

UNIVERSITY OF BELGRADE
FACULTY OF PHYSICS
INSTITUTE OF METEOROLOGY

Luka R. Ilić

NUMERICAL MODELING OF ICE
NUCLEATING PROPERTIES OF
ATMOSPHERIC MINERAL AEROSOL

Doctoral Dissertation

Belgrade, 2022

УНИВЕРЗИТЕТ У БЕОГРАДУ
ФИЗИЧКИ ФАКУЛТЕТ
ИНСТИТУТ ЗА МЕТЕОРОЛОГИЈУ

Лука Р. Илић

НУМЕРИЧКО МОДЕЛИРАЊЕ
НУКЛЕАЦИОНИХ ОСОБИНА
АТМОСФЕРСКОГ МИНЕРАЛНОГ
АЕРОСОЛА

докторска дисертација

Београд, 2022

Mentors:

Dr. Lazar Lazić, Full Professor
Faculty of Physics, University of Belgrade

Dr. Maja Kuzmanoski, Assistant Research Professor
Institute of Physics, University of Belgrade

Members of the Committee:

Dr. Vladimir Đurđević, Associate professor
Faculty of Physics, University of Belgrade

Dr. Vladan Vučković, Associate professor
Faculty of Physics, University of Belgrade

Dr. Ana Vuković Vimić, Associate professor
Faculty of Agriculture, University of Belgrade

Defense date:

Acknowledgments

I wish to express my sincere gratitude towards my mentors Lazar Lazić and Maja Kuzmanoski who went outside the requirements of the job to keep inspiring me to develop as a scientist and as a person in many unexpected ways. Although not in the official capacity of a mentor, I must add that research presented in this Thesis was made possible through generous support and supervision by the DREAM model original author, Slobodan Ničković, to whom I will also forever be grateful for helping me set my path as a scientist.

I would like to extend my appreciation to the members of the defense committee, Vladan Vučković, Vladimir Đurđević, and Ana Vuković Vimić for their very useful suggestions during my studies and research.

Of course, reaching this step in my academic pursuit would not have been possible without the guidance and inspiration instilled in me by the professors and lecturers at the Institute of Meteorology, Faculty of Physics, University of Belgrade. As complementary forces that helped me make my first steps in the research projects are the people who I am proud to call my colleagues from South Environment and Weather Agency (SEWA) and Meteos, Momčilo Živković, and Radomir Radojičić together with Veljko Milutinović from the School of Electrical Engineering and their teams.

Some of my first steps in the world of research were made through the cooperation of SEWA and the Institute of Physics Belgrade (IPB), a place that later became a home for me for so many years and where I conducted most of the research which is a part of this Thesis. I wish to thank the people who led the IPB and the Scientific Computing Laboratory (SCL), and who facilitated the setting up of a research environment and infrastructure which made this possible, Aleksandar Belić, Aleksandar Bogojević, and Antun Balaž. And especially the SCL team who maintained the HPC facilities at IPB helped me compile and run the code probably more times than they had planned, Dušan Vudragović, Petar Jovanović, and Vladimir Slavnić.

Another part of the IPB is the Environmental Physics Laboratory (EPL), coordinated for the most part of my time at IPB by Zoran Mijić. I am grateful for the opportunity to be a part of such a scientifically diverse team which is something, I believe, that had broadened the perspectives of all the EPL members.

A special place in this section is reserved for the developers of the DREAM model at the South East European Virtual Climate Change Center (SEEVCCC) of the Republic Hydrometeorological Service of Serbia (RHMSS), Goran Pejanović, Slavko Petković, Bojan Cvetković and other members of the cross-institutional “DREAM Team” for our fruitful discussions and cooperation.

Since the scientific results convey their meaning as they serve the society of today and the future, I was always eager to take the opportunities to present and discuss science with a broader auditorium. Therefore, I am grateful to the IPB Communications team led by Slobodan Bubnjević and Marija Đurić and to Jovana Vurdelja of the SEEVCCC for providing a platform and means to spread the message of science and understanding both to the curious and to the misinformed. Also, to Savremena International School and Savremena gimnazija and my IPB colleague Andrej Bunjac for giving me an opportunity to inspire younger generations to think critically and to imagine a world they will create.

And as the last item in the professional part of this list, only chronologically, I am proud to be a member of the Barcelona Supercomputing Center (BSC) Atmospheric Composition (AC) group. I am grateful to the AC coordinators Carlos Pérez and Oriol Jorba for believing in me and welcoming me to their group where I can make my next steps as a scientist.

As always, achievements like this are not possible without the support and understanding from family and friends, and unexpected mentors. To my parents, Biljana and Rodoljub, I am grateful for teaching me how to be curious and open-minded and to participate in fierce but kind discussions. To my brother, Nemanja, for being an immense personal and professional inspiration and someone to look up to while growing up and while overcoming many challenges. One more family member who played a vital part in this journey is my uncle Milenko Jovanović Bata the first meteorologist I have ever met and who always kept the level of professionalism and ethical standards that keep our profession at the place it deserves as it serves the society. Another meteorologist who has been a source of inspiration on this journey and to whom I am thankful for grounded advice is Dušanka Županski. I always appreciated the words of my rowing coach Vladan Milosavljević to stand up straight with my shoulders back and that submaximal effort can be maintained for unexpectedly long periods. To Rajko Šašić I am thankful for pushing me to use my intelligence while preparing for the exams and not to reinvent the wheel at the exams.

I will end this list by expressing gratitude for the love and support of the people close to me, who stood by me, sometimes levitating outside the limits of their patience, and understanding, through the many challenges faced during the research that led to the completion of this Thesis. Nikola Petrović Starac and MOR, Milica Kovačević Mačka, Nemanja Tončić Debeli, Martin Raspor Brat, Jovan Obradović Joca Panker, Dragana Đurić, Pavle Arsenović Ćorima, Nikola Jevtić Instruktor, Ivana Maksimović, Jadranka Vasiljević Jaca, Aleksandar Jovanović Coa, thank you!

Technical and financial support for this research was made possible through several projects and through the support of many colleagues from the international research networks and communities:

The funding was provided by the Institute of Physics Belgrade, through the grants by the Ministry of Education, Science, and Technological Development of the Republic of Serbia: III43007, III41011, 451-03-68/2020-14/200024.

GEO-CRADLE project (Coordinating and integRating state-of-the-art Earth Observation Activities in the regions of North Africa, Middle East, and Balkans and Developing Links with GEO-related initiatives towards GEOSS) has received funding from the European Union's Horizon 2020 research and innovation program under grant agreement No 690133.)

VI-SEEM was a three-year project that aimed at creating a unique Virtual Research Environment (VRE) in Southeast Europe and the Eastern Mediterranean (SEEM), to facilitate regional interdisciplinary collaboration, with a special focus on the scientific communities of Life Sciences, Climatology, and Digital Cultural Heritage under the European Union's Horizon 2020 research and innovation program under grant agreement No 675121.

The International Network to Encourage the Use of Monitoring and Forecasting Dust Products (inDust) is the COST Action CA16202. The overall objective of inDust was to

establish a network involving research institutions, service providers, and potential end-users of information on airborne dust.

Ioannis Biniotoglou led the activities in the systematic evaluation of dust models within the EARLINET. I thank EARLINET (<https://www.earlinet.org/>, last access: 12 December 2020), ACTRIS (<https://www.actris.eu>, last access: 12 December 2020), and PollyNET (<http://polly.tropos.de>, last access: 15 March 2021) for the data collection, calibration, processing, and dissemination, and for their investment into raising the capacities of EPL through numerous workshops and training.

Eleni Marinou provided lidar data from an instrument hosted by Jean Sciare in the Cyprus institute during the INUIT-BACCHUS-ACTRIS experiment. Jann Schrod and Bingemer Heinz G. provided the UAV-FRIDGE measurement data. The INUIT-BACCHUS-ACTRIS experiment received support from the Deutsche Forschungsgemeinschaft (Grant Nos. 1525, INUIT), the European Union's Seventh Frame-work Program (Grant Nos. 603445, BACCHUS), the European Union's Horizon 2020 research and innovation program (654109, ACTRIS-2). Eleni Marinou was funded by the European Research Council (Grant Nos. 725698, D-TECT) and by a DLR VO-R young investigator group and the Deutscher Akademischer Austauschdienst (Grant No. 57370121).

Fabio Madonna, Marco Rosoldi and Michail Mytilinaios provided data from the Potenza lidar and cloud radar observations.

Vassilis Amiridis coordinated the PRE-TECT campaign where the DREAM INPC experimental forecast was first used operationally. PRE-TECT experiment was focused on desert dust microphysical characterization from remote sensing, employing advanced inversion techniques developed in the framework of ACTRIS.

I am grateful to the AERIS/ICARE Data and Services Center for generating and storing the DARDAR products and for providing access to the CALIPSO data used and their computational center (<http://www.icare.univ-lille1.fr/>, last access: 8 August 2019). I thank the NASA CloudSat Project and NASA/LaRC/ASDC for making available the CloudSat and CALIPSO products, respectively, which are used to build the synergetic DARDAR products.

Luka Ilić

Numerical Modeling of Ice Nucleation Properties of Atmospheric Mineral Aerosol

Abstract

Mineral dust particles are one of the most abundant aerosol species in the atmosphere. They are very efficient ice nucleating particles (INPs). A mineralogy-sensitive immersion freezing parameterization in presence of dust particles has been implemented in Dust Regional Atmospheric Model (DREAM). Ice nucleating particle concentration (INPC) was also parameterized using two mineralogy-indifferent immersion freezing, and two deposition nucleation parameterizations. A two-year model dataset of dust vertical profiles in Europe was contributed to a model evaluation study at the European scale. Selected cases in the Mediterranean in April 2016, were analyzed in more detail and compared with the lidar-derived vertical profiles of cloud relevant dust concentrations and INPC and in situ INPC measurements. Predicted INPC values were compared to the ice crystal number concentration (ICNC) vertical profiles product during satellite overpasses over the dust plume. Ground-based cloud radar observations of ice water content (IWC) and satellite observations of ice water path (IWP) were used in a qualitative assessment of INPC and observed cloud correlation. While all three model setups agreed within one order of magnitude, the mineralogy-sensitive setup presented a sharp maximum in INPC at -25°C and the sharpest decrease of INPC at temperatures higher than -20°C , due to sensitivity to feldspar. It showed agreement with the in situ measurements at temperatures lower than -20° . It was also the most successful in predicting the ICNC profile shape and extent in the presented cases. Variations in the feldspar content influence the effectiveness of dust as an INP but this effect is reduced by the sedimentation of feldspar silt particles. The horizontal distribution of INPs was well predicted by all the model setups. The differences due to deposition nucleation parameterizations and feldspar content were more pronounced above sea surfaces, over the Atlantic, the Mediterranean and the Caspian Sea.

Keywords: Numerical Modeling, Atmospheric Modeling, Parameterizations, Aerosols, Mineral Dust, Ice Initiation, Lidar, Remote Sensing

Scientific field: Earth Science

Field of academic expertise: Meteorology

UDC: 551.5 (043)

Нумеричко моделирање нуклеационих особина атмосферског минералног аеросола

Сажетак

Честице минералног аеросола су један од најприсутнијих типова аеросола у атмосфери. Оне су веома ефикасна језгра нуклеације (INP). Параметризација имерзионог замрзавања у зависности од минералног састава честица песка је укључена у Dust Regional Atmospheric Model (DREAM). Концентрација језгара нуклеације (INPC) је такође параметризована коришћењем две параметризације имерзионог замрзавања и две параметризације депозиционе нуклеације које су индиферентне на састав песка. Подаци добијени двогодишњим симулацијама моделом су део студије евалуације модела регионалних размера у Европи. Одабрани случајеви у Медитерану током априла 2016. године су детаљније анализирани и поређени са вертикалним профилима концентрација песка релевантним за коришћене параметризације и INPC добијеним мерењима лидаром и *in situ* мерењима INPC. Прогнозиране вредности INPC су поређене са вертикалним профилима концентрација ледених кристала (ICNC) добијених током сателитских прелета изнад перјанице песка. Извршено је квалитативно поређење INPC са осматреним облацима на основу мерења садржаја леда (IWP) радаром са земље и сателитским осматрањима садржаја леда у стубу ваздуха (IWC). Сви избори параметризација у моделу се слажу до једног реда величине, међутим, минерално осетљива параметризација показује оштар максимум у INPC на -25°C и најстрмији пад INPC на температурама изнад -20°C због осетљивости на активност фелдспара. Ова параметризација се слаже са *in situ* мерењима на температурама нижим од -20°C . Такође је најуспешнија у представљању облика и вертикалне распрострањености ICNC у приказаним случајевима. Промене у садржају фелдспара утичу на ефикасност песка као INP али овај ефекат је смањен седиментацијом фелдспара у честицама прашине. Хоризонтална распрострањеност INP је добро прогнозирана у свим подешавањима модела. Разлике због избора шеме за депозициону нуклеацију и због садржаја фелдспара су више изражене изнад водених површина, изнад Атлантика, Медитерана и Каспијског језера.

Кључне речи: нумеричко моделирање, моделирање атмосфере, параметризације, аеросоли, минерална прашина, иницијација ледене фазе, лидар, даљинска мерења

Научна област: Геофизичка наука

Ужа научна област: Метеорологија

УДК број: 551.5 (043)

Table of Contents

1 Introduction.....	1
2 Numerical Modeling of Atmospheric Mineral Dust	6
2.1 Dust Regional Atmospheric Model (DREAM)	7
2.2 Mineral Composition of Atmospheric Dust.....	9
3 Remote Sensing and In Situ Observations of Dust and Clouds	12
3.1 Aerosol Lidar Remote Sensing and Dust Mass Concentrations Retrievals	15
3.1.1 LIRIC Algorithm.....	15
3.1.2 POLIPHON Algorithm	16
3.2 The CALIOP instrument.....	18
3.3 Cloud Radar Observations	19
3.4 DARDAR Satellite Products.....	20
3.5 CLAAS-2 dataset.....	20
3.6 In Situ Measurements	21
4 Simulation of Dust Episodes in Europe and the Mediterranean	22
4.1 A Systematic Study of Dust Model Performance	22
4.2 Systematic Study Evaluation Metrics	23
4.3 Evaluation Results	24
4.4 Simulations of Dust Episodes in Eastern Mediterranean.....	27
4.4.1 Major dust event, April 8 to 11	28
4.4.2 Intermediate Dust Event, April 14 to 16	30
4.4.3 Dust Plume in the Mediterranean, April 18 to 21	32
4.5. Comparison of Dust Mass Concentrations from DREAM and POLIPHON	35
5 Numerical Modeling of Ice Nucleating Properties of Atmospheric Mineral Dust	41
5.1. INPC Parameterizations in DREAM	42
5.2 Comparison of INPC resulting from DREAM and POLIPHON dust concentrations	46
5.3 Comparison of DREAM and In Situ INPC Measurements	51
5.4. Comparison with the IWC in Potenza.....	53
5.5 Comparison with the DARDAR Product during Dust Plume Overpasses.....	54
5.5 Comparison with the IWP.....	60
6 Summary and Conclusions	65
7 References.....	68
Appendix.....	84
Publications.....	84

Journals	84
Conferences.....	85
Presentations	87
Biography.....	88

1 Introduction

Dust aerosols in the atmosphere are one of the main contributors to the global aerosol burden (Huneeus et al., 2011; Kok et al., 2017). Dust is emitted from the sources in arid regions across the world, mainly from the so-called dust belt (Wu et al., 2020; Kok et al., 2021). It is considered that the dust belt covers areas from northern Africa, covering the sources in the Middle East and Central Asia to northern India, also including areas in China and Mongolia (Ginoux et al., 2001). Separated from these areas by oceans, dust sources in the northern hemisphere are also present in North America (Vuković et al., 2014) and Iceland (Sanchez-Marroquin et al., 2020). Dust regions are also present in the southern hemisphere, namely in Australia, South America, and southern Africa (Krätschmer et al., 2022). After emission, the dust particles in the atmosphere are distributed by the circulations of different scales and sometimes the particles originating from the Sahara are transported across the Atlantic reaching remote areas through long-range transport (Prospero et al., 2021). Dust can impact the Earth system and affect weather and climate through direct interaction with solar and terrestrial radiation (Ghan et al., 2012) and by influencing the cloud processes (Lohmann and Feichter, 2005; Kanji et al., 2017). Furthermore, dust can impact visibility, which affects tourism, road transport, and aviation (Papagiannopoulos et al., 2020). When surface concentrations become high enough, they can pose serious health risks (Giannadaki et al., 2014). Long-range transport and the associated processing of dust particles and their subsequent deposition can be a source of nutrients in some ecosystems (Jickells and Moore 2015; Ravi et al. 2011). Airborne dust may also contribute to the transport of fungal and viral microbial pathogens, which can lead to disease outbreaks (Sprigg et al., 2014).

One of the main drivers to increase interest in the dust research are conclusions of the Intergovernmental Panel on Climate Change (IPCC) Assessment Report 5 (AR5). It was reported that the role of dust in the Earth system is a source of significant uncertainties in climate modeling and numerical weather prediction, mainly due to its impact on radiation and clouds (Boucher et al., 2013). In the following years, studies of the role of dust in cloud microphysics led to an improved understanding of their impact (i.e., Villanueva et al., 2020) but future development is intended to ensure a more detailed representation of aerosol forcing in the Earth system models (Bellouin et al., 2020). The small-scale process of ice initiation in the presence of dust particles influences cloud extent, lifetime, particle size, and radiative properties (Cantrell and Heymsfield, 2005) and therefore affects the tropospheric composition (Abbatt, 2003) and hydrological cycle (Rogers and Yau 1989). Mineral dust particles have been shown to be one of the main reservoirs of ice-nucleating particles (INP) influencing ice initiation in areas distant from their sources (Cziczo et al., 2013). While the liquid water droplets in the atmosphere, without INPs present, can be supercooled to temperatures below about -37°C (Herbert et al., 2015; Ickes et al., 2015), INPs in the atmosphere can promote the heterogeneous freezing mechanisms (i.e. immersion freezing, contact freezing, condensation freezing, and deposition nucleation) at higher temperatures and therefore lower supercooling (Prupacher and Klett, 1997; Murray et al., 2012; Hoose and Möhler, 2012; Vali, 2015).

Our knowledge about dust and its role in ice initiation is being constantly improved through experimental and numerical modeling efforts (Kanji et al., 2017). Research in recent years was organized through laboratory studies (DeMott et al., 2010; 2015; Niemand et al., 2012; Atkinson et al., 2013; Steinke et al., 2015; Ullrich et al., 2017; Harrison et al., 2019),

observational efforts (Schrod et al., 2017; Price et al., 2018; Marinou et al., 2019), and numerical modeling and prediction (Atkinson et al., 2013; Nickovic et al., 2016; Vergara-Temprado et al., 2017; Suand Fung, 2018). Correct representation of dust in atmospheric models can lead to improvements in climate simulations, weather forecasts, and weather analysis and reanalysis. One direction in the model development regarding the dust role in the cloud process is oriented towards the use of cloud-microphysics schemes coupled with dust concentration and parameterization of dust INPC. In the atmospheric models in the past, parameterizations were proposed that would describe the INPC as a function of temperature (Fletcher et al., 1962; Bowdle et al., 1985; Dudhia 1989; Reisner et al., 1998; Roudier 2003). Meyers (1992) used a different approach and parameterized the ice crystal number concentrations (ICNC) as a function of temperature. In an atmospheric dust model, the INPC can be calculated as a function of cloud-relevant dust concentrations and meteorological parameters. In most cases, the mineral composition of dust is not considered in INPC parameterizations and those are referred to in the text as the mineralogy-indifferent parameterizations. In parallel, further investigation of the properties of dust responsible for its effectiveness as an INP has been conducted (Atkinson et al., 2013, Murray et al., 2017; Boose et al., 2016; Harrison et al., 2019; Holden et al., 2019). It was found that feldspars are the most effective minerals found in dust in the immersion freezing process at temperatures lower than -15 °C. Parameterizing feldspar INPC (Atkinson et al., 2013), Vergara-Temprado et al. (2017) found that feldspar particles were prevailing INPs near terrestrial sources, while marine organic aerosols (Wilson et al., 2015) were dominant INPs in remote ocean locations.

Remote sensing observations provide valuable data sets that have been used for aerosol model evaluation in numerous studies in recent years. Tsikerdekis et al. (2017) compared results of the RegCM4 regional model (Alexandri et al., 2015) in northern Africa, the Middle East, and the Mediterranean with the aerosol optical depth (AOD) LIVAS product (Amiridis et al., 2015) based on observations from the Cloud-Aerosol Lidar and Infrared Pathfinder Satellite Observations (CALIPSO; Winker et al., 2013). LIVAS 3D product of dust extinction was used in the same region for model evaluations: simulations for the period 2007-2012 (Georgoulias et al., 2018) with the MACC (Monitoring Atmospheric Composition and Climate) aerosol system of the European Centre for Medium-range Weather Forecasts (ECMWF) (Morcrette et al., 2009; Benedetti et al., 2009) and for the period 2009-2013 with the BSC-DREAM8b regional dust model (Konsta et al., 2018). Solomos et al. (2017) evaluated the Regional Atmospheric Modeling System (RAMS; Solomos et al., 2011) simulations of a dust storm that affected the Middle East and the eastern Mediterranean in September 2015. They used aerosol vertical profiling measurements from the European Aerosol Research Lidar Network (EARLINET; Pappalardo et al., 2014) and CALIPSO, and the qualitative dust RGB product from the geostationary Meteosat Second Generation (MSG) Spinning Enhanced Visible and Infrared Imager (SEVIRI) (Schmetz et al., 2002). Solomos et al. (2019) compared the AOD from the NMME-DREAM model (Nickovic et al., 2001, 2016; Pérez et al., 2006) simulations with MODIS AOD (Platnick et al., 2017) and the Aerosol Robotic Network (AERONET; Holben et al., 1998) AOD values for the mesoscale simulations in the Middle East in 2016. Kampouri et al. (2021) analyzed the development of a volcanic plume originating from Mt. Etna, Italy between 30 May and 6 June 2019. Lidar measurements performed at the PANhellenicGEophysical observatory of Antikythera (PANGEA) of the National Observatory of Athens (NOA), in Greece detected the particles of volcanic origin in the days following the eruption. FLEXiblePARTicle dispersion model (FLEXPART; Sthol et al., 2005) simulations

and satellite-based SO₂ observations from the TROPOspheric Monitoring Instrument onboard the Sentinel-5 Precursor (TROPOMI/S5P) (Veefkind et al., 2012) confirmed the volcanic plume transport. Varlas et al. (2021) evaluated the coupled Chemical Hydrological Atmospheric Ocean wave modeling System (CHAOS). CHAOS encompasses the wave model (WAM) two-way coupled through the OASIS3-MCT coupler with the Advanced Weather Research and Forecasting model coupled with Chemistry (WRF-ARW-Chem) against in-situ PM₁₀ and LIRIC lidar aerosol concentration retrievals at 2 stations in Greece (Finokalia on 4 and 15 July 2014 and Antikythera-PANGEA on 15 September 2018).

Dust models are routinely evaluated within the Sand and Dust Storm Warning Advisory and Assessment System (SDS-WAS) project (WMO, <http://www.wmo.int/sdswas>; Basart et al., 2012; Gama et al., 2015). Within the SDS-WAS, aerosol optical depth is compared with observations from the AERONET (Holben et al., 1998). Synergistic approaches using both lidar and AERONET data have been developed within the EARLINET (Pappalardo et al., 2014). These algorithms, namely the Generalized Aerosol Retrieval from Radiometer and Lidar Combined data algorithm (GARRLiC; Tsekeri et al., 2017); LIRIC algorithm (Lidar-Radiometer Inversion Code; Chaikovsky et al., 2016; Tsekeri et al., 2017) and the POLIPHON algorithm (Polarization Lidar Photometer Networking; Ansmann 2011; 2012) can provide vertical profiles of dust concentrations (Biniotoglou et al., 2015; Tsekeri et al., 2017; Ansmann et al., 2019b). Papayannis et al. (2014) retrieved and intercompared lidar-derived dust mass concentrations from two different synergistic methodologies, LIRIC and POLIPHON, highlighting that POLIPHON does not require spatiotemporally collocated lidar and AERONET measurements and that it can provide dust concentration profiles in presence of thin clouds, besides the cloud-free conditions. Having cloud-relevant dust concentration profiles as a product of remote sensing retrievals enabled applications of mineralogy-indifferent INPC parameterizations (Mamouri and Ansmann 2015; 2016; Ansmann et al., 2019a; Marinou et al., 2019; Haarig et al., 2019). The lidar-derived cloud-relevant dust concentrations have been intercompared with in situ measurements onboard unmanned aerial vehicles (UAVs), showing agreement within their uncertainties (Mamali et al., 2018; Marinou et al., 2019). Lidar INPC has also been compared to ICNC from ground-based and satellite-born cloud radar observations (Ansmann et al., 2019b; Marinou et al., 2019). These findings further encouraged the use of remote sensing instruments in model evaluation in terms of dust concentrations and INPC. Lidar-derived vertical profiles of cloud-relevant dust concentrations and INPC values calculated based on them also have the potential to be used in the data assimilation cycle (Ansmann et al., 2019b).

The main objective of this Thesis is to expand the capabilities of a regional atmosphere-dust model to describe ice initiation in presence of dust particles as a process dependent on thermodynamic quantities, dust concentrations, and dust mineral composition (Barreto et al., 2021; Ilić et al., 2021). Until now, parameterizations that can be applied to describe the immersion freezing in presence of mineral dust particles have been developed (Atkinson et al., 2013; Harrison et al., 2019). Parameterizations that do not take the mineral composition of dust into account (DeMott et al., 2015; Steinke et al., 2015; Ullrich et al., 2017) have been used in this type of model (Ničković et al., 2016, 2021). This Thesis presents the results of the implementation of INPC parameterization schemes to describe atmospheric mineral dust ice initiation in a regional atmospheric model with fully coupled dust transport processes. Dust INPC is analyzed using parameterizations as a step toward coupling the predicted dust

concentrations with a microphysics scheme (Thompson et al., 2014; Ničković et al., 2016). The main concepts of numerical modeling of atmospheric dust processes with a dust mineralogy representation are presented as they are described in Dust Regional Atmospheric Model (DREAM). The main aspect of the new development is the implementation of INPC mineralogy-sensitive parameterization for the immersion freezing ice initiation process in DREAM. Parameterizations for the immersion freezing process in the presence of feldspar and quartz minerals are implemented as they are the most active in the ice initiation process. Mineralogy-indifferent parameterizations for immersion freezing and deposition nucleation are also included. The model results using mineralogy-sensitive and mineralogy-indifferent parameterizations are used to estimate the relative contribution and the importance of feldspar and quartz in total INPC.

A significant component of this Thesis is the evaluation of DREAM results with reference to observations. An overview is given of the remote sensing algorithms, datasets, as well as products, and in situ measurements used in model evaluation. The evaluation presented here goes beyond the operationally established methodologies. State-of-the-art remote sensing retrieval products are used to evaluate DREAM model performance in dust concentration prediction. Vertical profiles of dust concentration outputs of two-year simulations of DREAM were contributed to a systematic model evaluation in the frame of the EARLINET lidar network (Biniotoglou et al., 2015). The model results are also compared with the retrievals of remote sensing observations for the numerical experiment performed in the Mediterranean in April 2016 (Ilić et al., 2022). During this period, INUIT-BACCHUS-ACTRIS experimental campaign was organized in Cyprus (Schrod et al., 2017; Mamali et al., 2018; Marinou et al., 2019). The lidar retrieval dataset from the campaign was used in the evaluation of the prediction of cloud-relevant dust concentrations and the related INPC. Apart from the measurements organized within the framework of the campaign, ground-based lidar and ground-based radar in Potenza, Italy, were used in quantitative and qualitative model evaluation, respectively. In situ measurements performed during the campaign were used to evaluate model INPC in Cyprus. Aerosol classification from Cloud-Aerosol Lidar with Orthogonal Polarization (CALIOP) aboard the CALIPSO (Winker et al., 2013) and ICNC product from combined CALIOP and CloudSat retrievals were used to evaluate the model results during satellite overpasses over the dust plume (Delanoë and Hogan, 2010). The horizontal distribution of INPs was compared to ice water path (IWP) from the Spinning Enhanced Visible and InfraRed Imager (SEVIRI) sensor aboard the METEOSAT second-generation satellite (MSG) (Schmetz et al., 2002). While not all the measurements used in the evaluation are suitable for quantitative comparisons, they provide valuable insight into model performance and the potential for use of INPC parameterizations in dust models.

The Thesis is organized into seven Chapters. The manuscript begins with the introduction with the motivation and objectives of the study in Chapter 1. In Chapter 2, the main concepts of dust modeling with reference to mineral composition representation are described as they are represented in the DREAM model. In Chapter 3, the observation methodologies, and datasets (both remote sensing and in situ) are described, as well as their applications in the model evaluation. Chapter 4 presents the validation of the model results for two years in several stations in Europe, and for selected cases in April 2016 in the Mediterranean. Chapter 5 presents the main results of the application of INPC parameterizations in the model and comparisons with the measurements. The Thesis concludes

with a summary of the main findings and conclusions with an outlook for the future given in Chapter 6. References are listed in Chapter 7.

2 Numerical Modeling of Atmospheric Mineral Dust

Dust aerosols are abundant in the atmosphere with an estimated production of several thousand megatons per year (Tegen and Fung 1994). The main dust sources on Earth are deserts, dried-out rivers, and lake beds. It is estimated that almost half of the global dust emissions occur in Africa (Huneeus et al., 2011), the location of the Sahara, the largest desert in the world. The role of mineral dust has been recognized to be important in a broad range of atmospheric phenomena at different scales. The role and interactions of dust in the environment are influenced by its chemical and mineral composition. Adequate description of the mineral composition of dust in numerical models can improve the representation of certain processes in weather prediction and climate simulations (Nickovic et al., 2012). The mineral composition of dust affects radiation, cloud processes, deposition of nutrients, and human health. The direct impact of mineral dust on both shortwave and longwave radiation is significantly affected by its mineral composition (Sokolik and Toon, 1999, Claquin et al., 1998; Balkanski et al., 2007). As a consequence of interaction with radiation, large dust loads can reduce the surface temperature by a few degrees (Perez et al., 2006). The indirect impact of dust on radiation is related to its role in the cloud process. Dust particles can serve as CCN (Koehler et al., 2009; Kumar et al., 2009, 2011) and INPs (DeMott et al., 2010; 2015). Several field experiments and laboratory studies have shown that mineral dust can be the dominant source of INPs (Hoose and Möhler, 2012; Murray et al., 2012; Cziczo et al., 2013). Some minerals found in dust are more efficient in ice initiation. Particles containing K-feldspar are considered to be the most efficient INPs, while quartz as a major component of dust can also contribute to ice nucleation (Atkinson et al., 2013, Boose et al., 2016; Harrison et al., 2016, 2019). The interaction of dust with the biosphere is related to the transport of nutrients found in dust and the atmospheric processing which makes the nutrients usable by living organisms. Long-range transport of dust increases the solubility of iron present in dust through interactions with cloud processes and radiation, making it bioavailable to ocean phytoplankton (Baker and Jickells, 2006; Journet et al., 2008). Nickovic et al. (2013) developed a regional model for atmospheric transport and transformation of iron in dust and its deposition over the Atlantic. High surface concentrations of dust are associated with a significant risk of respiratory and cardiovascular diseases in humans (Giannadaki et al., 2014). Iron in dust may be a contributor to bacterial growth and epidemics of meningococcal meningitis in the African Sahel (Pérez et al., 2014).

There are several modeling approaches to the exploration of the transport of mineral dust particles and their role in the atmosphere. Offline dust models rely on previously saved output with regular time intervals of meteorological fields from global or regional atmospheric models or reanalyses (Mahowald et al., 1999). Trajectory models can be used to calculate air mass trajectories and estimations can be made about air masses containing and transporting aerosol particles. Offline models can be more complex, including calculations of dust emission, transport, and wet and dry deposition. The first online models were focused on the analysis of specific events (Westphal et al., 1988). Several years later, global dust transport models were developed (Tegen and Fung 1994, 1995) to simulate long-range transport on seasonal scales. A more detailed view of the atmospheric dust process required higher spatial and temporal resolution available with regional models (Ničković and Dobričić 1996; Marticorena et al., 1997; Nickovic et al., 2001). In online models, it is feasible to perform online simulations of dust and its interaction with clouds, radiation, or biosphere (Perez et al., 2006b, Nickovic et al., 2013, Su et al., 2018). Resolution of the atmospheric driver of these models is chosen to describe a certain scale of the phenomena, several tens of kilometers for the global models, to several kilometers for high-resolution prediction of very strong smaller-scale dust events such as haboobs (Vuković et al., 2014).

2.1 Dust Regional Atmospheric Model (DREAM)

The Dust Regional Atmospheric Model (DREAM) (Nickovic et al. 2001; Nickovic 2005; Vuković et al. 2014) is an atmospheric dust cycle model, including emission, horizontal and vertical turbulent mixing, large scale transport, and deposition. It is coupled with an atmospheric driver model, the Nonhydrostatic Mesoscale Model (NMM) so that they share the same time step. In the coupled dust-atmosphere model, the dust cycle is driven by atmospheric variables, but dust does not influence the atmospheric variables as it is considered a passive tracer. Therefore, there are no parameterizations of dust interactions with the environment. NMM is a numerical atmospheric model capable of simulating atmospheric phenomena of different time and spatial scales, from high-resolution weather forecasts to regional climate studies. It was developed and run for several years operationally at National Centers for Environmental Prediction (NCEP) in Washington D.C., USA. It is being actively developed and used in operational forecasts and research in RHMSS/SEEVCCC (<https://www.seevccc.rs>). For the simulations used in this thesis, DREAM is set up with a domain covering Saharan and Middle Eastern dust sources and dust transport in the Mediterranean. The model is run with $0.1^\circ \times 0.1^\circ$ horizontal resolution and 28 vertical levels.

DREAM, as a fully coupled atmospheric dust cycle model, solves an Eulerian type dust mass (C) continuity prognostic equation:

$$\frac{\partial C}{\partial t} = -u \frac{\partial C}{\partial x} - v \frac{\partial C}{\partial y} - (w - w_t) \frac{\partial C}{\partial z} - \nabla \cdot (K_h \nabla C) - \frac{\partial}{\partial z} \left(K_z \frac{\partial C}{\partial z} \right) + \left(\frac{\partial C}{\partial t} \right)_{source} - \left(\frac{\partial C}{\partial t} \right)_{sink} \quad (2.1)$$

where u and v are horizontal components of velocity, w is vertical velocity, w_t is particle terminal velocity, K_h is the horizontal diffusion coefficient, K_z is the vertical diffusion coefficient. The first two right-hand side terms represent horizontal advection of dust, and the third is vertical advection. The fourth and fifth terms represent horizontal and vertical turbulent diffusion, respectively. The remaining two terms represent dust source and sink.

In DREAM, dust particle size distribution has been discretized and the particles are distributed in 8 size bins (Table 2.1) (Perez et al., 2006a). The size distribution in each size bin is considered to be log-normal with a mass median diameter of 2.524 μm (Shettle, 1984) and geometric standard deviation of 2.0 (Schulz et al., 1998). The sub-bin distribution is maintained throughout the model simulation (Zender et al., 2003). The analytic sub-bin distribution allows accurate prescription of physical and optical properties known to vary across the bin width (Perez et al., 2006). The first four bins with smaller effective radii represent clay particles, and the larger particles are in the silt category according to the United States Department of Agriculture (USDA) classification. Each of the size bins is represented by one mass continuity equation in the model.

The particle emission in the model is parameterized by an emission scheme. The particles can be injected into the atmosphere from the grid points in the model which are considered to be dust productive source points. To determine the dust productivity factor in dust sources in the model domain, land cover and soil type databases are used. USGS (United States Geological Survey, Olson 1994 a, b) land cover dataset provides information about vegetation cover which distinguishes between the desert and non-desert areas (Nickovic et al.,

2001; Walker et al., 2009). Land cover sources are combined with preferential sources originating from sediments in paleo-lake and riverine beds (Ginoux et al., 2001; Nickovic et al., 2016). Soil type information is used from a hybrid STATSGO (State Soil Geographic Database) – FAO (Food and Agriculture Organization of the United Nations) database (USDA, 1994), with 30s spatial resolution and 12 USDA soil type classes. In an atmospheric mineral dust regional model, clay and silt soil types are considered. Clay and silt soil type correspond to the particle bins 1-4 and 5-8 respectively (Table 2.1). Land cover and soil type maps are interpolated to the DREAM grid, creating source masks. Source masks provide land cover and soil type information in terms of fractions of area for which each model grid point is representative. Another parameter important for defining dust sources is the effectiveness of the dust source, the fraction of mass of particles available for emission as described by Tegen and Fung (1994). Additional parameters may be added when mineral-specific source masks are defined (Nickovic et al. 2013; Ilic et al., 2021). This parameter will be described in the next chapter.

Table 2.1 Effective radii and size limits for 8 bins in DREAM

Size fraction	Bin	Size limits (μm)	Effective radius (μm)
Clay	1	0.1-0.18	0.15
	2	0.18 - 0.3	0.25
	3	0.3 - 0.6	0.45
	4	0.6 - 1.0	0.78
Silt	5	1.0 - 1.8	1.3
	6	1.8 - 3.0	2.2
	7	3.0 - 6.0	3.8
	8	6.0 - 10.0	7.1

Dust productivity factor can be calculated for all potential source points and is defined for each size bin k as

$$\delta_k = \alpha\beta_k\gamma_k \quad (2.2)$$

where α is the fraction of the area from which emission is possible, β defines clay or silt fraction, and γ represents mass fraction available for emission (Nickovic et al., 2001).

In this model, dust emission parameterization includes a viscous sublayer between the surface and the lowest model layer (Janjic, 1994). The turbulent vertical transfer of dust into the lowest model layer is parameterized following different turbulent regimes (laminar,

transient, and turbulent mixing). When the particles are lifted through the boundary layer and into the free troposphere, they are transported by horizontal and vertical advection and horizontal and vertical turbulent diffusion processes. The particles' removal from the atmosphere (the sink term in the dust mass continuity equation 2.1) is described by dry and wet deposition processes. The dry deposition scheme includes processes of deposition by surface turbulent diffusion and Brownian diffusion, gravitational settlement, and interception and impaction on the surface roughness elements (Georgi, 1986). The wet dust deposition is proportional to the rainfall rate (Nickovic et al., 2001). Rainfall in the NMM atmospheric model can be produced by a convective cloud scheme (Janjic, 1994) and by the Ferrier et al. (2002) grid-scale cloud microphysics. The Ferrier et al. (2002) scheme is not aerosol-friendly, which means that it does not take forecasted aerosol concentrations as an input to cloud process calculations.

2.2 Mineral Composition of Atmospheric Dust

Capability of the dust model to reproduce the mineral content of atmospheric dust was enhanced with the development of mineralogical databases with estimates of mineral content in the dust (Claquin et al., 1999; Nickovic et al. 2012). GMINER30 gridded database has global coverage and is convenient for interpolation into various model grids (Figure 2.1). The minerals in the database are mapped based on the hybrid STATSGO – FAO soil type database and mineralogical tables of Claquin et al. (1999) which relate soil types to surface mineralogy. GMINER30 provides mineral fractions of illite, kaolinite, smectite, calcite, quartz, and hematite in clay fraction, and feldspar, gypsum, calcite, quartz, and hematite in silt fraction. For each of the minerals used in model simulations, source masks are created for clay and silt fractions and added as additional terms in the dust productivity equation. Each simulated mineral requires additional eight mass continuity equations for the eight size bins, and minerals are assumed to be externally mixed. Therefore, this type of model simulation can significantly increase the computational demands, even if the minerals are transported as passive tracers. Parameterizations of dust interactions with the environment would increase the computational complexity even further.

In simulations presented in this thesis, it was analyzed how the mineral composition of dust affects INPC. This is achieved by implementing appropriate INPC parameterizations in DREAM. Most of the INPC parameterizations presented in the literature do not take the mineral composition of dust into account (mineralogy-indifferent parameterizations). On the other hand, a study by Atkinson et al. (2013) showed that the main contributor to the effectiveness of dust as an immersion freezing INP is K-feldspar. They provided a mineralogy sensitive INPC parameterization, developed for several minerals present in dust. Further investigation confirmed that K-feldspars are generally very efficient ice nuclei although some alkali feldspars may have high nucleating abilities with implications on INPC prediction (Harrison et al., 2016). K-feldspar concentrations were found to be correlated with the ice-nucleating ability of nine desert dust samples (Boose et al., 2016). Quartz, as a major component of atmospheric mineral dust (Glaccum and Prospero, 1980), has been studied as a potential INP contributor and has proven to be active as an INP as well (Zolles et al., 2015; Holden et al., 2019; 2021). Several laboratory studies continued the development of mineralogy sensitive INPC parameterizations (Zolles et al., 2015; Harrison et al., 2016; Harrison et al., 2019). Harrison et al. (2019) analyzed the relative importance of quartz to feldspars in immersion ice nucleation, and as a result, developed new INP parameterizations for feldspar and quartz concentrations as main INPC contributors: feldspar due to its effectiveness, and quartz as a less effective but abundant mineral.

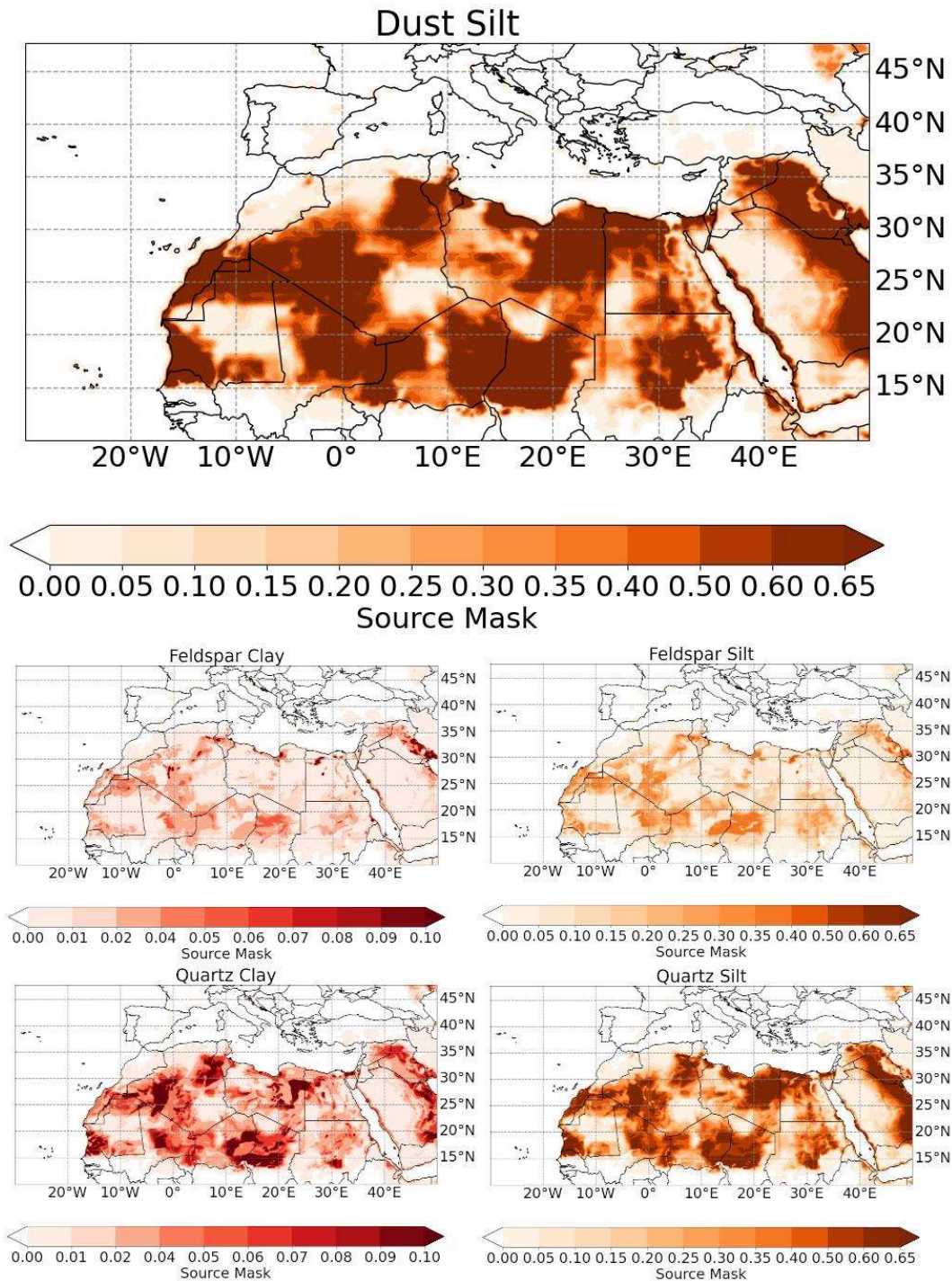


Figure 2.1 DREAM dust source masks for total dust, feldspar, and quartz in the model domain. Feldspar and quartz source masks are interpolated to model grid points from the GMINER30. Adapted from Ilić et al. (2022).

Therefore, feldspar and quartz minerals are considered in DREAM, since they are proven to be significant contributors to INPC. Mineralogy-sensitive parameterization by Harrison et al. (2019) is used. GMINER30 database does not provide feldspar fraction in the clay soil type but there is observational evidence of its presence (Kandler et al., 2009). Therefore, the same quartz-to-feldspar ratio as considered for silt-sized particles is used in silt to estimate feldspar fraction (Atkinson et al., 2013). Feldspar and quartz mineral fraction for clay and silt are created for the model domain (Figure 2.1). Fractions of feldspar and quartz

and their standard deviations across the whole model domain are given in Table 2.2. Considering the two mineral fractions and total dust concentrations in eight size bins, a total of 24 dust mass continuity equations are calculated in the model.

Table 2.2 Mean fractions and standard deviations for feldspar and quartz source masks for clay and silt, based on dust source grid points in the model domain used. Adapted from Ilic et al. (2022).

Mineral fraction	Mean fraction	Standard deviation
Feldspar in clay	0.03	0.02
Feldspar in silt	0.22	0.14
Quartz in clay	0.06	0.03
Quartz in silt	0.59	0.22

3 Remote Sensing and In Situ Observations of Dust and Clouds

To improve the prediction of clouds and the atmospheric cycle of aerosols, enhanced information is needed on aerosol horizontal and vertical distribution in the atmosphere and their interaction with weather systems. Such information has been made available through efforts in establishing ground-based remote sensing instrument networks for aerosol and cloud research (e.g., the Aerosol Robotic Network (AERONET; Holben et al. 1998), Cloudnet cloud radar observation network (Illingworth et al., 2007), the European network of ground-based aerosol lidars (EARLINET; Pappalardo et al., 2014). Satellite-borne sensors have also been used to observe aerosols and clouds. Products from selected sensors are used in this Thesis: Cloud-Aerosol Lidar with Orthogonal Polarization (CALIOP) onboard Cloud-Aerosol Lidar and Infrared Pathfinder Satellite Observation (CALIPSO) provides information on the vertical profiles and optical properties of aerosols and clouds (Winker et al., 2013); Cloud Radar aboard CloudSat provides the altitude and microphysical properties of clouds (Delanoë and Hogan, 2010); the Spinning Enhanced Visible and InfraRed Imager (SEVIRI) sensor aboard the METEOSAT second-generation satellite (MSG), among other products, provides cloud imaging and tracking (Schmetz et al., 2002).

Important properties of satellite or ground-based remote sensing observations are their spatial and temporal coverages and resolutions depending on the observation platform and instruments used. Satellite measurements can provide long-term observation data with global coverage or with a relatively high vertical resolution compared to conventional radio-sounding measurements. Ground-based remote sensing stations can provide global coverage but can be sparse in some geographical areas. On the other hand, they can also provide long-term higher vertical and temporal resolution measurements. However, besides the operational observations, field campaigns are organized to observe dust events in limited time periods, often using a variety of instruments for remote sensing and in situ measurements, based on the ground or aboard unmanned aerial vehicles (UAVs) and airplanes (Schrod et al., 2017; Price et al., 2018; Konsta et al., 2020). Regardless of the measurement platform, the characterization of aerosols in the elevated layers is important in studies of aerosol long-range transport and their role in the cloud process. A number of experimental campaigns were organized, for which one of the objectives was to investigate the role of dust in ice initiation: e.g., the Ice in Clouds Experiment – Tropical (ICE-T), based in St. Croix, US Virgin Islands in June 2011 (Heymsfield et al., 2014); the Ice in Clouds Experiment-Dust (ICE-D) field campaign, organized in the region of the Cape Verde archipelago in August 2015 (Price et al., 2018). The INUIT-BACCHUS-ACTRIS campaign in Cyprus in April 2016 was organized within the framework of three projects: Ice Nuclei Research Unit (INUIT); Impact of Biogenic versus Anthropogenic emissions on Clouds and Climate: towards a Holistic UnderStanding (BACCHUS); and Aerosols, Clouds, and Trace gases Research Infrastructure (ACTRIS) (Schrod et al., 2017; Marinou et al., 2019).

In aerosol research, lidar, as an active remote sensing instrument, can be used for the vertically resolved characterization of aerosols, necessary in the investigation of their impact on the Earth's environment. Atmospheric lidars have high vertical resolution when compared to common meteorological measurements such as radiosondes. This enables lidars to provide information about the fine features of elevated aerosol layers. It should be considered that thick cloud layers limit the altitudes from which the signal can be retrieved and consequently limit the lidar data analysis. The use of lidar data in model evaluation and the data assimilation cycle can lead to improvements in the quality of forecasts (Konsta et al., 2021; Escribano et al., 2022). Ground-based lidar measurements are organized in the frame of the GAW Aerosol Lidar Observation Network (GALION) initiative of WMO to form a global observational capacity

(Hoff and Pappalardo, 2010). Individual networks which compose the GALION are the European Aerosol Research Lidar Network (EARLINET; Pappalardo et al., 2014), the Micropulse Lidar Network (MPLNET; <https://mplnet.gsfc.nasa.gov/>; Welton et al., 2001), a NASA-supported network of comparatively low-cost micropulse backscatter lidars, the Latin America Lidar Network (LALINET; <http://www.lalinet.org/>; Antuña-Marrero et al., 2017) in Latin America, and the Asian dust and aerosol lidar observation network (AD-Net; Nishizawa et al., 2017).

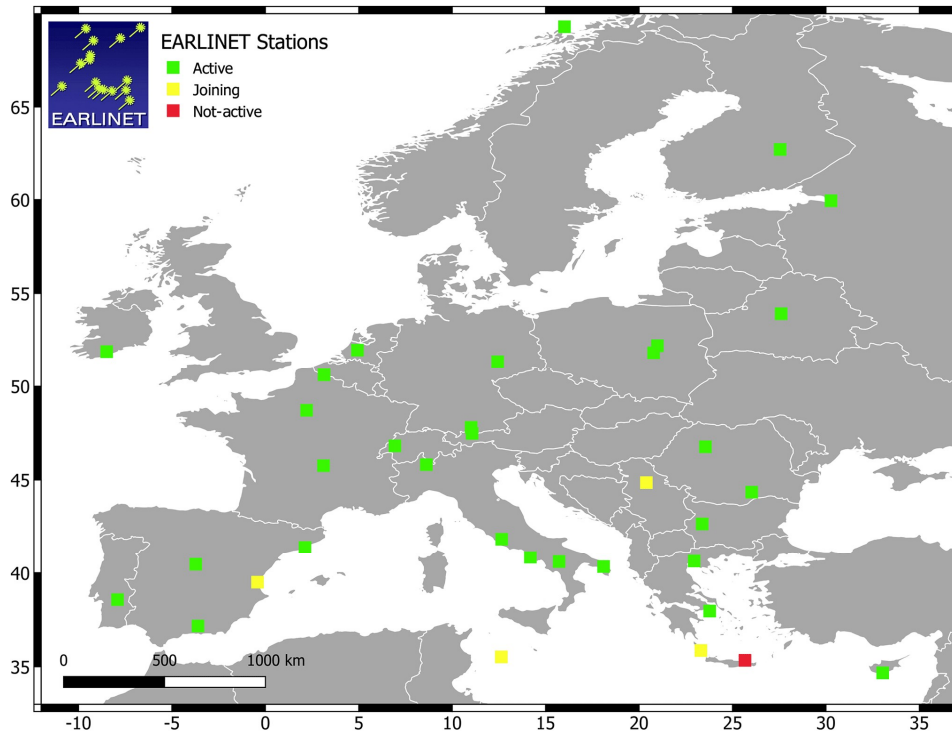


Figure 3.1 The EARLINET network in Europe. The green squares indicate the active stations, the yellow squares indicate the joining stations, and the red square indicates the non-active Finokalia, Greece, station. Adapted from Papagiannopoulos et al., 2020.

EARLINET is a European network of ground-based aerosol lidars (Bösenberg et al., 2001; Pappalardo et al., 2014). The lidar systems within EARLINET have diverse technical characteristics (Matthias et al., 2004). To overcome possible discrepancies in the lidar data analysis, standardization is established through a set of quality assurance tests (Freudenthaler et al., 2018) and inter-comparison campaigns (Wandinger et al., 2016). Significant efforts have been made toward an automated lidar data analysis through the development of the Single Calculus Chain tool (SCC) (D’Amico et al., 2015). Lidar observations within EARLINET are performed on a regular schedule which provides long-term, quality-assured aerosol data on a European scale (Bösenberg et al., 2003). In addition to the routine measurements, additional observations are organized to monitor Saharan dust episodes, volcanic eruptions, forest fires, and satellite overpasses (CALIOP, AEOLUS). Leibniz Institute for Tropospheric Research (TROPOS) made an effort to develop a lidar network with the advantages of using standardized instrument design, automated continuous operation during day and night in a wide range of weather conditions, and unified data processing (Althausen et al., 2009; Baars et al., 2016; Engelmann et al., 2016). This resulted in the development of multi-wavelength polarization Raman lidars called PollyXT lidars, which have been used within the so-called PollyNET international network of independent, voluntary, measurement stations (Althausen et al., 2013).

The map of the stations is shown in Figure 3.2. Some of the PollyNET stations have been part of EARLINET and the associated lidars have been used in experimental campaigns organized close to Sahara dust source regions (e.g., SAMUM-1 and SAMUM-2, Ansmann et al., 2011b; INUIT-BACCHUS-ACTRIS; Schrod et al., 2017; SALTRACE, Weinzierl et al. 2017; PRETECT, Konsta et al., 2021) and aboard the research vessel Polarstern (Rittmeaister et al., 2017; Ansmann et al., 2017).



Figure 3.2 Operational (green) and non-operational (red) PollyNet lidar stations. Adopted from <https://polly.tropos.de> (last access: 18 March 2022).

A global network of sun photometers, the AERONET, has been in operation since the 1990s (Holben et al. 1998). AERONET provides globally distributed observations of spectral aerosol optical depth (AOD) at seven wavelengths in the range 340 - 1020 nm, precipitable water vapor, and inversion products including aerosol size distributions and refractive indices at four wavelengths in the range 440 - 1020 nm. AERONET sun photometer measurements provide volume concentration for 22 size classes in particle size range from 0.05 μm to 15 μm . AERONET data analysis is centralized at the NASA processing facility, providing operational products several hours after measurements are performed. The near real-time quality control algorithm for sun photometer AOD measurements is described by Giles et al. (2019). The algorithm for retrieval of inversion products is described in Dubovik and King (2000) and Dubovik et al. (2006).

Multiwavelength lidar systems, with Raman and depolarization capabilities, can be used to differentiate the layers in terms of dominant aerosol type (e.g., smoke, dust, marine, volcanic, continental) (Nicolae et al, 2018). In synergy with columnar photometer measurements, lidars are used to retrieve dust concentration profiles (Lopatin et al., 2013; Mamouri and Ansmann, 2015, 2016; Chaikovsky et al., 2016), as explained in more detail later in this chapter. In this Thesis, vertical profiles of dust concentration, retrieved from ground-based measurements using lidar and sun photometer, which are parts of EARLINET and PollyNET lidar networks and AERONET photometer network, respectively, are used in model evaluation. Additional insight into the dust plumes and associated cloud formation is provided by other remote sensing systems (i.e., CALIOP, Cloudsat, MSG-SEVIRI, Cloudnet), described later in this chapter.

3.1 Aerosol Lidar Remote Sensing and Dust Mass Concentrations Retrievals

Evaluation of dust model outputs can be performed by calculation of vertical profiles of dust extinction coefficient and their comparison with lidar measurements (Perez et al., 2006 a, b; Mona et al., 2014). Another approach relies on retrieval algorithms to calculate dust concentration profiles based on lidar and sun photometer measurements, which are then used for the evaluation of modeled dust concentrations. The latter approach is used in this Thesis, since it focuses on ice nucleating particle concentrations (INPC) and cloud-relevant dust concentrations are necessary input parameters for parameterization schemes (along with thermodynamic quantities).

In this Thesis, the results of the evaluation of the model by comparison with dust concentration retrievals by two retrieval algorithms are shown: LIRIC (Chaikovsky et al., 2016) and POLIPHON (Mamouri and Ansmann 2015; 2016). LIRIC and POLIPHON belong to two different categories of algorithms. LIRIC is used to find the optimal aerosol profile which fits both the vertically resolved lidar measurements and the columnar sun photometer measurements. This approach requires the measurements to be collocated and simultaneous, thus limiting the number of available measurements. Moreover, since sun photometer measurements require daylight and a clear sky, it makes the use of LIRIC impossible in case of nighttime lidar measurements or in presence of clouds. As opposed to LIRIC, the POLIPHON algorithm does not require the lidar and sunphotometer measurements to be collocated and simultaneous. A comparison of LIRIC and POLIPHON algorithms regarding the retrieved aerosol concentrations was performed in earlier studies. A good agreement between LIRIC and POLIPHON non-spherical particle mass concentration was reported for a Saharan dust case at Leipzig in 2008 (Wagner et al., 2013). Papayannis et al. (2014) analyzed vertical profiles of the aerosol optical, size, and mass properties retrieved from lidar and sunphotometer measurements in EARLINET/AERONET stations in Greece and Romania during a two-day experiment in September 2012. They found that aerosol mass concentrations obtained using LIRIC and POLIPHON retrievals over Bucharest differed by less than 20% for layers with significant non-spherical aerosol loads, indicative of dust. The two algorithms are described in more detail in further text.

3.1.1 LIRIC Algorithm

LIRIC algorithm is used to derive vertical profiles of aerosol volume and mass concentrations (Kokkalis et al., 2013; Tsekeri et al., 2013; Wagner et al., 2013; Chaikovsky et al., 2016) separately for fine, coarse spherical, and coarse spheroidal particles. Thus, it allows differentiation of contributions of different aerosol types to the aerosol vertical profile. Irregularly shaped dust particles are represented in LIRIC algorithm as spheroidal particles. The coarse spheroidal particles are of primary interest in this Thesis as they represent the dust. LIRIC is based on coincident lidar and AERONET sunphotometer measurements. It uses the elastically backscattered lidar signals at three wavelengths (355, 532, 1064 nm) as input and makes use of the AERONET inversion products: aerosol columnar size distribution, refractive index, and sphericity parameter (which represents the percentage of spherical particles). It is assumed in LIRIC that the microphysical properties of aerosols above the measurement station do not change with altitude. Moreover, the aerosol complex refractive index and the sphericity parameter are assumed to be the same for fine and coarse-mode aerosols. The lidar signals are cut off at the altitude of full overlap between the laser beam and the receiver field of view of the instruments. Based on the assumption that the particles below the full overlap height are well mixed, it is assumed that the vertical profiles of aerosol concentrations are constant at

these altitudes. Above the altitude of full overlap, the concentration profiles are dependent on height. Using a least squares algorithm, LIRIC optimizes volume concentration profiles to fit the lidar signals, AERONET columnar volume concentration and user-defined smoothness constraints. Since the scattering of polarized laser beam by non-spherical particles can result in depolarization of the incident light, the distinction between the spherical and non-spherical components of the coarse mode particles is based on depolarization measurements at 532 nm (Chaikovsky et al., 2016). Some lidar instruments do not provide depolarization measurements, and therefore they lack the capability to separate between the non-spherical and spherical components, so the coarse mode would be representative of both the marine and dust particles. While important in individual cases, in systematic statistical comparisons, such as the systematic study by Biniotoglou et al., (2015) this limitation does not significantly affect the outcome of the whole study.

3.1.2 POLIPHON Algorithm

POLIPHON algorithm can be applied to lidar profiles from both ground-based and space-borne instruments. Based on the particle depolarization ratio the desert dust particles can be separated from marine and other continental particles. As previously mentioned, desert dust particles can be identified because of the high depolarization of backscattered linearly polarized laser light. On the other hand, typical mixtures of non-desert aerosols cause very low depolarization (Mamouri and Ansmann, 2015; 2016). In this Thesis, cloud-relevant dust concentrations retrieved from ground-based lidar are discussed. In the first part of the POLIPHON algorithm, the lidar observations are analyzed to calculate the vertical profiles of the backscatter coefficient at the wavelength of 532 nm. The height-dependent volume depolarization ratio ($\delta_{v,532}$) can be expressed as:

$$\delta_{v,532} = \frac{\beta_{532}^{\perp}}{\beta_{532}^{\parallel}} = \frac{\beta_{m,532}^{\perp} + \beta_{p,532}^{\perp}}{\beta_{m,532}^{\parallel} + \beta_{p,532}^{\parallel}} \quad (3. 2)$$

where β^{\parallel} and β^{\perp} are the vertical profiles of parallel- and cross-polarized components of the backscatter coefficient, respectively. The indexes p and m denote particle and molecular contributions, respectively. The particle and molecular depolarization ratios can be expressed by similar equations (Tesche et al., 2009). The expression for the particle depolarization ratio is:

$$\delta_{p,532} = \frac{\beta_{p,532}^{\perp}}{\beta_{p,532}^{\parallel}} = \frac{\beta_{n,532}^{\perp} + \beta_{d,532}^{\perp}}{\beta_{n,532}^{\parallel} + \beta_{d,532}^{\parallel}} \quad (3. 3)$$

where the indexes n and d denote non-dust and dust contributions, respectively. The particle depolarization ratio is then used to separate the contributions of dust and non-dust particles to the particle backscatter coefficient. The separation method is based on changes in the polarization of an emitted laser beam as it interacts with a dust layer (Tesche et al., 2009; Groß et al., 2011). After rearrangement and appropriate substitutions, described in detail by Tesche et al. (2009), the following expression is obtained:

$$\delta_{p,532} = \frac{\beta_{n,532}\delta_{n,532}(1 + \delta_{d,532}) + \beta_{d,532}\delta_{d,532}(1 + \delta_{n,532})}{\beta_{n,532}(1 + \delta_{d,532}) + \beta_{d,532}(1 + \delta_{n,532})} \quad (3.4)$$

where $\beta_{p,532}$ the total particle backscatter coefficient, $\beta_{d,532}$ is the dust backscatter coefficient, $\delta_{p,532}$ is total particle depolarization ratio, $\delta_{d,532}$ is dust depolarization ratio, $\delta_{nd,532}$ is non-dust particle depolarization ratio and. After substitution the expression for dust backscatter coefficient is obtained:

$$\beta_{d,532} = \beta_{p,532} \frac{(\delta_{d,532} - \delta_{nd,532})(1 + \delta_{d,532})}{(\delta_{d,532} - \delta_{nd,532})(1 + \delta_{p,532})} \quad (3.5)$$

For the separation criteria, a dust particle depolarization ratio needs to be used. The dust depolarization ratio values measured at several locations have been reported in literature. The average value of 0.31 ± 0.02 at 532 nm was reported for 19 dust cases near the dust sources in Morocco during SAMUM-1 campaign (Freudenthaler et al., 2009). The values obtained for transported but pure Saharan dust from measurements during SAMUM-2 at Cape Verde were 0.30 ± 0.01 (Groß et al., 2011). Depolarization ratio values of other aerosol types at different locations are also reported in literature. The comprehensive study by Baars et al. (2016) gives an overview of the observations on four continents and two research vessels obtained with eight Polly systems and analyzed particle depolarization ratio values (along with other optical properties), of several aerosol types (mineral dust, smoke, dust-smoke and other dusty mixtures, urban haze, and volcanic ash) at multiple locations. Groß et al. (2013) analyzed optical properties of continental pollution aerosol EUCAARI-LONGREX field experiment over Europe in May 2008. Ansmann et al. (2010) measured particle depolarization ratios at several locations in central Europe during eruptions of the Icelandic Eyjafjallajökull volcano in 2010. Haarig et al., 2017 performed profiling the the Saharan dust during the SALTRACE campaign in the Caribbean in 2013 and 2014. In the retrievals performed to provide data used in this Thesis dust depolarization ratio of 0.31 ± 0.04 and a non-dust aerosol depolarization ratio of 0.05 ± 0.03 were assumed, based on data from the literature and long-term measurements at the measurement stations in focus. Then, the dust extinction coefficient was calculated as follows:

$$\sigma_{d,532} = LR_{d,532} \times \beta_{d,532} \quad (3.6)$$

where $\sigma_{d,532}$ is the dust extinction coefficient, $LR_{d,532}$ is the dust lidar ratio and $\beta_{d,532}$ is the dust backscatter coefficient at 532 nm wavelength. The assumed value of lidar ratio was 45 ± 10 sr for Saharan dust at 532 nm. This value was estimated based on analyses of several years of lidar measurements in Europe (Müller et al., 2007), Cape Verde (Tesche et al., 2011), Middle East (Nisantzi et al., 2015) and Africa (Veselovskii et al., 2016).

The obtained dust extinction profiles have been converted to dust particle number, surface area and volume concentrations using AERONET-based parameterizations (Ansmann et al., 2011a; 2012; Mamouri and Ansmann 2015; 2016). The dust volume concentration is calculated as:

$$v_d(z) = c_{v,d,532} \times \sigma_{d,532}(z) \quad (3.5)$$

where v_d is height-dependent dust volume concentration, $c_{v,d,532}$ is dust extinction-to-volume conversion factor at 532 nm wavelength and $\sigma_{d,532}$ is the dust extinction coefficient at the same wavelength. Dust mass concentrations are calculated by multiplication of Equation 3.5 with the dust particle density ρ_d of 2.6 g/cm³ (Ansmann et al., 2012):

$$M_d(z) = \rho_d \times v_d(z) \tag{3.6}$$

In this Thesis, results of POLIPHON algorithm are used to derive vertical profiles of cloud-relevant dust concentrations, necessary as inputs to INPC parameterizations. Thus, the profiles of concentrations of dust particles with radii greater than 250 nm (n_{250}) and dust dry particle surface area concentrations (S_d) are calculated similarly to Equation 3.5, based on appropriate conversion factors given in Ansmann et al (2019).

The conversion factors are based on good correlation found between columnar particle concentration values from appropriate class to AOD at 500 nm, at stations dominantly under the influence of dust aerosol (Ansmann et al., 2019a). From that relationship the dust extinction-to-volume conversion factors are determined. To select AERONET data pertaining to dust, Ansmann et al (2019) used the following criteria: 440-870 nm Ångström exponent value less than 0.3 and AOD value at 532 nm greater than 0.1. POLIPHON retrieval dataset of extinction coefficients for Nicosia on April 2016, used in this Thesis, has been obtained from NOA (Eleni Marinou, personal communication, 2020) and appropriate conversion factors have been applied. POLIPHON retrieval data for Potenza on April 18, 2016, used in this Thesis has been obtained from CIAO (Fabio Madona, personal communication, 2021). Conversion factors used for provision of the POLIPHON data were provided in work by Ansmann et al. (2019). For the Nicosia, Cyprus station, conversion factors obtained using observation data for the closest AERONET station at Limassol, Cyprus were used. The stations are at around 60 km distance. For the Potenza station, conversion factors based on AERONET data from the North African stations at Tamanrasset, Izana, Tenerife, Sal, Cabo Verde; Dakar, Banizoumbou, and Ilorin have been used.

3.2 The CALIOP instrument

CALIOP is a nadir-viewing standard dual-wavelength (532 and 1064 nm) elastic backscatter lidar with a polarization channel at 532 nm, operating aboard the CALIPSO satellite. CALIPSO was launched in 2006 as the first satellite to carry a lidar specifically designed to study aerosols and clouds (Winker et al., 2009). In the period analyzed in this Thesis, CALIPSO and CloudSat were among five satellites in the A-train satellite constellation (Figure 3.3). All the satellites in the A-train are in a 705 km sun-synchronous polar orbit with a 16-day repeat cycle. Polar-orbiting satellites in the A-train provide observations of aerosols and clouds globally. The A-train constellation enables the use of products derived from synergies of instruments aboard several satellites. CALIPSO and CloudSat provide vertically resolved observations of aerosols and clouds. More information on CALIPSO and CloudSat synergetic products related to ice clouds is given later in this chapter.

CALIOP lidar measures vertical profiles of the attenuated backscatter of aerosols and clouds at 532 and 1064 nm with a resolution of 1/3 km in the horizontal direction and 30 m in the vertical direction (Winker et al., 2009). The retrieval algorithm uses altitude, location, surface type, depolarization measurements at 532 nm, and integrated attenuated backscatter to classify aerosols (Omar et al., 2009). Aerosols layers are classified into layer types and sub-types: dust, marine, smoke, polluted dust, polluted continental, and clean continental (Liu et

al., 2009; Omar et al., 2009). The products used in this thesis are the Level 2 products, version 4.20 (Kim et al., 2018). Specifically, the aerosol subtype product was used to provide qualitative observations of types of the aerosol present in the dust plume cross section.

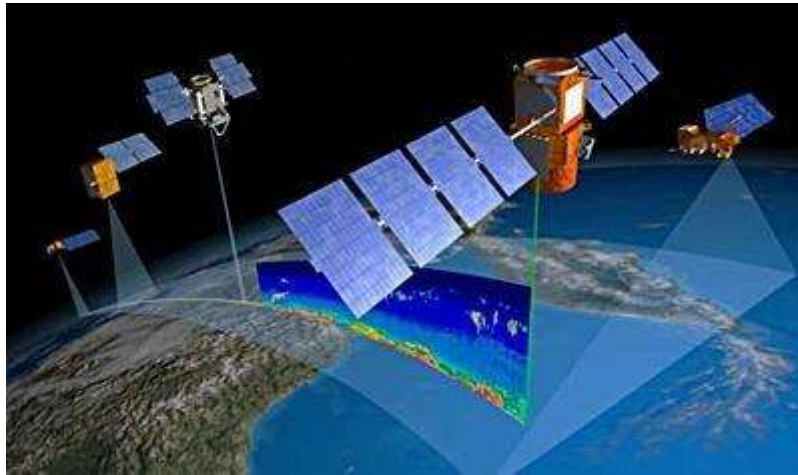


Figure 3.3. An illustration of the A-Train satellite constellation. CALIOP measurements are depicted as a quicklook image of the lidar range corrected signal along the satellite ground track. The image was adapted from <https://www-calipso.larc.nasa.gov/>.

3.3 Cloud Radar Observations

Numerical models typically do not fully resolve clouds as they are a phenomenon of subgrid-scale. Therefore, the cloud processes are parameterized. To contribute to numerical weather prediction and improve our knowledge of cloud processes, the Cloudnet cloud radar observation network (Stephens et al., 2002; <https://cloudnet.fmi.fi>) provides data that is designed for systematic evaluation of weather forecast models and cloud research. Cloudnet algorithm uses observational data retrieved by several instruments: cloud radars, ceilometers, microwave radiometers, and radiosondes (e.g., water vapor path, liquid water path, cloud base height) to calculate the liquid water content (LWC) and ice water content (IWC). The observations are supplemented by the vertical profiles of temperature, wind speed, and humidity from an operational model. These quantities are interpolated to a common grid at the cloud radar resolution and used as input to the Cloudnet algorithm. To retrieve LWC and IWC profiles, a target categorization is performed. Several different target categories can be determined: hydrometeors forming clouds and precipitation (liquid droplets, ice crystals, drizzle, and rain), aerosols, and insects.

In this Thesis, IWC data from CNR-IMAA Atmospheric Observatory (CIAO), a Cloudnet station located in Potenza, Italy (Madonna et al., 2011), are used. The datasets were provided by CIAO (Fabio Madona, personal communication, 2020). CIAO is equipped with near-infrared ceilometers (Vaisala CT25k and Jenoptik CHM15k), a microwave radiometer (Radiometrics MP3014), and a Ka-band pulsed polarimetric Doppler radar (Metek Mira 36). All datasets from instruments are processed using the Cloudnet algorithm (Illingworth et al., 2007), interpolated to the radar time and height resolution at a common grid of 30 s and 30 m in height. IWC is estimated using the approach by Hogan et al. (2006) from measured radar reflectivity and temperature from the ECMWF forecast model, using a power-law relationship between IWC and radar reflectivity at 36 GHz. The formula is only applied when the target is composed of ice, according to the target categorization. The retrieval is not reliable above rain or melting ice when attenuation cannot be estimated accurately.

3.4 DARDAR Satellite Products

DARDAR satellite products provide ice cloud properties derived from Cloud Profiling Radar measurements aboard CloudSat and CALIOP observations aboard CALIPSO (Delanoë and Hogan, 2010). Both CloudSat and CALIPSO satellites were parts of the A-Train satellite constellation during the period from which the data are used in this analysis. DARDAR variational framework uses collocated observations from the instruments aboard the A-train satellite platforms to produce vertical profiles of ice cloud properties. The number concentration of ice crystals (ICNC) in clouds (DARDAR-Nice) is a product intended for use in studies of aerosol-cloud interactions and it is used in this Thesis. DARDAR-Nice product is available at a 60 m vertical and 1.7 km horizontal resolution (Delanoë et al., 2014). This product is only available for ice clouds with an IWC larger than 10^{-8} kg/m³. Delanoë et al. (2005) compared the DARDAR retrievals with the in situ measurements from mid-latitude and tropical regions and concluded that a four-parameter modified gamma distribution allows the parameterization to properly fit the observations. Two of the parameters are fixed to best fit with the in situ measurements from mid-latitude and tropical regions. The remaining two are iteratively adjusted during retrieval to fit the observational constraints (Sourdeval et al., 2018). The choice of one of the fixed parameters puts a limitation on the retrievals. The analytical solution for ICNC can only be found when the minimum particle diameter is set and not equal to zero. To overcome the resulting discontinuity in ICNC when the diameter equals zero, the ice crystal size distribution is integrated from three minimum size thresholds of 5, 25, and 100 μm . The thresholds are chosen to be within the validity range of the in situ measurements used for the algorithm evaluation (Sourdeval et al., 2018). Different physical processes can influence the ICNC uncertainty depending on the integration threshold. If homogeneous nucleation rates are very high, the number of ice crystals can be underestimated. Also, the shattering of ice crystals can significantly increase their number. If aggregation of ice crystals is the dominant process, their number can be overestimated. These processes increase the retrieval uncertainty by an additional 50 % due to deviations from the assumed particle size distribution. Smaller minimum radii, which are considered when a 5 μm threshold is used, can be affected by the instrumental uncertainties of the in situ measurements used in validation (Jensen et al., 2013; Gurganus and Lawson, 2018). The moderate size crystals are represented with the use of the 25 μm threshold. The data from the in situ measurements is considered to be of higher confidence in this size range of the ice crystals. The most accurate in situ measurements are for the largest minimum size threshold used in the DARDAR product. Therefore, for the 100 μm threshold the assumed ice crystal particle size distribution (PSD) is a correct representation of the ICNC (Sourdeval et al., 2018).

DARDAR-Nice has been evaluated against theoretical considerations and a large amount of in situ measurements and its estimates are expected to have uncertainties from 25% up to 50% (Sourdeval et al., 2018). Larger uncertainties are expected in mixed-phase cloud retrievals. Therefore, these retrievals are flagged in the dataset to inform the users to consider them in their analyses. In this Thesis, mixed-phase clouds are of interest, especially because the mineralogy-sensitive immersion freezing parameterization is analyzed. DARDAR-Nice product has been used in the evaluation of INPC applied to cloud-relevant dust concentrations retrieved using POLIPHON and predicted by DREAM (Marinou et al., 2019; Ilić et al., 2022).

3.5 CLAAS-2 dataset

The Satellite Application Facility for Climate Monitoring (CM SAF) provides products related to climate from geostationary satellites. CM SAF cloud products are based on observations from EUMETSAT Meteosat Second Generation satellites (MSG). The Spinning

Enhanced Visible and InfraRed Imager (SEVIRI) sensor aboard the MSG performs measurements in 12 spectral bands: four in the visible and near-infrared (0.4 – 1.6 μm) wavelength range and 8 in the infrared range (3.9 – 13.4 μm). SEVIRI is used to derive the CLAAS-2 (CLOUD property *dAtAset* using SEVIRI, Edition 2) cloud property dataset. The cloud products available from CLAAS-2 are cloud mask/type, cloud top temperature, pressure, and height, cloud phase, as well as cloud microphysical properties such as optical thickness, effective droplet radius and cloud water path. Uniformity of the CLAAS-2 dataset was achieved by inter-calibration of the SEVIRI solar channels of MSG-1, MSG-2, and MSG-3 (Meirink et al., 2013) with MODIS Aqua before performing the cloud retrievals. The results of the comprehensive evaluation of CLAAS-2, with the data and documentation are provided in Benas et al. (2016). The SEVIRI products are available with a 15-minute repeat cycle and around 4 km spatial resolution in the domain covered by DREAM (Stengel et al., 2014). The comprehensive dataset can be used in regional and large-scale cloud process studies with a wide range of temporal scales, from minutes to years. Ničković et al. (2016) used the ice water path (IWP) from the CLAAS-2 dataset to evaluate the model prediction of the horizontal distribution of cold clouds. Although the dust particles are efficient ice nuclei, their results show that the patterns of horizontal distribution of dust do not necessarily coincide with the patterns of clouds indicated by IWP. Therefore, they used INPC parameterizations within the model to consider the thermodynamic conditions needed for cloud development. They concluded that the qualitative comparison of horizontal distribution of predicted INPC and observed IWP showed considerable similarity to the pattern shapes and locations. In this Thesis, a qualitative comparison was performed between the IWP product and integrated columnar values of INPC predictions from DREAM as a proxy for cloud ice.

3.6 In Situ Measurements

Unmanned Aerial Vehicles (UAVs) can be used to collect samples up to a few kilometers height due to legal and technical limitations in operating these measurement platforms. In this Thesis, INPC data were used from the INUIT-BACCHUS-ACTRIS campaign. The samples were collected using onboard miniaturized electrostatic precipitators (Schrod et al., 2017; Marinou et al., 2019). Immediately after collection they were analyzed in the FRankfurt Ice nucleation Deposition freezinG Experiment (FRIDGE) (Bundke et al., 2008) chamber to estimate sample efficiency as an INP source. In the FRIDGE, the samples were exposed to water saturation of 101% and temperatures within the immersion freezing temperature regime. UAV-FRIDGE data and uncertainties presented here are adopted from Marinou et al. (2019). Marinou et al. (2019) consider the errors of the INP measurements to be around 20%, and the same estimation is used when presenting the measurements for the purpose of this Thesis. Their estimate takes into consideration the statistical reproducibility of an individual sample.

4 Simulation of Dust Episodes in Europe and the Mediterranean

The interest in aerosol prediction and application of aerosol forecasts is growing in areas of climate research and operational numerical weather forecasts. Several regional dust models participate in operational efforts of the Sand and Dust Storm Warning Advisory and Assessment System (SDS-WAS) program established by the World Meteorological Organization (WMO) in September 2004. The main purpose of the program is to coordinate forecast and observational efforts and improve the capabilities of dust models. This is achieved through a coordinated global network of SDS-WAS centers. A partnership of two research Spanish institutions, the Barcelona Supercomputing Center-Centro Nacional de Supercomputación (BSC-CNS; www.bsc.es) and the Spanish National Agency of Meteorology (AEMET, www.aemet.es), host Northern Africa-Middle East-Europe Node (NA-ME-E; <http://sds-was.aemet.es/>) and its partners include several international organizations and institutions. This regional node covers the area of Saharan dust sources, the Mediterranean, and Europe, which are also of interest in this study. The DREAM model runs operationally in the framework of the South East European Virtual Climate Change Centre (SEEVCCC) of the Republic Hydrometeorological Service of Serbia (RHMSS). Operational products are submitted to SDS-WAS every day in a gridded form containing 72 h forecasts of the surface dust concentration and aerosol optical depth (AOD) at 550 nm, with a time resolution of 3 h. This operational evaluation, although very valuable, does not provide information on model performance regarding the dust vertical profiles. A detailed evaluation of the representation of dust vertical profiles is needed to better understand its role in the atmospheric processes of different scales and interactions with the environment (e.g., long-range transport, aerosol-radiation interactions, aerosol-cloud interactions, effects on aviation, etc.). Such evaluations have been performed for individual cases (Papayannis et al., 2014) or systematically for dust extinction coefficients (Mona et al., 2014). However, to complement SDS-WAS routine model evaluation and improve numerical dust forecasts, Biniotoglou et al. (2015) carried out a systematic analysis of model predictions of dust mass concentration vertical profiles. The DREAM model was part of this model validation effort. In this Chapter, the approach to systematic model evaluation used by Biniotoglou et al (2015) is described, and the performance of the DREAM model in predicting dust vertical structure is presented. As the next step, a similar approach is used in case studies of DREAM prediction of dust plumes in the Mediterranean, selected for evaluation of dust effects on INPC.

4.1 A Systematic Study of Dust Model Performance

Validation of DREAM model dust vertical profiles as part of a systematic atmospheric dust model performance study at the European scale (Biniotoglou et al., 2015), based on synergistic lidar and sunphotometer retrieval algorithm, LIRIC. The study of such a scale was possible through collaboration within the EARLINET network. The DREAM-NMME-MACC model used in the study differs from the one presented in this Thesis only in its use of the dust assimilation scheme described in Chapter 2 and will be referred to as DREAM hereon. In addition to this model, the study evaluated the other three dust models (BSC-DREAM8b v2, NMMB/BSC-DUST, DREAM-ABOL). The model evaluation methodology relied on retrievals of dust concentration profiles from simultaneous collocated lidar and sunphotometer measurements. Ten measurement stations equipped with multi-wavelength lidar and sunphotometer, which are part of EARLINET and AERONET networks were involved in the study (Athens, Barcelona, Belsk, Bucharest, Évora, Granada, Lecce, Leipzig, Potenza, and Thessaloniki). Their locations are shown in Figure 4.1. A total of 55 dust profiles were provided for the measurement period from January 2011 to February 2013. The case selection and

measurement data analysis were performed independently for each station. However, the uniform quality of data analysis and dust concentration retrievals is achieved by the established practices of EARLINET and AERONET networks. The number of cases was limited by the LIRIC requirements of simultaneous lidar and AERONET observations, commitments of available personnel, the episodic character of dust transport in Europe, and specific requirements of the proposed methodology. The time difference between lidar and photometer measurements was kept as small as possible (in 65 % of cases it was less than 1 h and in 87 % of cases less than 3 h). The requirement of the minimal time difference between the profiles of 24 h was set to remove the profiles too close in time representing the same case. In this way, the situation in which one dust episode is represented with many cases and the second episode with too few cases was avoided. Only cases in which dust was observed were analyzed. Cases in which the dust was predicted, but not observed were not a part of the dataset used for model evaluation.

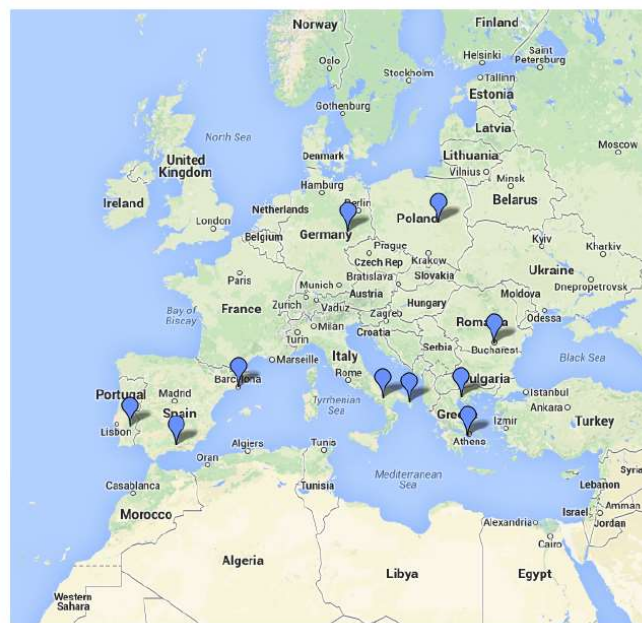


Figure 4.1. Map of the ACTRIS/EARLINET remote sensing stations providing data for testing the proposed methodology. Adapted from Biniotoglou et al. (2015).

4.2 Systematic Study Evaluation Metrics

The set of parameters was used to evaluate average vertical dust profiles while being compatible with the SDS-WAS evaluation of AOD columnar property. A set of statistical indicators was used for each measurement case to evaluate the overall performance of the model.

Center of mass (CoM) was calculated for both observed (O) and modeled (M) profiles:

$$CoM = \frac{\int_{z_{min}}^{z_{max}} z \times c \times dz}{\int_{z_{min}}^{z_{max}} c \times dz}$$

where c is height dependent dust mass concentrations and z is the vertical coordinate.

(Eq. 4. 1)

Correlation coefficient between the observed and modeled data is calculated as

$$r = \frac{\sum_{i=1}^N (M_i - \underline{M})(O_i - \underline{O})}{\left[\sum_{i=1}^N (M_i - \underline{M})^2 \sum_{i=1}^N (O_i - \underline{O})^2 \right]^{\frac{1}{2}}}$$

(Eq. 4. 2)

with range [-1,1] and 1 is the perfect score.

Fractional bias, as a normalized measure of the mean bias, indicates the models' systematic underestimations and overestimations of the observed values:

$$F_B = \frac{2}{N} \sum_{i=1}^N \left(\frac{M_i - O_i}{M_i + O_i} \right)$$

(Eq. 4. 3)

Fractional bias takes values between -2 and 2, with a perfect score being 0.

4.3 Evaluation Results

The aim of this analysis was to understand how the model represents the vertical profile of dust concentration. The analysis was performed in three ways: for a total of 55 cases and two regional clusters of stations (Figure 4.2) and in a case-by-case comparison. The single parameters examined are center of mass, total concentration in a vertical column, peak concentration, and dust-layer thickness. The correlation coefficient and fractional bias for these metrics are given in Table 4.1. In case-by-case comparisons, the vertical correlation coefficient and the fractional bias of the volume concentration profiles represent the model's ability to predict the shape of the profile, and the total amount of dust, respectively.

It should be noted that LIRIC retrievals are representative of a vertical column directly above the station, while the model predictions are representative of a grid point. Besides, DREAM vertical resolution is variable due to the hybrid sigma-pressure vertical coordinate (Janjic, 2001). The model has 28 vertical levels, having a vertical resolution of several hundreds of meters in the immersion temperature range. This resolution is lower than the vertical resolution of LIRIC retrievals. Therefore, the sometimes very complex vertical structure of aerosol layers and their finer features might not be resolved by the model.

The results of the analysis of DREAM performance are presented using the described datasets and the set of metrics. The results show that DREAM places the transported dust in agreement with observations, according to the dust layer CoM evaluation with a correlation coefficient of 0.83 (Table 4.1). Only in 6 out of 55 cases (11 %) is the difference in CoM altitude between model and observations larger than 1 km. In these cases, the model usually overestimates the CoM altitude, as shown in the fractional bias value of 0.14. The overestimation is more frequent in cases where CoM is observed above 3 km. The model overestimates dust concentration at altitudes above 5 km, therefore positioning CoM above the observed ones. Additionally, this affects the thickness of the dust layer since DREAM does not reproduce the altitude of the top-layer boundary. Dust layer thickness is determined using a dust concentration threshold value of 5 $\mu\text{g}/\text{m}^3$ to locate the top and bottom of the dust layer. According to this criterion, DREAM places the top of the dust layer at a higher altitude than was observed. Dust concentrations of 10 $\mu\text{g}/\text{m}^3$ are observed at altitudes just above 6 km, while they are predicted even above 8 km. Increased concentration at high altitudes in the prediction could be related to limitations of model representation of thermal inversion related to the

tropopause (Janjic, 1994; Mona et al., 2014). Removal of dust that reaches very high altitudes is slower than at lower altitudes since the main mechanism for that process is sedimentation. This could result in increased dust concentrations at high altitudes. DREAM systematically underestimates the total concentration values with a fractional bias of -0.22. Furthermore, peak values are underestimated with the fractional bias of -0.27, and this can be related to the prediction of the intensity of the episode and systematic underestimation of total concentration. Possible causes for the underestimation are insufficient dust source strength, overestimated deposition, and wet scavenging parameters, or a combination of these effects (Biniotoglou et al., 2015). It was not feasible to discriminate between these factors based on model outputs and measurement data used. The model's horizontal and vertical resolutions and setup can partly contribute to these discrepancies.

Table 4.1 Correlation coefficient (r) and fractional bias (FB) for single value metrics of the DREAM profiles. Adopted from Biniotoglou et al., 2015.

Center of Mass		Total Concentration		Peak Value		Layer Thickness	
r	FB	r	FB	r	FB	r	FB
0.83	0.14	0.74	-0.22	0.78	-0.27	0.56	0.0

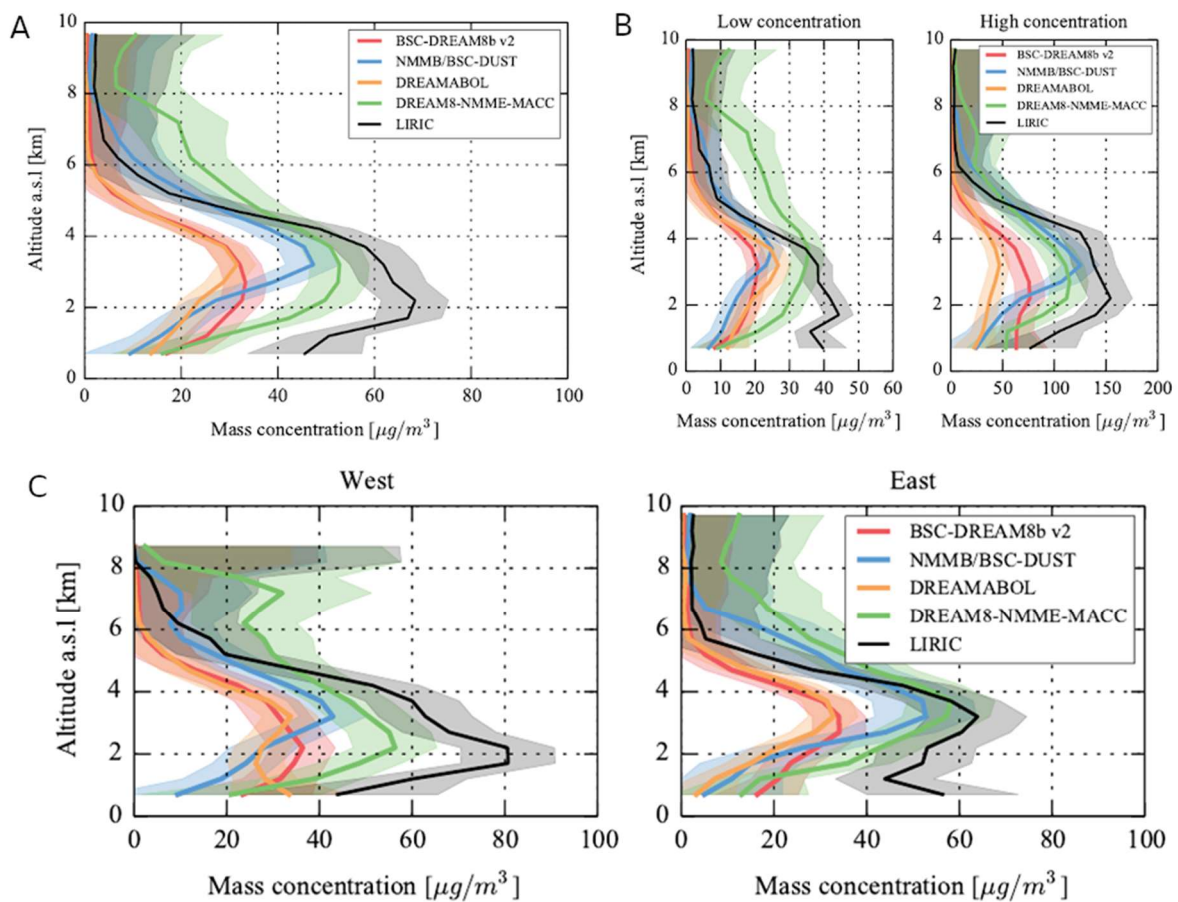


Figure 4.2. Average profile comparison as simulated by four models and retrieved by LIRIC (A), for low and high concentration cases (B) and for the west and east clusters (C). Shaded

areas indicate the standard deviation of the mean values. DREAM8-NMME model was used in this Thesis. Adopted from Binietoglou et al. (2015).

The mean modeled concentration profile for all 55 cases is compared with the corresponding measurement profiles (Figure 4.2 A). Visual inspection of the profiles indicates that DREAM correctly captures the shape of dust profiles with the most significant differences in peak concentrations and overestimation at higher altitudes. LIRIC's maximum concentration of $65 \mu\text{g}/\text{m}^3$ at the altitude of around 2 km was underestimated by DREAM, which predicted the maximum dust concentration region at 3-4 km altitude with a peak value of $50 \mu\text{g}/\text{m}^3$. The difference in layer placement is more pronounced in the low concentration cases (Figure 4.2 B). Conversely, in the high concentration cases, DREAM shows a particularly good agreement with LIRIC. In case-by-case analysis, DREAM fractional bias for total concentration is distributed near zero, which confirms previous analysis that DREAM can predict dust concentration. The correlation shows greater variability, highlighting the potential difficulty for the model in representing the shape of the profile or the position and thickness of the main dust layer.

Additional consideration regarding the regional analysis provides results based on the separation of stations into two clusters (Figure 4.2 C). Évora, Granada, and Barcelona constitute the western cluster of stations, while Potenza, Lecce, Athens, Thessaloniki, and Bucharest constitute the eastern cluster of stations. Separation of the dataset in clusters reduced the number of available cases for each cluster. Nevertheless, the regional evaluation of dust models is beneficial for further analysis. Specifically, the results of the model comparisons with lidar-derived dust concentrations in the east cluster of stations are of particular interest here, as the Thesis focuses on the case studies of the model comparisons with lidar-derived cloud-relevant dust concentrations and INPC estimations in Potenza and Nicosia stations. It should be noted that Nicosia was not part of the systematic study of model performance; however, it is geographically closer to the east cluster. The main difference in western and eastern stations is seen in the observed position of the maximum value of dust concentration. For the west cluster, the maximum value is at the altitude of around 2 km and for the east cluster, it is at 3 km. DREAM predicts the observed peak position in the west cluster, with an overestimation of peak altitude in the east cluster, as was shown in the overall analysis of 55 cases discussed earlier. The correlation coefficient shows a similar performance of DREAM in both clusters, with the best correlation at altitudes between 2 km and 3 km in the west (0.80 – 0.85) and between 4 km and 5 km in the east (0.75 – 0.85) cluster. The number of available profiles with dust at altitudes above 6 km is less than 15, limiting the number of data points for statistical analysis. As discussed in Binietoglou et al. (2015), the differences between the DREAM model performances for the two clusters can be attributed to different dust transport paths and transport duration to the stations. The Atlas Mountains with associated difficulties with wet convection (Reinfried et al., 2009; Solomos et al., 2011) and the complex terrain of the Iberian Peninsula on the path to the west cluster can form a challenge in successful prediction. The transport to the east cluster typically avoids those mountainous regions and dust event homogenizes during additional 1-2 days of transport over the Mediterranean.

As it was stated in the outset of this chapter, it is difficult to distinguish between different atmospheric processes that could lead to differences between the observed and predicted values using this kind of dataset. Although the models generally underestimate the concentrations, DREAM has the best performance. It has the highest correlation coefficient in CoM predictions. On the other hand, the BSC-DREAM8b v2 and DREAMABOL models show almost zero bias in placing CoM. All the models have a negative fractional bias by systematically underestimating the total amount of dust and peak concentrations (Figure 4.2 A). Overall, DREAM predictions show the lowest absolute value of fractional bias for total

concentrations. The same considerations apply to the peak value, with DREAM showing the smallest bias and the strongest correlation. The average result of the DREAM model shows no bias when layer thickness predictions are evaluated. In regional analysis, the cluster differences in altitude of transported dust are captured by all models. The correlation coefficient reveals a better representation of profile shape in the east cluster. These differences were previously attributed to the possible effects of orography and transport paths (Biniotoglou et al., 2015). It should be highlighted that the assimilation scheme used only by DREAM could be contributing to better performance in comparison to other models. DREAM tends to overestimate the amount of dust at higher altitudes, but this issue is less pronounced in high concentration cases. This should be considered when analyzing the INPC estimations. The variation of the model performance in case-by-case analysis indicates the need for more statistical comparisons. Participation from a larger number of stations and longer-term studies in the future can provide additional insight, especially in terms of regional and seasonal variability in model performance.

4.4 Simulations of Dust Episodes in Eastern Mediterranean

To evaluate DREAM model dust mass concentration in this Thesis predictions and cloud-relevant dust concentrations, a month-long simulation of dust transport over the Mediterranean was carried out, covering the period of the INUIT-BACCHUS-ACTRIS campaign. The campaign was organized in April 2016 within the framework of the projects Ice Nuclei Research Unit (INUIT; <https://www.ice-nuclei.de/the-inuit-project>); Impact of Biogenic versus Anthropogenic emissions on Clouds and Climate: towards a Holistic UnderStanding (BACCHUS; <http://www.bacchus-env.eu>); and Aerosols, Clouds, and Trace gases Research Infrastructure (ACTRIS; <https://www.actris.eu>). The focus of the campaign was a study of aerosols, clouds, and ice nucleation within dust-laden air over the Eastern Mediterranean (Schrod et al., 2017; Mamali et al., 2018; Marinou et al., 2019). In operational dust forecasts and numerical experiments, this model can be run with an assimilation scheme using (European Centre for Medium-Range Weather Forecasts) ECMWF dust analysis in the initial dust field (Pejanovic et al., 2012; Biniotoglou et al., 2015). In simulations presented here, the DREAM model was set up to run with a ‘cold start’ for several days prior to the campaign (‘warm up’) to reach a reasonable dust concentration field in the atmosphere (Nickovic et al., 2016).

The model simulations were evaluated using observations from two EARLINET lidar stations: Potenza, Italy, and Nicosia, Cyprus. Potenza station is a permanent EARLINET station operating MUSA (Multiwavelength System for Aerosol), a mobile multi-wavelength Raman lidar system. It is located in the CNR-IMAA Atmospheric Observatory (CIAO) in Tito Scalo, 6 km far from Potenza, Southern Italy, on the Apennine Mountains (40.60N, 15.72E, 760 m a.s.l.) (Madonna et al., 2011). The site is on a plain surrounded by low mountains (<1100 m a.s.l.). Lidar in Nicosia is a PollyXT-NOA lidar system (Engelmann et al., 2016; Baars et al., 2016). It is a multiwavelength Raman lidar system operated by the National Observatory of Athens (NOA). During the INUIT-BACCHUS-ACTRIS campaign, it was located in The Cyprus Institute in Nicosia (35.14 N, 33.18 E; 181 m a.s.l.).

At the beginning of April, a dust plume formed in North-West Africa reached Cyprus on April 4. After this event, several dust episodes occurred in Cyprus during the month (Schrod et al., 2017; Marinou et al., 2019). The intensity of these dust episodes can be classified based on continuous dust concentrations as simulated by DREAM during a 12h period, following Schrod et al. (2017). Events are classified as major when model dust concentrations above the station exceed $200 \mu\text{g}/\text{m}^3$, intermediate for concentrations between 100 to $200 \mu\text{g}/\text{m}^3$ and

minor for concentrations between 50 and 100 $\mu\text{g}/\text{m}^3$. Biniotoglou et al. (2015) classify individual dust profiles as low concentration ones if total concentrations are lower than 0.3 g/m^2 , and high concentrations for total concentrations greater than 0.3 g/m^2 . In this Thesis, the two analyzed dust events in Nicosia are a major one from April 8 to 11 and an intermediate one from April 14 to 16. Additionally, a dust plume was analyzed during transport using ground-based measurements at Potenza, Italy on April 18 and at Nicosia, Cyprus on April 21. This event was classified as intermediate.

4.4.1 Major dust event, April 8 to 11

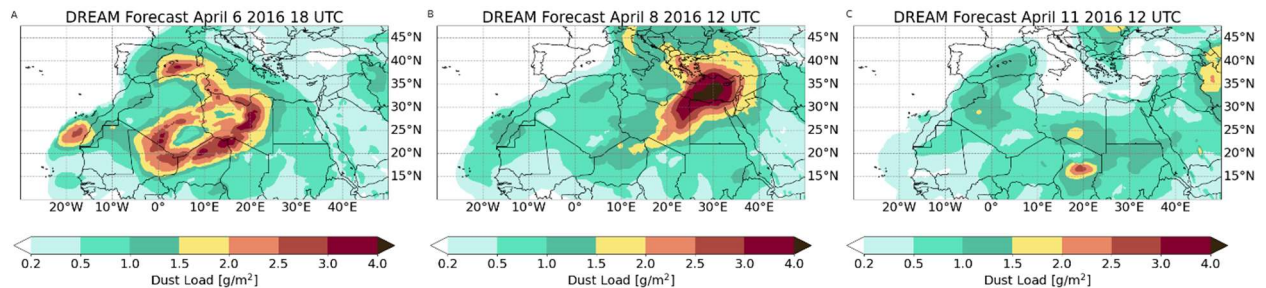


Figure 4.3 DREAM simulated dust load (shaded contours) for April 6 at 18UTC (A), April 8 at 12 UTC (B), and April 11 at 12UTC(C).

Some amount of dust was present above the Nicosia station most of the time during April 2016. DREAM simulations show that a large amount of dust, with a dust load above 3 g/m^2 , was introduced into the atmosphere from central Sahara on 6 April (Figure 4.3). The dust plume carried by the southwesterly flow reached Nicosia on April 8. On April 9, dust layers were detected in the PBL and at heights between 2 km and 4 km. The attenuated backscatter intensity and volume depolarization ratio were higher in the PBL than in the lofted layer (Figure 4.4 A and B). A high volume depolarization ratio indicates the presence of non-spherical particles (i.e., dust) or ice crystals. Clouds containing ice crystals were forming atop the dust layer from 19 UTC and 20 UTC between 5 km and 7.5 km. A weaker signal can be seen around 21 UTC at 6 km height. After 22 UTC, clouds were present at the top of the dust layer until 00 UTC on the next day. The cloud top height descended from 7 km to 6.5 km. The dust layer itself gradually descended on April 9, as well. From April 9 to 11, dust concentrations decreased until the next dust event starting on April 14.

The evolution of the dust plume above Nicosia can be clearly seen in Figure 4.4 (C). A significant increase in dust concentrations, above 50 $\mu\text{g}/\text{m}^3$, was predicted on April 8. In the afternoon of April 8 and during April 9, concentrations above 300 $\mu\text{g}/\text{m}^3$ were predicted at altitudes between 2 km and 6 km. DREAM successfully predicted the observed descent and intrusion of the dust layer in the PBL on April 9. DREAM overestimated the vertical extent of the layer significantly, with dust concentrations reaching altitudes above 9 km. It is possible that the clouds obscured the lidar measurements, and therefore the full extent of the dust layer cannot be seen in the attenuated backscatter quicklook. Moreover, as pointed out in section 4.3, a systematic analysis of model performance showed that DREAM overestimates dust concentrations at altitudes above 5 km and can predict the top layer boundary at higher altitudes than shown by observations.

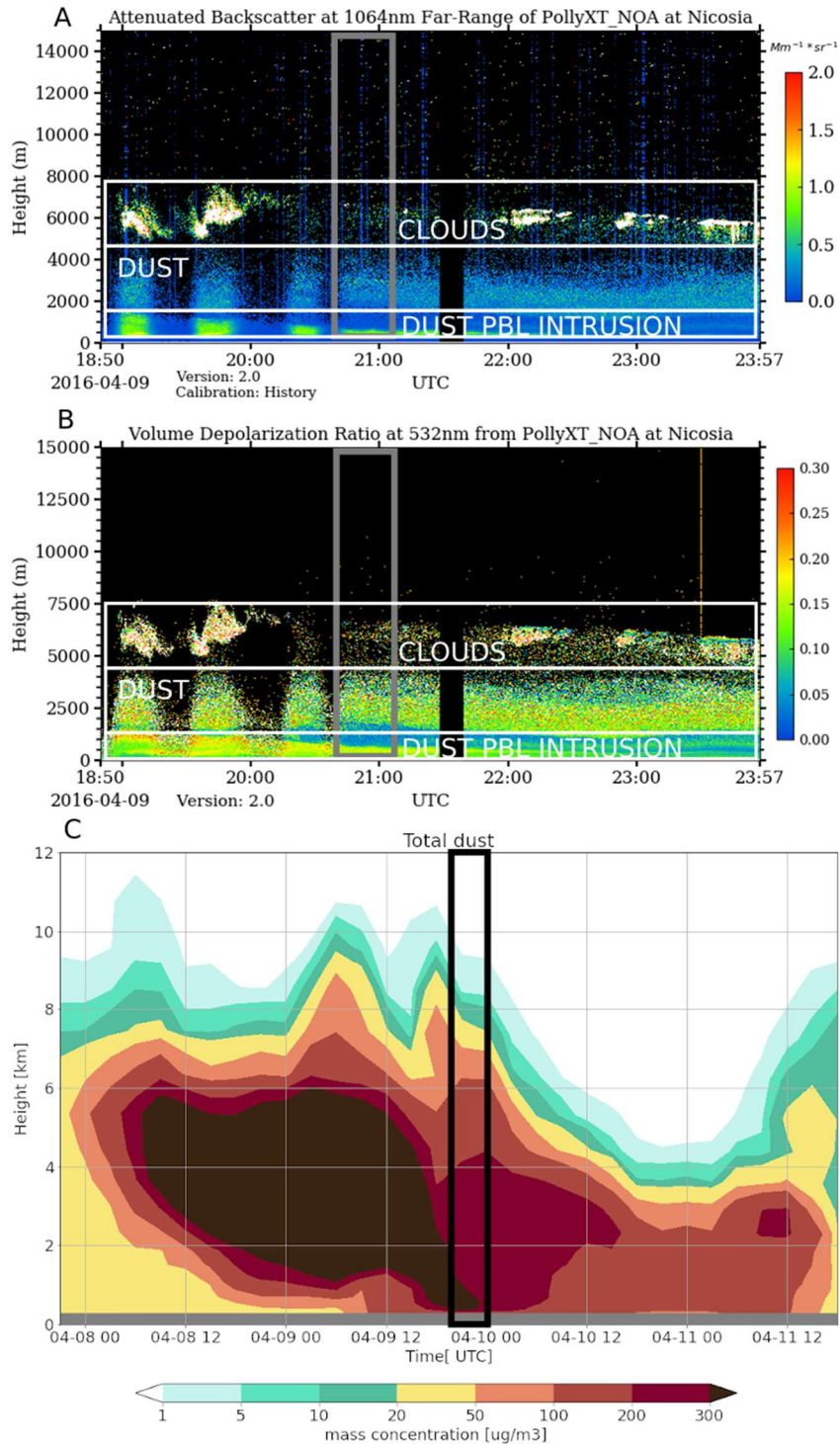


Figure 4.4 Quicklook of the lidar attenuated backscatter at 1064 nm for Nicosia lidar (A). The Grey rectangle indicates data used with the POLIPHON algorithm. White rectangles indicate cloud and aerosol layers. Volume depolarization ratio at 532 nm for Nicosia lidar (B). DREAM-simulated dust concentration at Potenza from April 8 to 11 (C). A black rectangle indicates the period of lidar measurements shown in the quick look.

4.4.2 Intermediate Dust Event, April 14 to 16

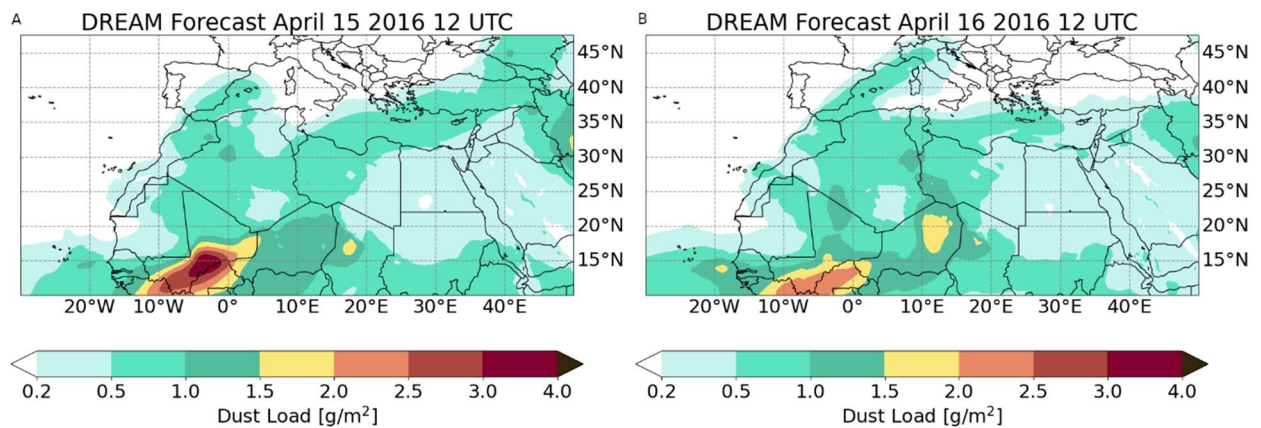


Figure 4.5 DREAM simulated dust load (shaded contours) for April 15 at 12UTC (A) and April 16 at 12 UTC (B).

A dust plume, formed in western and central North Africa and spread over the Mediterranean on April 11, reached Nicosia on April 14 carried by westerly flow (Figure 4.5). It was an intermediate dust event that lasted between April 15 and 16. The intensity of the attenuated backscatter and volume depolarization ratio increased during the evening of April 14 after 22 UTC (Figure 4.6 A and C). On April 15, an elevated dust layer can be seen between 2.4 km and 5 km (Figure 4.6 B and D). By the morning of April 15, the altitude and vertical extent of the layer decreased, but the signal intensified. The cirrus clouds were observed on April 14 from 18:30 to 20:00 UTC and from 21:00 to 23:00 UTC. On April 15, cirrus clouds were present above 10 km at 00- 03 UTC, and 04 UTC - 04:30 UTC. The intensity of the signal in the aerosol layer continued to steadily increase throughout the measurement. After this dust layer passed over Cyprus, concentrations decreased by April 17.

DREAM predicts the increase of dust concentration to above $50 \mu\text{g}/\text{m}^3$ at altitudes of 4 - 6 km on April 14. The evolution of the layer is correctly represented by the model. A decrease in both the altitude and the vertical extent of the layer can be seen in Figure 4.6 (E). Dust intruded into the PBL in the afternoon of April 15 and kept on descending until April 17. Dust concentrations reached values between $100 \mu\text{g}/\text{m}^3$ and $200 \mu\text{g}/\text{m}^3$ on April 15 and 16.

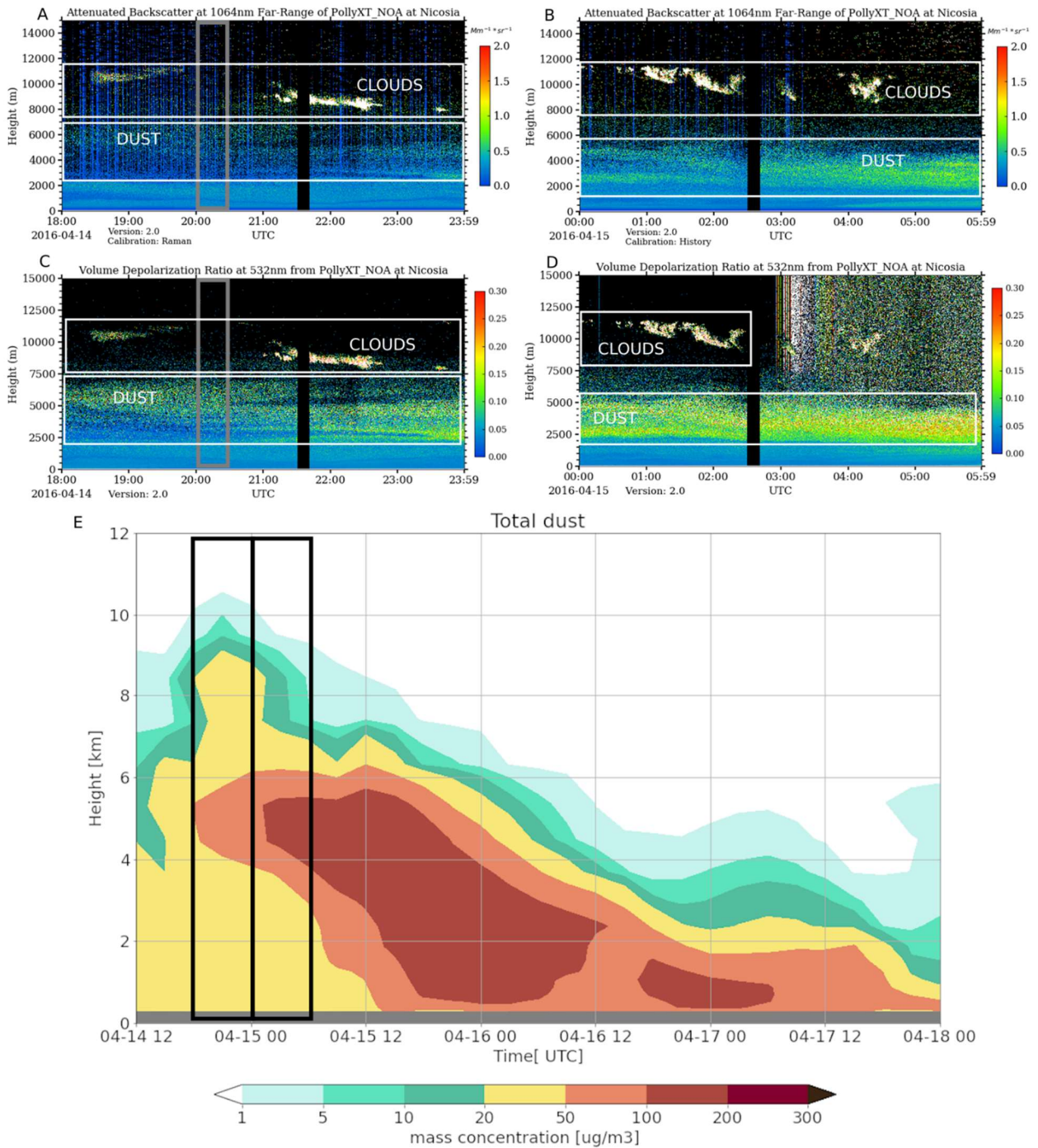


Figure 4.6 Quicklook of the lidar attenuated backscatter at 1064 nm for Nicosia lidar (A) and (B). The Grey rectangle indicates data used with the POLIPHON algorithm. Volume depolarization ratio at 532 nm for Nicosia lidar (C) and (D). White rectangles indicate cloud and aerosol layers. DREAM-simulated dust concentration at Potenza from April 15 to April 18 (E). A black rectangle indicates the period of lidar measurements shown in the quick look.

4.4.3 Dust Plume in the Mediterranean, April 18 to 21

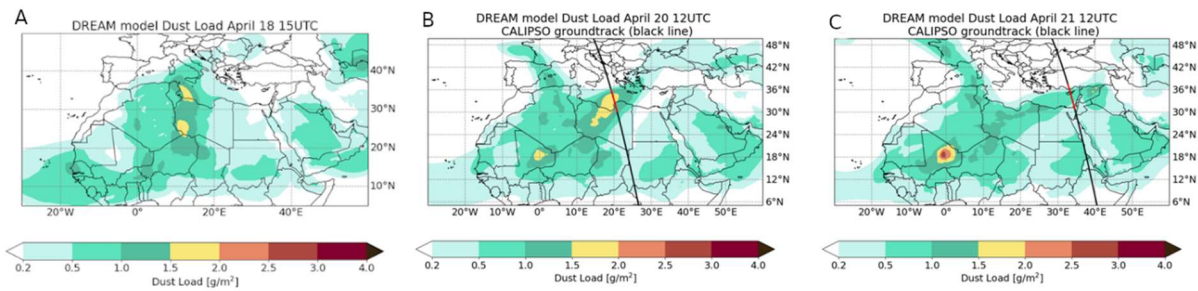


Figure 4.7 DREAM-simulated dust load (shaded contours) and A-Train constellation track (black and red line) for April 20 at 12 UTC during overpass A (A) and April 21 at 12 UTC during overpass B (B). The red part of the satellite track indicates the cross-section used in the comparisons with DARDAR products. Adapted from Ilic et al. (2021).

The DREAM model simulation results are compared with ground-based measurements in Potenza on 18 April and in Nicosia on April 21, 2016, during a Saharan dust episode in the Mediterranean (Figure 4.7). Saharan dust was observed above both lidar sites during this period and during the two A-Train constellation overpasses. Dust was introduced to the atmosphere from sources in Algeria on April 15. The dust plume reached Potenza a day later as a minor dust event. Dust was transported northward on April 17, reducing the concentrations. On the same day, the dust plume started forming from the sources in central North Sahara. The new plume reached Potenza on April 18 and mixed with the small concentrations of dust already present above the station. The increase in concentrations caused an intermediate dust event in Potenza on April 18 and 19. During the corresponding intermediate dust event, dust was present in Nicosia when the plume reached Cyprus on April 21.

Figure 4.8 (A) shows lidar range-corrected signal (RCS) in Potenza on April 18, from 12 UTC to 15:30 UTC. Strong RCS between 4 and 6 km height indicates the presence of a dust layer. During the first 1.5 hours of measurements, clouds were present within and above the dust layer. After the period of cloud formation, the layer somewhat descended and the intensity of the signal increased in the last 1.5 hours of measurements. Cirrus clouds were observed during the whole measurement period between 7.5 and 12 km height. DREAM predicted the dust plumes above Potenza starting on April 16 until April 19 (Figure 4.8 B). Maximum dust concentrations at 5 km altitude on April 18 around 12 UTC and later descent of the dust layer were predicted in agreement with the lidar observations.

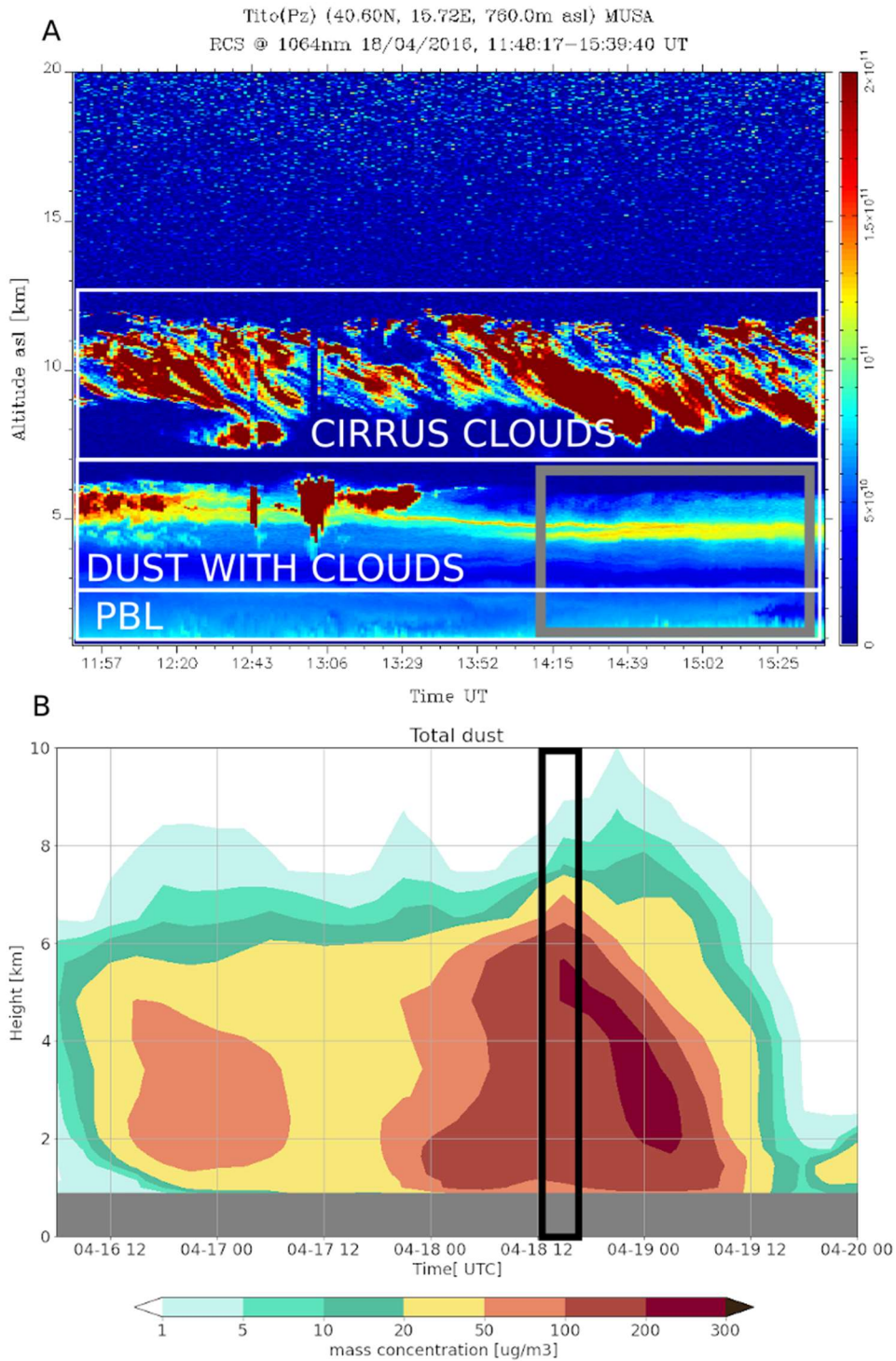


Figure 4.8 Quicklook of the lidar range-corrected signal at 1064 nm for Potenza lidar (A). The Grey rectangle indicates data used with the POLIPHON algorithm. White rectangles indicate cloud and aerosol layers. DREAM-simulated dust concentration at Potenza from April 16 to April 20 (B). A black rectangle indicates the period of lidar measurements shown in the quick look. Adapted from Ilic et al. (2021).

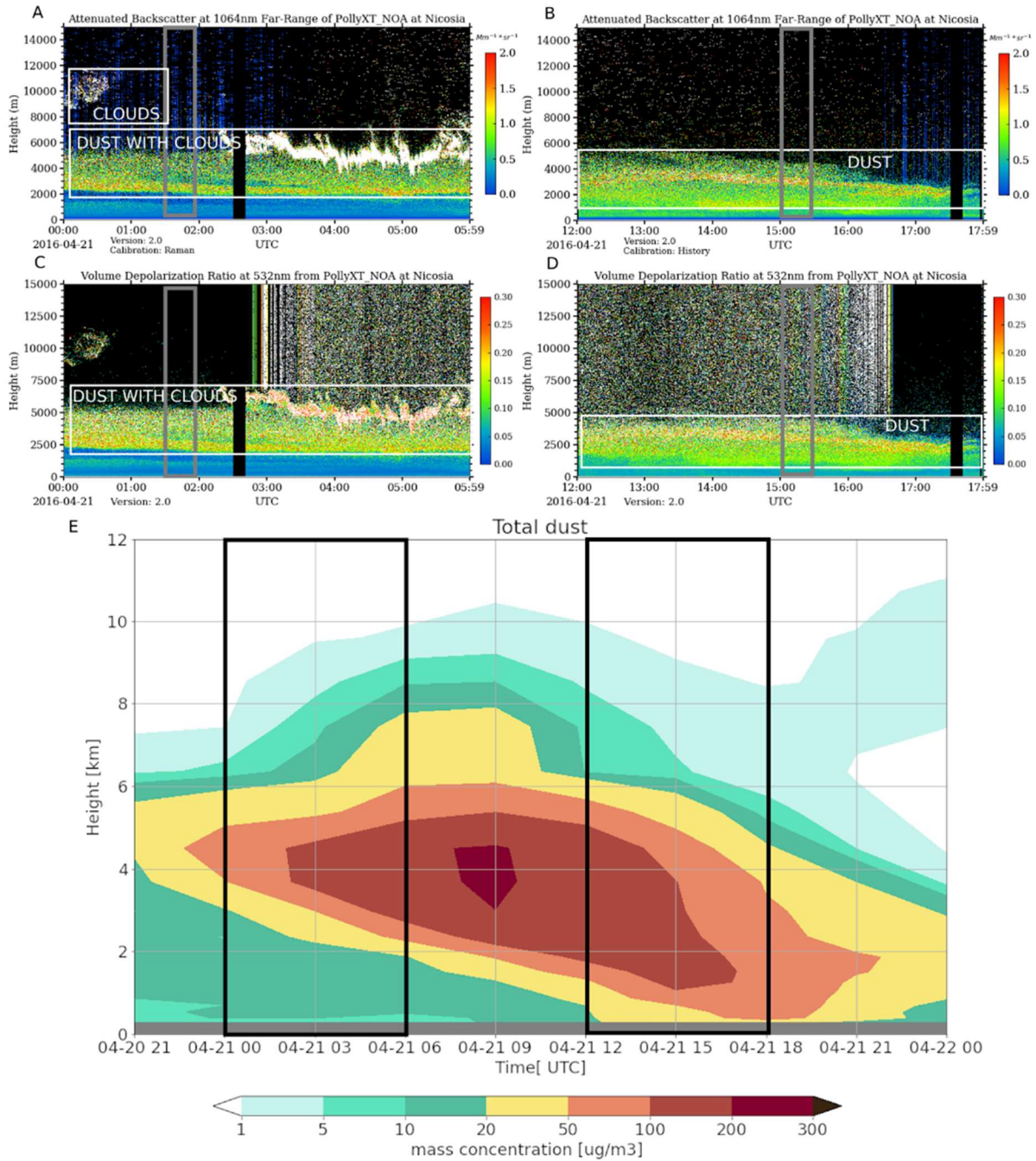


Figure 4.9 Quicklook of the lidar attenuated backscatter at 1064 nm for Nicosia lidar (A) and (B). A black rectangle indicates data used with the POLIPHON algorithm. The Grey rectangle indicates data used with the POLIPHON algorithm. White rectangles indicate cloud and aerosol layers. Volume depolarization ratio at 532 nm for Nicosia lidar (C) and (D). DREAM-simulated dust concentration at Nicosia on April 21 (E). A black rectangle indicates the period of lidar measurements shown in the quick look. (Adapted from Ilic et al. (2021).

Attenuated backscatter shows a dust layer above Nicosia at altitudes between 2 km and 6 km on April 21 until 6 UTC (Figure 4.9 (A and C)). The layer gradually descended and mixed with the planetary boundary layer after 12 UTC. Ice-containing clouds formed within the dust layer after 2 UTC, as indicated by volume depolarization ratio profiles. DREAM simulations predict the dust layer arriving above Nicosia on April 20 after 18 UTC and the altitude of the concentration peak gradually descending while the vertical extent of the layer increased until

April 22. The top boundary of the layer was placed approximately 1 km above the height seen in the lidar quicklook. After 2 UTC on April 21, the dust layer reached 8 km altitude. This event coincided with the period of cloud formation, and therefore could not be observed by lidar.

4.5. Comparison of Dust Mass Concentrations from DREAM and POLIPHON

In this chapter, six vertical profiles of dust concentration were chosen for comparison of DREAM and POLIPHON (five profiles over Nicosia and one over Potenza). The profiles were selected to evaluate dust concentration predictions and to provide input parameters for immersion freezing and deposition nucleation INPC parameterizations. For the INPC parameterizations to be valid, the profiles should be available to sufficient heights and reach sub-zero temperatures. The presence of clouds during the observations can limit the maximum altitude up to which the POLIPHON products can be retrieved. Therefore, profiles were selected during periods prior to or after observations of clouds above the station when they were available. A detailed description of the INPC parameterizations used in this Thesis and the results of their implementation are given in the next chapter.

The POLIPHON algorithm is applied to the lidar profiles from Potenza, Italy, and Nicosia, Cyprus to provide dust mass concentration retrievals. POLIPHON extinction-to-volume conversion factors described in Chapter 3 are derived from North African and Cyprus AERONET stations for Potenza and Nicosia, respectively (Ansmann et al., 2019a). Vertical profiles of particle backscatter coefficient and linear depolarization ratio at 532 nm have been retrieved at both stations. For the Potenza station, the EARLINET Single Calculus Chain (SCC) (D'Amico et al., 2016; Mattis et al., 2016) was used with a vertical resolution of 60 m and temporal integration of 100 minutes. For the Nicosia lidar, the PollyNET algorithm (Baars et al. 2016) was used with temporal integration of 30 minutes and vertical resolution of 7.5 m for the Nicosia lidar. The different integration time in the lidar observations is due to the need to keep a balance between the homogeneity of the observed aerosol layer in the selected time window and the signal-to-noise ratio for the retrieval of lidar profiles. Uncertainties in SCC products, as well as in dust and non-dust linear depolarization ratio, dust lidar ratio, and conversion factors have been propagated through all the steps of the POLIPHON algorithm. The uncertainties in the products are as follows: the dust extinction coefficients can be obtained with the uncertainty of the order of 20% – 40%, while the uncertainty in the microphysical parameters is of the order of 20% – 50% for the dust component (Marinou et al., 2019).

In the April 9 case (N11), POLIPHON and DREAM vertical profiles around 21 UTC are compared, during a period when there were no clouds observed above the station. On April 14 around 21 UTC and on April 15 around 3 UTC, two vertical profiles were analyzed, before and after the formation of cirrus clouds above the dust layer (Ni21 and Ni22). At Potenza, one POLIPHON profile is available around 15 UTC on April 18 (Po31) after the formation of clouds embedded in the dust layer. Two profiles were analyzed around 02 UTC on April 21 prior to the cloud formation (Ni31) and at 15 UTC on April 15 when the clouds were no longer present above Nicosia station (Ni32). In order to compare DREAM and POLIPHON profiles of dust concentrations, the nearest model outputs in time to the POLIPHON products were used. Since DREAM was set to produce outputs every 3 h, the maximum possible time difference between measurement and model profiles was 3 h. Therefore, the model variability for each studied case was represented by the profiles ± 3 h of the observation times. The

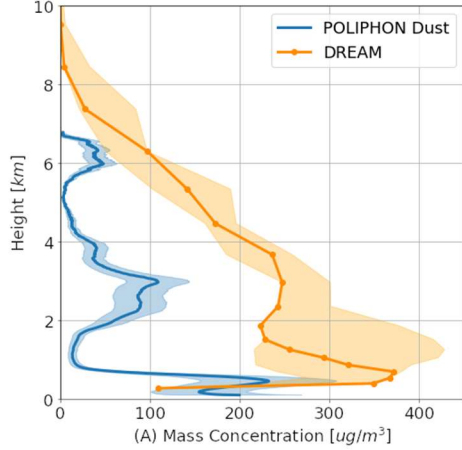
uncertainties of POLIPHON products are described in the previous section. Dust concentrations from POLIPHON and DREAM were interpolated to a common vertical resolution of 100 m for the purpose of the comparison. The calculated metrics are the CoM, the correlation coefficient, the total concentration, and its peak value from mass concentration profiles from both DREAM and POLIPHON (given in Table 4.2). The estimated effect of interpolation on the values of comparison metrics is less than 1%. Figure 4.13 presents dust mass concentrations from DREAM and POLIPHON for each of the analyzed cases. In some of the analyzed cases (Po31, Ni32), the presence of thick clouds limited the POLIPHON profiles at height levels above 6 km: therefore, the evaluation metrics are based on data points where both DREAM and POLIPHON are available. Additionally, CoM and total concentrations for the whole DREAM vertical extent are provided.

HYSPLIT back trajectories corresponding to distinct features of each profile are presented in Figure 4.10, as well. Three local maxima can be seen in the Ni11 profile, at 0.5 km, 3 km, and 6 km. The lowest one can be influenced by mixing in the planetary boundary layer. According to the back trajectory analysis, the other two layers correspond to the southwesterly flow over the central Sahara. The profile is categorized as a high concentration profile according to the classification of Biniatoglou et al. (2015). The overall shape of the simulated profile corresponds to the POLIPHON retrieval, but the concentrations were overestimated by the model.

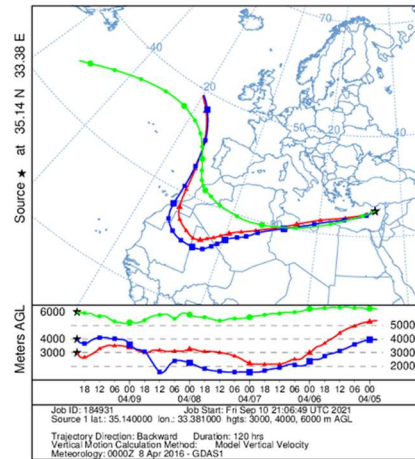
Both Ni21 and Ni22 profiles are low concentration cases. Some of the cases during the same dust episode in the Mediterranean were previously analyzed by Marinou et al. (2019). Their backward trajectory analysis implies that the dust reaching Nicosia in cases Ni21 and Ni22 was coming from the sources in Algeria. On its way to Cyprus it crossed Greece and Turkey, reaching the island from the north. In both cases, continental and marine aerosols were present in the boundary layer, at altitudes below 2.5 km. Their concentrations were significantly lower than dust concentration (less than $10\mu\text{g}/\text{m}^3$). In case of profile Ni21 DREAM simulated the observed dust present below 3 km and a more distinct dust layer between 4 km and 7 km. Additionally, DREAM suggests that dust was present up to 10 km altitude, but this is not supported by the observations. This behavior was noticed and discussed in the systematic study by Biniatoglou et al., 2015. DREAM placed the elevated dust layer and its peak below the observed altitudes. Ni22 profile shows an increase in observed and modeled dust concentrations, and a decrease in observed layer height in comparison to N21. Model places the main dust layer above the observed one (Table 4.2). Total and peak concentrations are overestimated by a smaller amount than in N21 case and within the range of variability of the model.

The Po1 high concentration profile provides data between 2 to 6 km altitudes. Back trajectories confirm that dust present above Potenza was lifted from central Saharan sources and then reached the station. CoM comparisons and correlation coefficients show that DREAM successfully simulated the altitude of transported dust and its vertical distribution (Table 4.2). The model suggests that dust was present even at lower heights with concentrations of $\sim 30\%$ of the peak value.

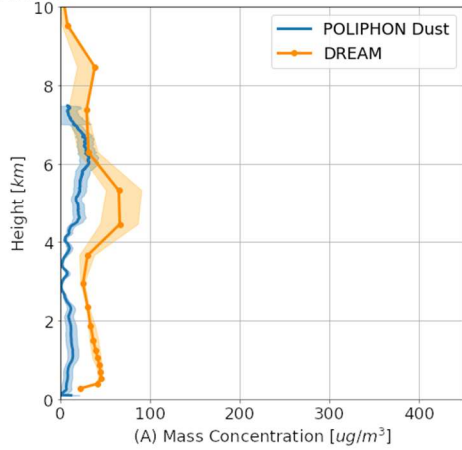
measurements: 2016-04-09 20:39 - 2016-04-09 21:08
Ni11
 DREAM: 2016-04-09 21:00



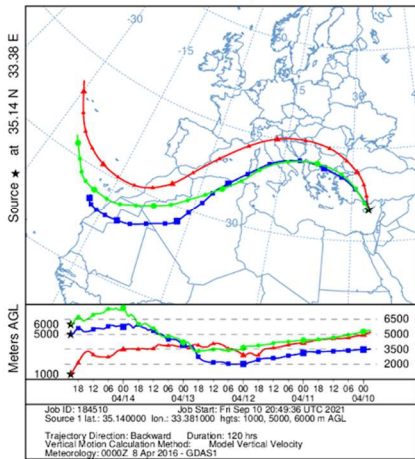
NOAA HYSPLIT MODEL
 Backward trajectories ending at 2100 UTC 09 Apr 16
 GDAS Meteorological Data



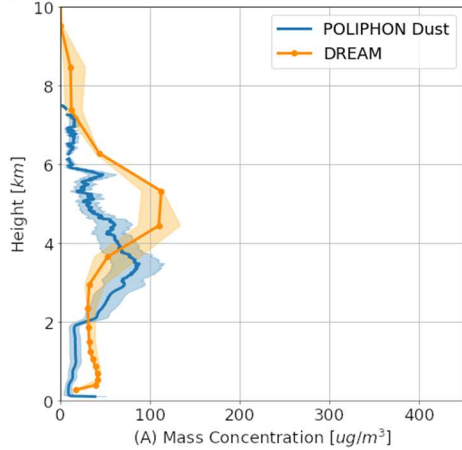
measurements: 2016-04-14 20:02 - 2016-04-14 20:31
Ni21
 DREAM: 2016-04-14 21:00



NOAA HYSPLIT MODEL
 Backward trajectories ending at 2100 UTC 14 Apr 16
 GDAS Meteorological Data



measurements: 2016-04-15 03:03 - 2016-04-15 03:32
Ni22
 DREAM: 2016-04-15 03:00



NOAA HYSPLIT MODEL
 Backward trajectories ending at 0300 UTC 15 Apr 16
 GDAS Meteorological Data

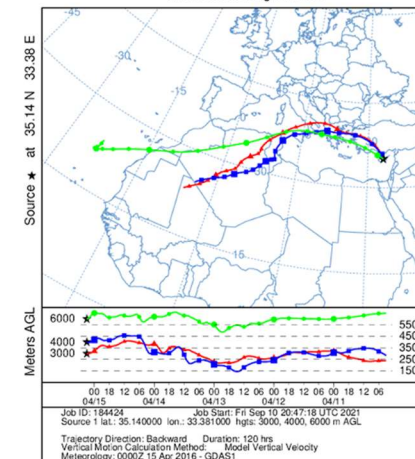
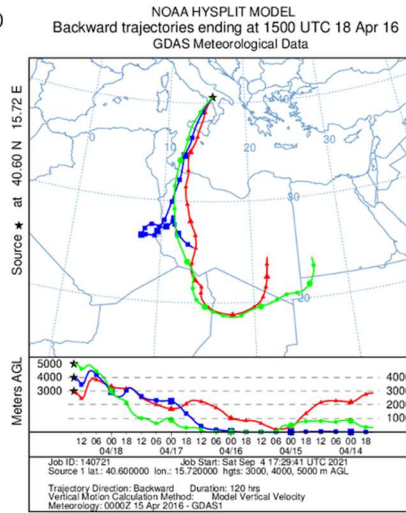
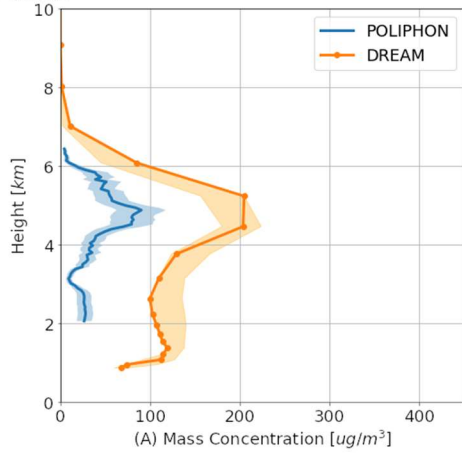
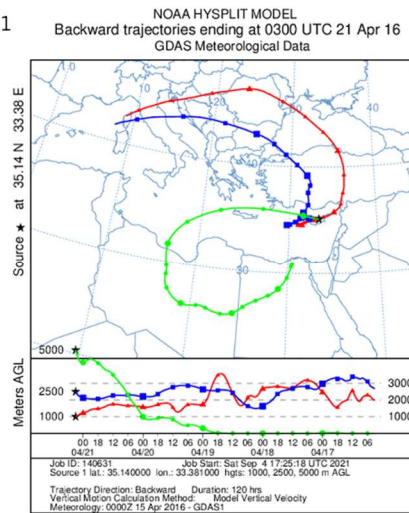
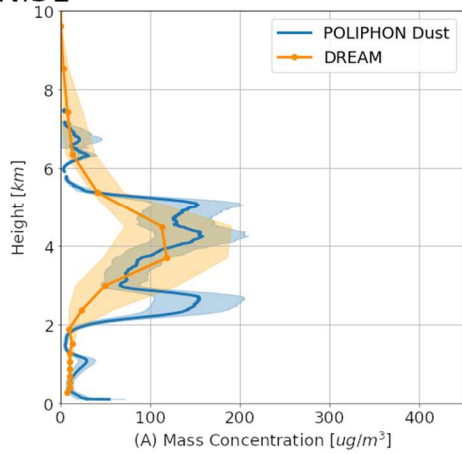


Figure 4.10a POLIPHON and DREAM profiles of dust mass concentration, HYSPLIT back trajectories corresponding to the profiles on April 9 at 21 UTC (Ni11), April 14 at 21 UTC (Ni21), April 15 at 03 UTC (Ni22) at Nicosia. Adapted from Ilic et al. (2021).

measurements: 2016-04-18 14:00 - 2016-04-18 15:40
Po31 DREAM: 2016-04-18 15:00



measurements: 2016-04-21 01:31 - 2016-04-21 02:01
Ni31 DREAM: 2016-04-21 03:00



measurements: 2016-04-21 15:03 - 2016-04-21 15:32
Ni32 DREAM: 2016-04-21 15:00

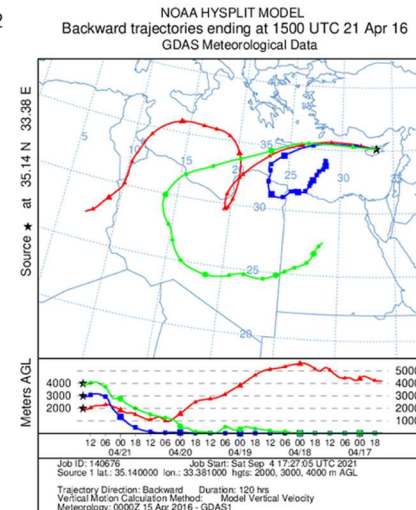
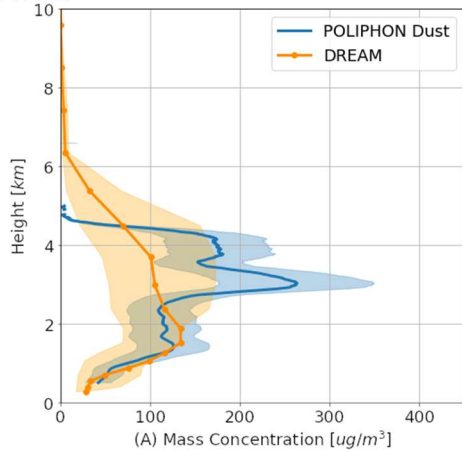


Figure 4.10b POLIPHON and DREAM profiles of dust mass concentration, HYSPLIT back trajectories corresponding to the profiles on April 18 at 15 UTC at Potenza (Po31), on April 21 at 03 UTC (Ni31) and April 21 at 12 UTC (Ni32) at Nicosia. Adapted from Ilic et al. (2021).

Table 4.2 POLIPHON (P) and DREAM (D) comparison metrics (center of mass, total concentration, peak value, and correlation coefficient) for the analyzed cases on April 9 at 21 UTC (Ni11), April 14 at 21 UTC (Ni21), April 15 at 03 UTC (Ni22) at Nicosia, on April 18 at 15 UTC at Potenza (Po31), on April 21 at 03 UTC (Ni31) and April 21 at 12 UTC (Ni32) at Nicosia. D-all represents the metrics for the whole DREAM profile (not limited to data points where POLIPHON products are available). Lower and upper values due to the uncertainties of POLIPHON (coming from the natural variability and the retrievals uncertainties) are given in brackets.

Location	Episode	Case	Center of Mass [m]			Total concentration [g/m ³]			Peak Value [μg/m ³]		Correlation Coefficient
			P	D	D-all	P	D	D-all	P	D	
Ni11	Ma	H	2313 (2301, 2318)	2961	2994	0.36 (0.23, 0.45)	1.41	1.42	223 (150, 295)	369	0.54
Ni21	In	L	4410 (4266, 4732)	3744	4647	0.10 (0.06, 0.14)	0.24	0.36	32 (22, 42)	66	0.55
Ni22	In	L	3619 (3614, 3628)	4126	4298	0.26 (0.17, 0.34)	0.39	0.41	85 (58, 112)	113	0.53
Po31	In	H	4412 (4393, 4422)	4310	3556	0.16 (0.11, 0.21)	0.64	0.82	87 (60, 114)	205	0.92
Ni31	In	H	3778 (3597, 3864)	4133	4143	0.45 (0.29, 0.61)	0.32	0.32	155 (105, 205)	119	0.79
Ni32	In	H	2819 (2797, 2831)	2857	2841	0.56 (0.42, 0.63)	0.49	0.50	263 (177, 349)	134	0.84

Both Ni31 and Ni32 profiles from Nicosia on April 21 are high concentration cases. Comparison of DREAM and POLIPHON Ni31 profiles shows that the model predicted presence of the main dust layer above 4 km but missed the dust layer at 2.5 km height. This results in CoM placement in DREAM higher than the observed one. For Ni32 profile, position of CoM from the model agrees with observations. According to the correlation coefficients, the main vertical structure of the dust plume was well represented by the model in both

cases. DREAM-simulated total concentrations are within the uncertainties of the POLIPHON retrievals in these cases. For most altitudes DREAM simulated dust concentrations within the POLIPHON uncertainties. The layer below 3 km for Ni31 and layer between 2.5 and 4.5 km for Ni32 was underestimated. In Ni31, peak of the modeled concentration agreed with POLIPHON within the uncertainties, but in Ni32 underestimation of the modeled concentration peak was larger.

In the 6 presented cases, the quality of the comparison of DREAM predictions with POLIPHON is consistent with the results presented in Chapter 4.1 (Table 4.2) regarding the shape of the profiles and altitude of the dust layer. The correlation coefficient is lower in Ni11, Ni21 and Ni22 cases than in the systematic study. In most of the presented cases, observed and simulated heights of the dust layer were above the average height of 3 km reported for east cluster by Binietoglou et al. (2015). The overestimations in dust concentrations above 6 km altitude were evident in Ni11, Ni21 and Ni22 cases. The low and high concentration case comparison is also similar to the previously reported results. In the low concentration cases (Ni21 and Ni22), DREAM overestimates dust concentrations above 5 km and therefore places the top of the dust layer above the observed one. In the high concentration cases, DREAM overestimation at high altitudes is less pronounced. In these 6 cases, DREAM typically overestimates the concentrations, in contrast to the average result of the systematic study. The dataset consisting of 6 cases presented here is very limited and does not allow a detailed statistical analysis of the overestimations. These results are a starting point for the analysis of dust related INPC model predictions discussed in the next chapter, considering the discrepancies between the observational and simulated datasets.

5 Numerical Modeling of Ice Nucleating Properties of Atmospheric Mineral Dust

The ice nucleation processes occur on a molecular scale and are therefore a sub-grid scale phenomenon in numerical models of the atmosphere. These processes are described in the models in a simplified way using parameterizations. The parameterizations are developed with the intention to represent the relationships between the physical quantities in the model as they are in the atmosphere. Typically, this is achieved by relating the overall effects of small-scale processes within a model grid-box to the thermodynamic quantities averaged over the model grid-box. The role of aerosols as a CCN or an INP in the cloud process can also be parameterized. CCN particles are more abundant in the atmosphere, whereas INPs are much rarer but have an impact on cloud cycle. INPs have historically been represented in numerical models with their climatological concentrations and ice nucleation efficiencies. Development of atmospheric models and their capabilities to describe aerosol and specifically mineral dust transport opened a pathway to represent ice initiation in more detail. Mineral dust has shown to be one of the main sources of INPs in the atmosphere (Cziczo et al., 2013). Improved characterization of particles that can participate in ice formation in the atmosphere allowed development of INPC parameterizations, which are specific for a particle type, such as dust (DeMott et al., 2015) or marine biogenic particles (Wilson et al., 2015). Since INPC parameterizations use particle concentrations and thermodynamic quantities as input, they can be implemented in atmospheric models (Niemand et al, 2012; Ničković et al., 2016) or used as a final component in remote sensing retrieval algorithm workflow (Marinou et al., 2019).

INPC parameterizations used in models are based on laboratory and field measurements. The main principle in development of INPC parameterizations is exposure of collected aerosol particles to controlled experimental conditions inside cloud chambers. In an experiment conducted in such a chamber, dust particle size distribution and mineral composition are known while the environmental factors such as water vapor content and temperature can be controlled. Then, at specified conditions, the INP fraction of particles can be determined. Since there are several modes of ice nucleation occurring in the atmosphere in a wide range of temperature regimes, it is not possible to use a single type of chamber to investigate all these processes. Ice nucleation chambers are therefore designed to study specific ice nucleation mechanisms and temperature ranges (DeMott et al. 2011). The developed parameterizations used in models to evaluate the dust contribution to INPC typically describe immersion freezing and deposition nucleation (Niemand et al, 2012; DeMott et al, 2015; Ullrich et al, 2017). In numerical weather prediction models mineralogy indifferent INPC parameterizations have mostly been used (Niemand et al., 2012; Ničković et al., 2016) to account for dust particles' contribution to INPC. However, evaluation of contributions of individual minerals found in dust to INPC can be described using mineralogy-sensitive parameterizations by Atkinson et al. (2013) and Harrison et al. (2019). In this Thesis, both mineralogy-indifferent and mineralogy-sensitive dust INPC parameterizations are used. The parameterizations used in this Thesis and results of their implementation in DREAM are presented and discussed in more detail in this Chapter.

5.1. INPC Parameterizations in DREAM

The INPC parameterizations in DREAM are used to predict the INPC in immersion freezing and deposition nucleation. In immersion freezing mode at or above water saturation, three different parameterizations are used: two mineralogy-indifferent parameterizations, by DeMott et al. (2015) (D15i) and by Ullrich et al. (2017) (U17i); and one mineralogy-sensitive parameterization by Harrison et al. (2019) (H19i). Deposition nucleation is described by two parameterizations, both mineralogy-indifferent: Steinke et al. (2015) (S15d) and Ullrich et al. (2017) (U17d). All the INPC parameterizations used in this Thesis, with their valid temperature ranges and input parameters used, are summarized in Table 5.1, and presented in the text.

Table 5.1. INPC parameterizations used in this study, with references, lists of input parameters, and temperature ranges. Adapted from Ilić et al. (2022).

Parameterization	Reference	Nucleation mode	Input parameters	T range [°C]
H19i	Harrison et al. (2019)	Immersion	K-feldspar S_d, T	-37.5 to -3.5
			plagioclase S_d, T	-38.5 to -12.5
			albite S_d, T	-35.6 to -6.5
			quartz S_d, T	-37.5 to -10.5
D15i	DeMott et al. (2015)	Immersion	Dust n_{250}, T	-36.0 to -5.0
S15d	Steinke et al. (2015)	Deposition	Dust S_d, T	-55.0 to -36.0
U17i	Ullrich et al. (2017)	Immersion	Dust S_d, T	-30.0 to -14.0
U17d	Ullrich et al. (2017)	Deposition	Dust S_d, T	-67.0 to -33.0

Parameterizations by Harrison et al. (2019) for quartz and feldspar minerals (H19i) are given below. Valid temperature ranges and standard deviations for $\log(n_s(T))$, where n_s is the nucleation site density in units of cm^{-2} , are shown in parentheses.

Quartz: (-10.5 °C to -37.5 °C; $\sigma=0.8$):

$$\log(n_s(T)) = -1.709 + (2.66 \times 10^{-4}T^3) + (1.75 \times 10^{-2}T^2) + (7 \times 10^{-2}T); \quad (5.1)$$

K-feldspar: (-3.5 °C to -37.5 °C; $\sigma=0.8$):

$$\log(n_s(T)) = -3.25 + (-0.793T) + (-6.91 \times 10^{-2}T^2) + (-4.17 \times 10^{-3}T^3) + (-1.05 \times 10^{-4}T^4)(-9.08 \times 10^{-7}T^5);$$

(5. 2)

plagioclase feldspar: (-12.5 °C to -38.5°C; $\sigma=0.5$):

$$\log(n_s(T)) = (-3.24 \times 10^{-5}T^4) + (-3.17 \times 10^{-3}T^3) + (-0.106T^2) + (-1.71T) - 12.00;$$
(5. 3)

Albite: (-6.5 °C to -35.5 °C; $\sigma=0.7$):

$$\log(n_s(T)) = (3.41 \times 10^{-4}T^3) + (1.89 \times 10^{-2}T^2) + (-1.79 \times 10^{-2}T) - 2.29.$$
(5. 4)

INPC is calculated for each size bin and mineral fraction in case of H19i, for nucleation site density-based parameterizations using the expression:

$$INPC = n_{250}(1 - \exp(-n_s\sigma))$$
(5.5)

where σ is the surface area of dust particles in a size bin. Then, total INPC is calculated as a sum of contributions from all size bins.

D15i parameterization is defined by the equation (DeMott et al., 2015):

$$INPC = f_d n_{250}^{(\alpha(273.16-T)+\beta)} \exp(\gamma(273.16-T)+\delta)$$
(5. 6)

where n_{250} is the concentration of dust particles with diameter larger than 0.5 μm , T is the air temperature in degrees Celsius, $\alpha = 0$, $\beta = 1.25$, $\gamma = 0.46$, and $\delta = -11.6$. To calibrate the parameterization scheme to the dust measurements, the factor $f_d=3$ is used (DeMott et al., 2015; Ničković et al., 2016). The equation, as well as the laboratory and field experiment results from which it was derived, are described in detail in DeMott et al. (2015). As shown in Table 5.1, D15i is the only parameterization used in this thesis which, besides thermodynamic quantities, relies only on dust particle concentrations as input.

The deposition parameterization S15d is based on the ice nucleation site density approach (Steinke et al., 2015):

$$n_s = 1.88 \times 10^5 \exp(0.2659 \times t_{therm}),$$
(5. 7)

where n_s is the ice-active surface site density and x_{therm} is a function of temperature and saturation in respect to ice:

$$x_{therm} = -1.085 \times (T - 273.16) + 0.815 \times (S_i - 1) \times 100$$
(5. 8)

where T is temperature in degrees Celsius, and S_i saturation ratio with respect to ice. In this case, the INPC is calculated using the Equation 5.4. The operational version of DREAM INPC forecasts uses D15i and S15d parameterizations to cover the immersion freezing and deposition

nucleation range (Ničković et al., 2016). The forecast is performed by the RHMSS/SEEVCCC, with the assistance of the Environmental Physics Laboratory (EPL) at the Institute of Physics Belgrade (IPB), Serbia.

Ullrich et al. (2017) proposed an immersion freezing parameterization (U17i) and a deposition nucleation parameterization (U17d), both based on the ice nucleation site density. U17i and U17d, as well as the previously described S15d parameterizations, are based on laboratory studies performed within the AIDA (Aerosol Interaction and Dynamics in the Atmosphere) cloud chamber of the Karlsruhe Institute of Technology. U17i and U17d are based on desert dust samples collected from Sahara, Taklamakan Desert, Canary Islands, and Israel.

The U17i parameterization is defined by the equation:

$$n_s = \exp (150.577 - 0.517T) \quad (5.9)$$

where T is temperature in Kelvins. Then the INPC can be calculated using the Equation 5.4.

The U17d parameterization is defined by the equation:

$$n_s = \exp \{ \alpha (S_i - 1)^{0.25} \cos[\beta(T - \gamma)]^2 \cot^{-1}[\kappa(T - \lambda)] \pi \} \quad (5.10)$$

where the parameters $\alpha = 285.692$, $\beta = 0.017$, $\gamma = 256.692$, $\kappa = 0.080$, $\lambda = 200.745$ are defined for dust aerosol, T is temperature in Kelvins and S_i saturation ratio with respect to ice. INPC in parameterization U17d is calculated using the Equation 5.4.

In this Thesis, the parameterizations described above have been used in DREAM model the in three different model setups (Ilić et al., 2022):

- the H19i_U17d setup, which is mineralogy-sensitive in the immersion freezing mode, uses H19i parameterization for immersion freezing and mineralogy indifferent U17d for the deposition mode;
- the D15i_S15d setup, the operational forecast setup described by Ničković et al. (2016), uses D15i and S15d parameterizations for the immersion freezing and deposition, respectively;
- the U17i_U17d setup is based on immersion freezing parameterization U17i and deposition nucleation parameterization U17d from Ullrich et al. (2017).

As shown in the equations 5.2-5.4, the INPC parameterization H19i for feldspar is intended to be applied to K-feldspar, plagioclase, and albite components of feldspar separately. The information about these feldspar components is not available in the GMINER30 database. To use the three components in H19i parameterization, it is considered that, based on compiled measurement data, K-feldspar accounts for 35% of total feldspar, with 65% being plagioclase (Atkinson et al., 2013). In this Thesis, a common assumption that albite account for 10% of plagioclase is used (Harrison et al., 2019). Having in mind these feldspar components, and the fact that GMINER30 does not differentiate between them, in the further text, they are referred to as feldspar. Due to the assumption of external mixture used in the model, the total INPC is calculated as the sum of INPC contributions from quartz and the three components of feldspar.

As a first step, an offline comparison of feldspar and quartz INP fractions has been performed to provide an estimate of the expected contribution of mineral components of dust to INPC (Figure 5.1) (Ilić et al., 2022). In Figure 5.1A, H19i parameterization is compared to D15i and U17i, as well. In Figure 5.1B, D15i values are not shown as the site nucleation density values are not parameterized by it. This is an offline comparison because it does not rely on the model simulations for the input parameters. For this purpose, temperature values used as input were selected to cover the validity range of each of the parameterizations, with a step of 0.1°C. The particle size distribution used to calculate input mass concentration is the same as that used in the model, a monomodal lognormal mass size distribution at dust sources (Zender et al., 2003; Perez et al. 2006). Mass concentration can be arbitrary, as the INPC fraction does not depend on it. Feldspar and quartz fractions at the dust source points in the model were calculated using the GMINER30 database (Figure 2.2). The mean values and the standard deviations of feldspar and quartz fractions in clay and silt at the source points within the model domain were used (Table 2.2). Since GMINER30 does not consider feldspar in clay fraction, two estimates were made: one with feldspar absent from clay, and another one where it is assumed that quartz to feldspar fraction in silt is valid in clay particles, as well (Atkinson et al., 2013). It should be noted that parameterization for quartz (equation 5.1) is valid for freshly milled quartz, and it results in an upper limit estimate of quartz contribution to INPC. Experiments with quartz exposure to air and water have shown that active sites on quartz can be removed due to aging (Zolles et al., 2015; Harrison et al., 2019). The results of the analysis in this Thesis show the highest fraction of feldspar INPs at around -25°C, as expected due to K-feldspar activity (Atkinson et al., 2013). At higher temperatures quartz contributes to about 7% of INPC. At temperatures above -10.5°C, parameterization for quartz is not defined, while at temperatures below -25°C, quartz contribution becomes increasingly important with decrease of temperature. This contribution is up to 30% at -35°C when feldspar is present in clay particles and increases to 51% with the assumption of no feldspar in clay particles. These results agree with findings of Boose et al. (2016), who showed that at temperatures between the homogeneous freezing limit and -33°C quartz can be a significant contributor to INPC. When compared to U17i and D15i, mineralogy-sensitive results fall between them in range of temperatures between -35°C and -15°C. At higher temperatures, H19i is expected to significantly underpredict INPC when compared to mineralogy-indifferent parameterizations. The analysis in Figure 5.1B shows the activity of feldspars, especially K-feldspar increasing at temperatures below -20°C above the U17i values for dust. INP Fraction in Figure 5.1A does not follow this trend since the feldspar fraction in dust is less than 30% by mass.

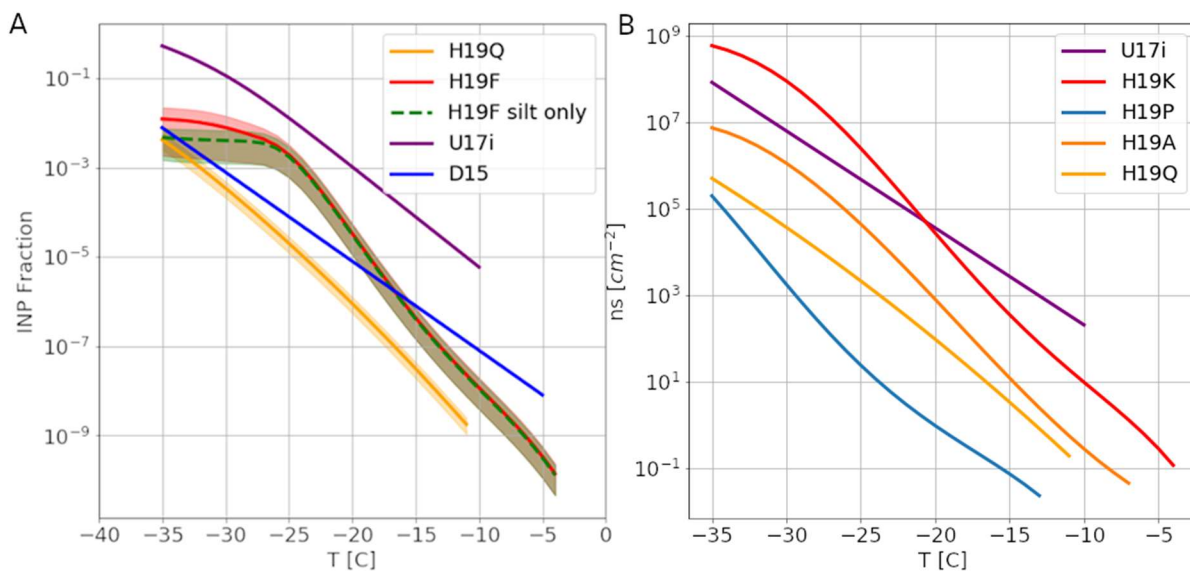


Figure 5.1 The comparison of INP fractions of quartz, feldspar, and feldspar in silt fraction, based on H19 parameterization (A). U17i and D15i are added for reference. Comparison of n_s -T graphs for H19 parameterizations and U17i parameterization (B). Adapted from Ilić et al. (2022).

5.2 Comparison of INPC resulting from DREAM and POLIPHON dust concentrations

Some weather and climate models can run INPC forecasts routinely (e.g., Ničković et al., 2016; Hande et al., 2015; Su et al., 2018). Several attempts have been made to validate these model results (Niemand et al., 2012; Atkinson et al., 2013; Vergara-Temprado et al., 2017) with in situ measurements. Direct comparisons can be made with ice nucleating properties of particle samples collected using unmanned aerial vehicles (UAV) or ground based measurements, but those sampling strategies typically rely on samples collected at altitudes where temperatures are too high to form clouds (Atkinson et al., 2013; Vergara-Temprado et al., 2017, Schrod et al., 2017). The evaluation of INPC prediction is also possible using ground-based and satellite-borne lidar aerosol concentration retrievals, with certain limitations. The INPCs based on lidar-derived aerosol concentration typically rely on atmospheric models for meteorological parameters. Additionally, the retrieval algorithms do not differentiate between different minerals found in dust and therefore only the mineralogy indifferent INPC parameterizations are used in such applications (Marinou et al., 2019; Ilić et al., 2022). Usefulness of lidar retrievals in INPC evaluation has been confirmed by the outcomes of the studies by Mamali et al., (2018) and Marinou et al., (2019). Mamali et al. (2018) found agreement within uncertainty limits between POLIPHON retrievals of dust concentration and optical particle counter (OPC) in situ measurements aboard UAVs within dust layers mixed with near-spherical particles and continental/pollution particles. They considered that the two techniques could be used interchangeably and systematically with numerical models. To evaluate lidar-derived cloud-relevant dust concentrations and INPC in Cyprus, Marinou et al. (2019) performed comparisons with the in situ measurements onboard unmanned aerial systems. They found agreement within the uncertainties of the measurements. Additionally, they reported that D15i applied to POLIPHON retrievals agrees within the uncertainty range in the immersion range and U17d (2017) parameterization agrees within one order of magnitude for deposition range, with the results derived from UAV measurements. Other two parameterizations used in their study, S15d and U17i were less successful in predicting the

INPC. S15d parameterization showed an enhanced freezing efficiency in the deposition mode by 3 to 4 orders of magnitude, while U17i showed agreement within 2 to 3 orders of magnitude. Bearing in mind these findings, we compare DREAM and POLIPHON cloud-relevant dust concentrations and INPC.

In this Thesis, mineralogy-indifferent parameterizations are applied to DREAM and POLIPHON profiles. The mineralogy-sensitive immersion parameterization was also implemented in DREAM, and it was compared with mineralogy-indifferent INPC parameterization results. The total dust concentration simulated by DREAM in the three types of numerical experiments is the same since the dust-atmosphere model was set up in the same way. Simulated cloud-relevant dust concentrations are used as input in the mineralogy-indifferent parameterizations. Feldspar and quartz cloud-relevant concentrations are used as input to mineralogy-sensitive parameterization. The POLIPHON cloud-relevant dust concentration profiles were used to calculate INPC from the observations. In addition to the cloud-relevant dust concentrations, meteorological properties, temperature, and humidity are used as input to INPC parameterizations. For the DREAM profiles, dust concentrations are available from the dust model, and thermodynamic quantities from the atmospheric driver. For the lidar retrievals, atmospheric parameters are used from the operational system GDAS (Global Data Assimilation System) of the National Weather Service's National Centers for Environmental Prediction (NCEP) (Ansmann et al., 2019a; Marinou et al., 2019).

Figure 5.2 presents the lidar-derived POLIPHON profiles and DREAM profiles of cloud-relevant dust concentrations and INPC. Each of the cases, previously analyzed in Chapter 4 cases is represented by four panels. Along with the dust concentrations, the feldspar and quartz contributions are presented. DREAM profiles are presented for the three INPC setups, as well. In all the presented profiles, POLIPHON data is limited up to a certain height, usually below 8 km and therefore temperatures above -33 °C. In the analyzed cases, only dust observed or predicted above approximately 4 km was relevant for the INPC parameterizations due to the temperature range for which parameterizations are valid (Table 5.1 and Figure 5.2). Due to these circumstances, the use of the deposition parameterizations was impossible with the POLIPHON data and only immersion parameterizations were implemented. On the other hand, DREAM does provide data in the deposition range and the appropriate parameterizations have been used with the model simulations.

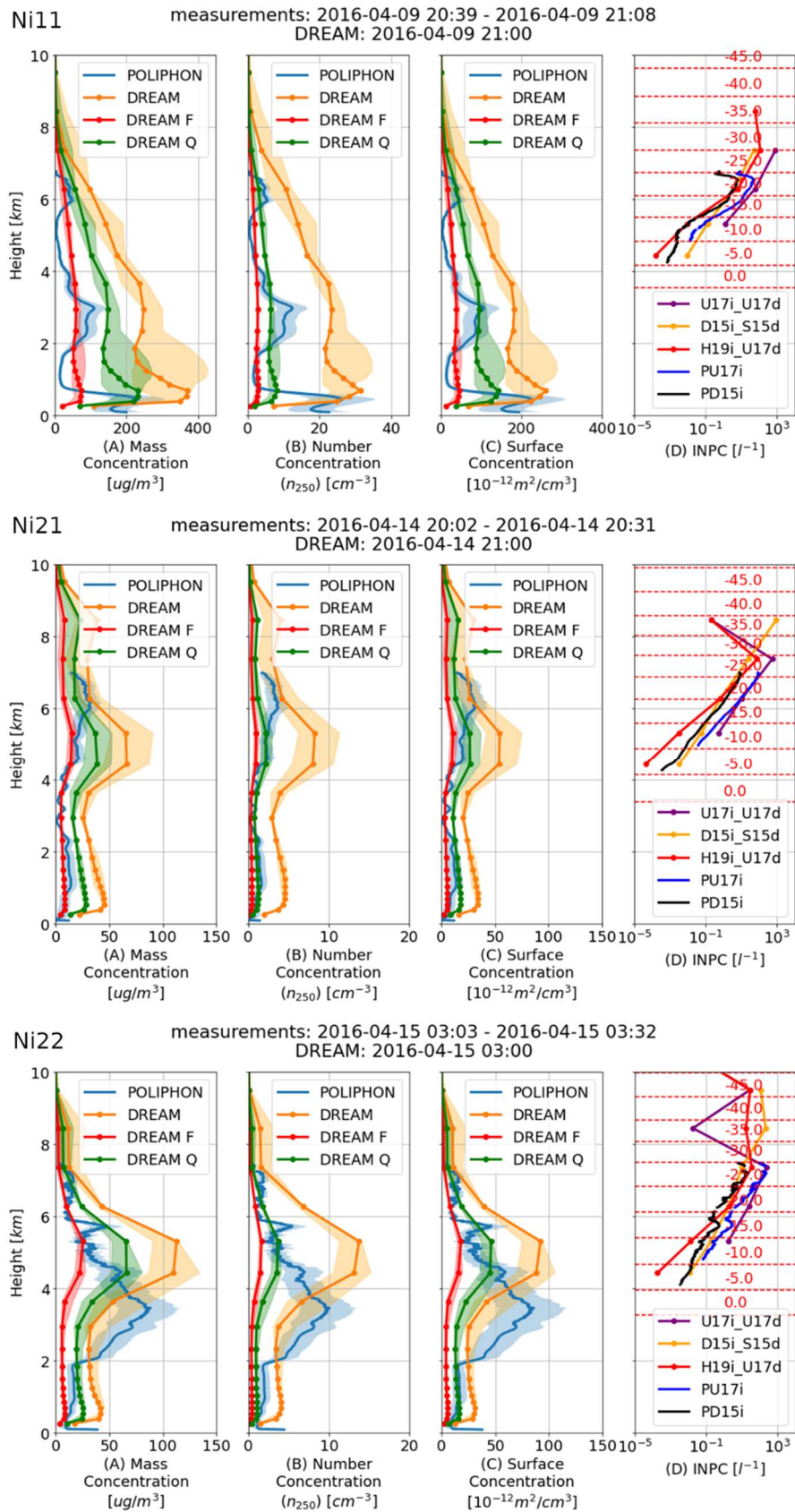


Figure 5.2a POLIPHON and DREAM profiles of cloud-relevant dust concentrations, INPC on April 9 at 21 UTC (Ni11), April 14 at 21 UTC (Ni21), April 15 at 03 UTC (Ni22) at Nicosia. Adapted from Ilić et al. (2022).

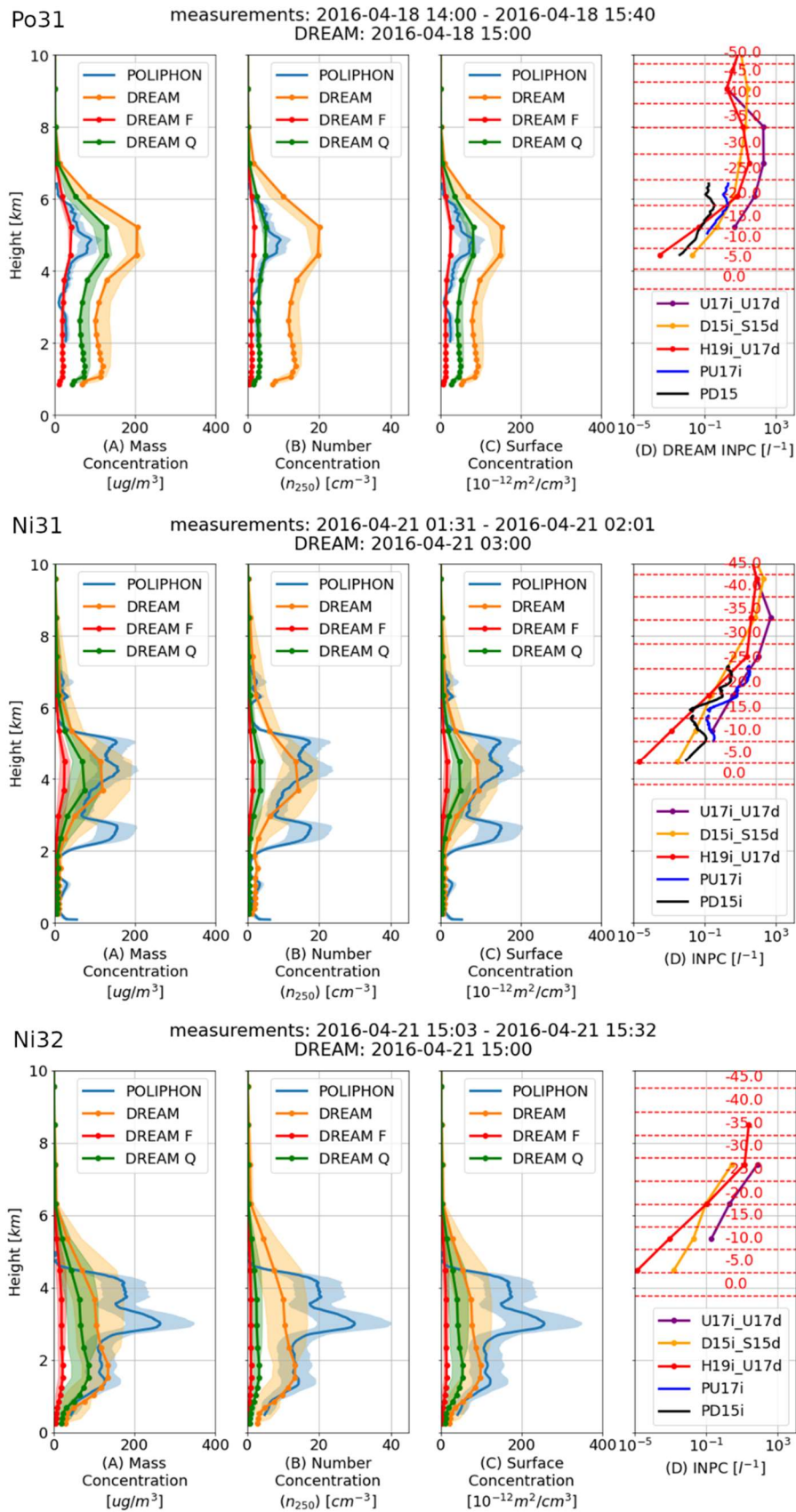


Figure 5.2b POLIPHON and DREAM profiles of cloud-relevant dust concentrations, INPC on April 18 at 15 UTC at Potenza (Po31), on April 21 at 03 UTC (Ni31) and April 21 at 12 UTC (Ni32) at Nicosia. Adapted from Ilić et al. (2022).

The DREAM and POLIPHON dust mass concentration profiles were compared in the previous Chapter for the cases in Nicosia (Ni11, Ni21, Ni22, N31, Ni32) and Potenza (Po31). Here, more information is given on the analysis of concentrations at heights at which immersion freezing INPC parameterizations are applied. In the high dust concentration case Ni11, the mass concentration was overestimated by the model, in comparison with POLIPHON, by a factor of up to 25 between 5 and 6 km altitudes. In the upper part of the mentioned altitude range a reasonable agreement in INPC can be seen. In the lower part with the largest overestimations in dust prediction, INPC differences are within one order of magnitude. In the second analyzed episode, two low concentration cases were analyzed, Ni21 and Ni22. Agreement in INPC is very good with overestimation of dust mass concentrations by the model in comparison with POLIPHON. The overestimations were much lower than in Ni11 case: Ni21 was overestimated by up to a factor of 4, and Ni22 up to a factor of 6 in mass concentrations. In the Ni22 profile, slightly more noise can be seen in the POLIPHON retrieval. In Ni21 and Ni22, the shape of the dust profiles is better represented than in the Ni11 case, leading to better representation of INPC profiles, as well. Po31 profile provides data up to 6 km height and is used only in estimation of immersion mode INPC at temperatures higher than -25°C , at altitudes around and slightly above the altitude of maximum dust concentration. The Po31 profile showed the highest overestimations of peak and total concentrations by the model in comparison to other analyzed profiles. In the immersion freezing altitude range, overestimations were between a factor of 2 and factor of 8 in mass concentrations. Overestimations are clearly noticeable in the INPC profiles, in this case within a range of magnitude. In the case of the same dust plume, when it reached Nicosia, DREAM underestimated dust concentrations in Ni31 and Ni32 according to peak and total concentration analysis. In the immersion range, in the case of Ni31 underestimations were by around a factor of 2. In the case of Ni32, in the immersion range, dust concentrations were overestimated by the model. In the Ni31 case, observations were available at altitudes which enabled the use of D15i and U17i INPC parameterizations. The POLIPHON Ni32 profile did not provide information at sufficiently high altitudes to compare the INPC results. The Ni31 results differ from those obtained using the same parameterizations in the DREAM model, within one order of magnitude. Overestimation of dust concentrations by DREAM compared to POLIPHON is around 100% (Table 4.2) and produces corresponding differences of one order of magnitude for INPC values predicted by D15i (setup D15i_S15d) and two orders of magnitude in INPC values for U17i (setup U17i_U17d).

Mineral fraction of feldspar and quartz in the immersion range are presented in Figure 5.2 and in Table 5.2. It should be noted in this discussion that very high quartz contribution to INPC can be influenced by the atmospheric model vertical resolution as described in the Chapter 4.1. A model layer can be several hundreds of meters thick in the immersion temperature range. Therefore, the highest vertical level at which the immersion parameterizations are applicable can be at relatively high temperatures, where the quartz contribution to INPC is below 5%. On the other hand, that vertical level can be at temperatures below -30°C where quartz contribution is significant.

Although the largest feldspar mass fraction was predicted in the Ni11 case, it did not significantly affect the mineral contribution to particle number concentrations or to INPC. In this case the highest feldspar fraction in the dust surface area concentration was predicted, as an expected consequence of the high mass fraction and the fact that most of the feldspar mass is in silt particles. Quartz contribution to INPC increased at temperatures below -30°C . In the second analyzed episode, the feldspar and quartz fractions and their respective contributions to INPC were almost constant. Profiles Ni21 and Ni22 showed very similar mineral dust fractions over a course of 8 hours. In this episode a significantly lower contribution of quartz to INPC

was predicted, in comparison with other cases, even though the quartz fraction in dust was similar to those in the presented cases during other episodes. The large difference between quartz contribution to INPC in the Ni11 case on one side and in the cases Ni21 and Ni22 on the other side can be explained by the main points of the discussion of model vertical resolution. Apparently, the temperature representative for the lower of the two neighboring model layers was too high for quartz to be efficient INP source in immersion freezing, and in the upper layer, the temperature was too low for the immersion freezing parameterization to be used.

Table 5.2 Mean values of feldspar and quartz contributions to dust mass concentrations, number particle concentrations, and surface area concentrations in the immersion freezing temperature range in DREAM. Mean values of feldspar and quartz contributions to INPC based on immersion freezing parameterization by Harrison et al. (2019) (H19i). Maximum and minimum values of mineral contributions are given in the brackets.

	Mass Concentration [%]		Number Concentration [%]		Surface Area Concentration [%]		INPC [%]	
	F	Q	F	Q	F	Q	F	Q
Ni11	25 (25,26)	58 (58,59)	8 (8,9)	20 (20,21)	22 (22,23)	50 (49,51)	86 (61,99)	14 (1,39)
Ni21	22 (21,23)	58 (57,59)	8 (8,9)	19 (19,20)	19 (18,20)	50 (48,52)	95 (93,98)	4 (2,7)
Ni22	20 (21,23)	58 (56,60)	8 (8,9)	19 (19,20)	19 (18,20)	49 (47,51)	95 (93,98)	4 (2,7)
Po31	19 (19,20)	61 (59,63)	6 (6,7)	18 (18,19)	17 (16,19)	51 (49,54)	91 (73,98)	9 (2,27)
Ni31	22 (21,23)	58 (57,60)	8 (8,9)	18 (18,19)	19 (18,20)	49 (47,51)	89 (74,97)	11 (3-26)
Ni32	21 (20,22)	58 (57,60)	9 (8,10)	17 (17,18)	18 (18,19)	50 (47,53)	87 (67,98)	13 (2-33)

As discussed in Chapter 4.2, cases Po1, Ni31 and Ni32 are parts of the same dust episode in the Mediterranean. The dust plume, which travelled from Potenza to Nicosia, went through some minor changes in the mineral composition, as shown by the DREAM model results. These changes affected the INPC contributions of feldspar and quartz to some extent, but the temperature and model resolution again played a role in determining specific mineral contributions to INPC. Like the episode described by the cases Ni21 and Ni22, this episode, in cases Ni31 and Ni32, shows almost constant mineral contributions above Nicosia over the course of 12 hours.

5.3 Comparison of DREAM and In Situ INPC Measurements

To provide additional insight into model performance, a comparison was performed to evaluate DREAM INPC against the available in situ measurements on April 21. UAV-FRIDGE data and uncertainties used here are adopted from Marinou et al. (2019). As reported in the Section 3.6, the estimated error of the INP measurements is around 20%. When discussing comparison of DREAM INPC with these in situ measurements, it is useful to consider their results. They compared the POLIPHON-derived INPC and UAV-FRIDGE results and found

that D15i immersion parameterization and U17d deposition parameterizations were applicable in dust dominated cases.

For comparison of model results with UAV-FRIDGE data presented in Figure 5.3, the INPC parameterizations were used in offline mode. At the sample collecting altitudes, immersion freezing conditions were not met. Therefore, as opposed to calculating immersion freezing INPC in the model where the thermodynamic conditions are met, it was necessary to use mineral dust concentrations from the model at the same latitude, longitude, and height at which the UAV samples were collected. Thus, the predicted cloud-relevant dust concentrations are used as input to the D15i, U17i and H19i parameterizations. The thermodynamic conditions used as input to the parameterizations were those to which the samples were exposed to in the FRIDGE. The DREAM results are presented with typical uncertainties of the INPC parameterizations (Harrison et al., 2019; Marinou et al., 2019). The variability of DREAM results described by the +3h and -3h profiles would introduce variability in INPC estimations of 27%, 30% and 33% for H19i, D15i and U17i, respectively (not shown on the plot).

The DREAM results of D15i underestimate INPC in comparison with FRIDGE measurements. It should be noted that at 2.5 km height, DREAM underestimated the cloud-relevant dust concentrations in comparison with POLIPHON retrievals (Figure 5.2b), contributing to INPC underestimations. Predictions obtained using the mineralogy-sensitive parameterization (H19i) at -30°C and -25°C are between those obtained using mineralogy indifferent parameterizations D15i and U17i. At these temperatures H19i results are in agreement with UAV-FRIDGE measurements within the uncertainties. However, at -20°C , H19i underestimates INPC in comparison to D15i parameterization and UAV-FRIDGE measurements. To explain this result, it should be noted that D15i parameterization is based on particle concentration as input, and it is not affected by changes in particle size. On the other hand, H19i predictions are influenced by particle size and mineral composition of dust. At the temperatures used in the FRIDGE experiment ($> -30^{\circ}\text{C}$), quartz contribution to INPC is expected to be small, so the most of the H19i INPC can be attributed to feldspar. Majority of feldspar is present in the silt particles, while its efficiency as an INP source is reduced with increase of temperature. It should be noted that in this case, relative contribution of silt particles to total dust particle concentration is smaller than in the mean particle size distribution at the sources in the model domain. Therefore, because feldspar is mostly present in silt particles, the feldspar fraction of dust is reduced. This suggests that sedimentation of silt particles is a possible cause of the underestimation of H19i prediction of INPC when compared to D15i at -20°C . DREAM results of H19i show closer agreement with UAV-FRIDGE data at -25°C and -30°C , in comparison with the results of the mineralogy-indifferent parameterizations, but the sensitivity to mineral composition contributed to underestimation at -20°C in this case.

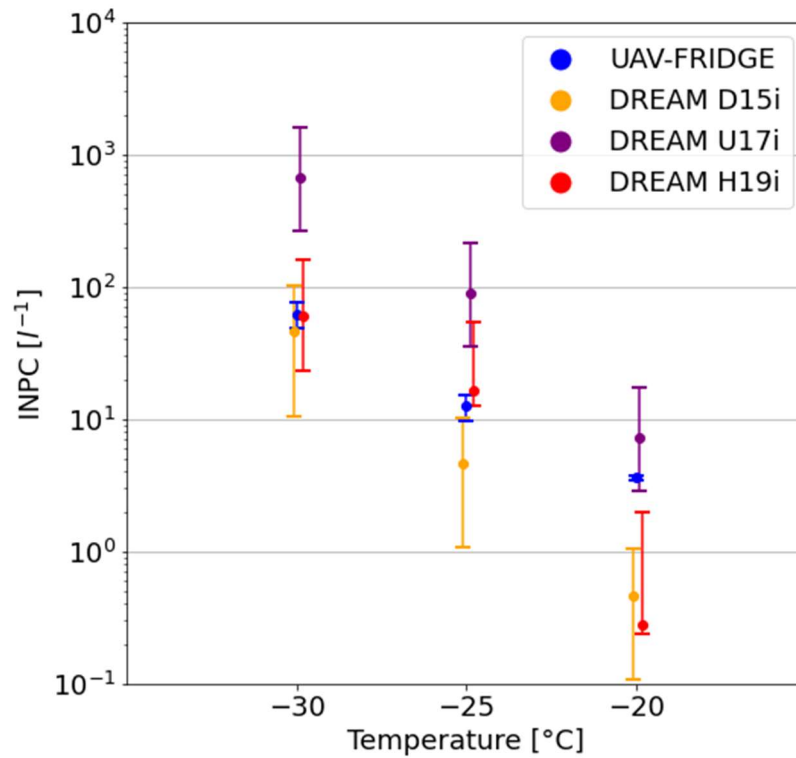


Figure 5.3 INPC prediction by DREAM on 21 April 2016 and the UAV-FRIDGE measurements for immersion freezing, as a function of temperature. The data points are slightly shifted from the actual temperature for clearer presentation. UAV-FRIDGE data are adapted from Marinou et al. (2019). Figure is adapted from Ilić et al. (2022).

5.4. Comparison with the IWC in Potenza

Qualitative comparisons of INPC prediction from the models can be made with ground-based or satellite observations of cloud properties such as IWC (Ničković et al., 2016). These comparisons are indicative in terms of model prediction of thermodynamic conditions and cloud-relevant dust concentrations as factors contributing to cloud process. For comparison of cloud properties, a cloud microphysics scheme fully coupled with a dust model is necessary. Observations from the Cloudnet station in Potenza were used to perform a qualitative comparison with the DREAM INPC prediction using the H19i_U17dsetup with the IWC product for the period of April 16-22 (Figure 5.4).

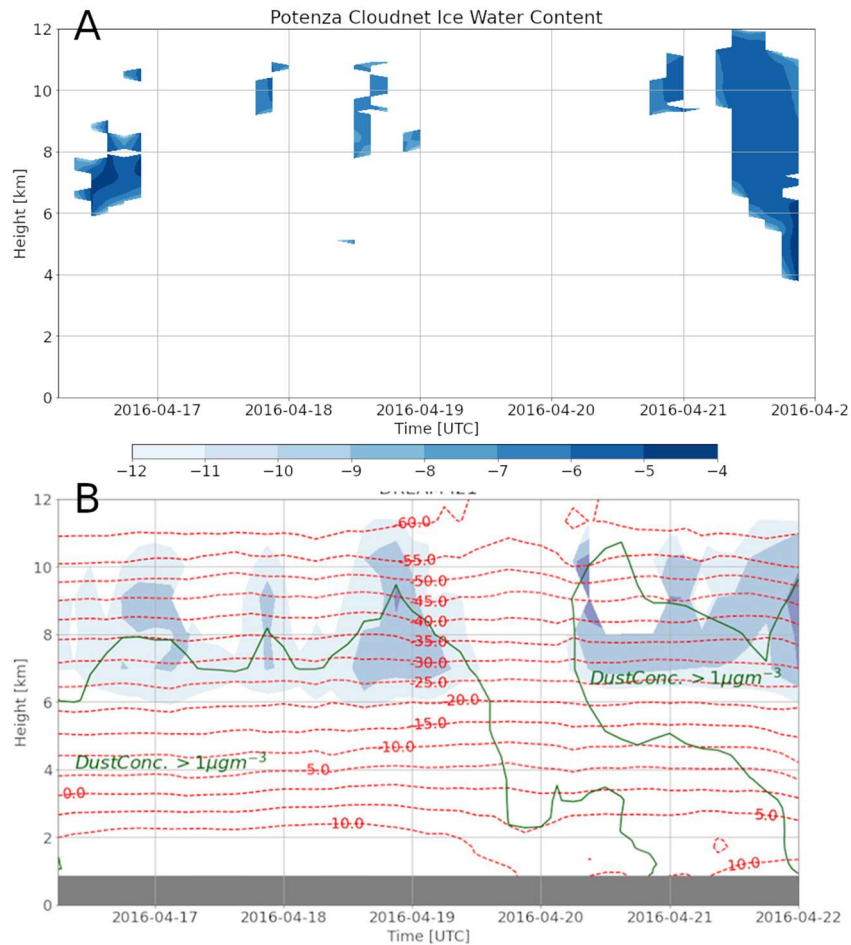


Figure 5.4 Ice water content retrieved in Potenza using the Cloudnet retrieval scheme coarse-grained to model resolution (A) and DREAM H19i_U17d INPC (B) from April 16 to 22. Green contour line represents $1 \mu\text{g}/\text{m}^3$ dust mass concentration. Adapted from Ilić et al. (2022).

During the period of measurements, DREAM predicted two Saharan dust plumes reaching Potenza. The dust-laden air masses and associated INPC were collocated with the observed cloud development. Due to westerly flow, the first dust plume was developing in the Mediterranean on April 14 and was above Potenza on April 16. The DREAM-predicted INPC production coincided with the observed clouds above 6 km. The dust plume was transported northward on April 17, reducing the dust concentrations. Cirrus cloud development on April 17 was not indicated by INPC predicted by the model. On April 18, covering the period of Po31 profile measurements, the observed clouds and the predicted INPC were vertically collocated. On April 19 - 20, advection of a drier air mass from northwest, with no dust present, was predicted by the model. Thus, dust related INPC were not predicted in that period. On April 21-22, another dust plume reached Potenza, influencing pre-frontal cloud development which was also indicated by the model INPC. The qualitative comparison in the case presented here indicates possible correlation between predicted INPC and observed IWC.

5.5 Comparison with the DARDAR Product during Dust Plume Overpasses

Since this version of the model does not include a microphysics scheme which takes predicted dust concentrations as an input, the discussion analyzes whether INPC parameterizations are a good proxy for ICNC estimation and whether the mineralogy-sensitive

parameterization presents a considerable improvement in INPC estimation. A recently published closure study presented the relationship between the INPC and ICNC in clouds at temperature ranges which promote immersion freezing and deposition nucleation mechanisms, based on ground-based active remote sensing (Ansmann et al., 2019b). In the three closure experiments, in which clouds formed in Saharan dust layers, the estimated INPC and ICNC values agreed within an order of magnitude. Previously discussed study of Marinou et al. (2019) presented results of DARDAR-Nice estimates with INPC values derived from remote sensing measurements. The cloud-relevant dust profiles were retrieved from CALIPSO measurements using the POLIPHON algorithm. Two immersion parameterizations (D15i and U17i) were used. DARDAR-Nice values were between the values of D15i and U17i within the errors of the two parameterizations.

While results of Ansmann et al., (2019) and Marinou et al., (2019) suggest that a reasonably good agreement (within an order of magnitude) can be expected between DREAM INPC and DARDAR-Nice, there are certain limitations that must be considered in this kind of comparison. The INPC parameterizations provide predictions of ice-initiation in clouds and not the ICNC values. The INPC can be considered as a reservoir of particles on which ice phase may initiate but not necessarily grow to the size of ice crystals that can be observed. The secondary ice production (SIP) processes at temperatures between -3°C and -8°C can be present in clouds, and contribute to the ICNC (Hallett and Mossop, 1974; Field et al., 2017). Due to the strong INPC dependence on temperature, high INPC values are expected close to the top of the upper aerosol–cloud layers. Additionally, liquid water droplets can be supercooled to temperatures around -37°C . In the following discussion an assumption is made that the ice crystals nucleate close to the cloud top and then grow and fall through the lower layers of clouds.

Following the results of Marinou et al. (2019), in this Chapter a comparison of vertical profiles of DREAM INPC and ICNC from the DARDAR-Nice product is discussed for two cases of mixed-phase clouds during A-train overpasses over dust plume in the Mediterranean. Overpass A was in the central Mediterranean on April 20 around 12 UTC. Overpass B was above east Mediterranean and Cyprus on April 21 around 12 UTC. The satellite overpasses and parts of the trajectories used in the analysis are shown in Figure 4.10. A qualitative comparison with CALIPSO satellite observations of the dust plume on April 20 and 21 is performed, as well. Specifically, CALIPSO subtyping products are used for that purpose (Figure 5.5). CALIPSO detected both the dust layers and clouds present on the top of the dust layers in both cases. In case of overpass B, additional presence of some pollution in the dust layers is also observed. The DREAM model successfully forecasted the dust advection (in space, top height, and time), as shown in the vertical cross sections of the dust plume. CALIPSO products show that there are also marine and dusty-marine (marine and dust) particles present in the lower troposphere of overpass A.

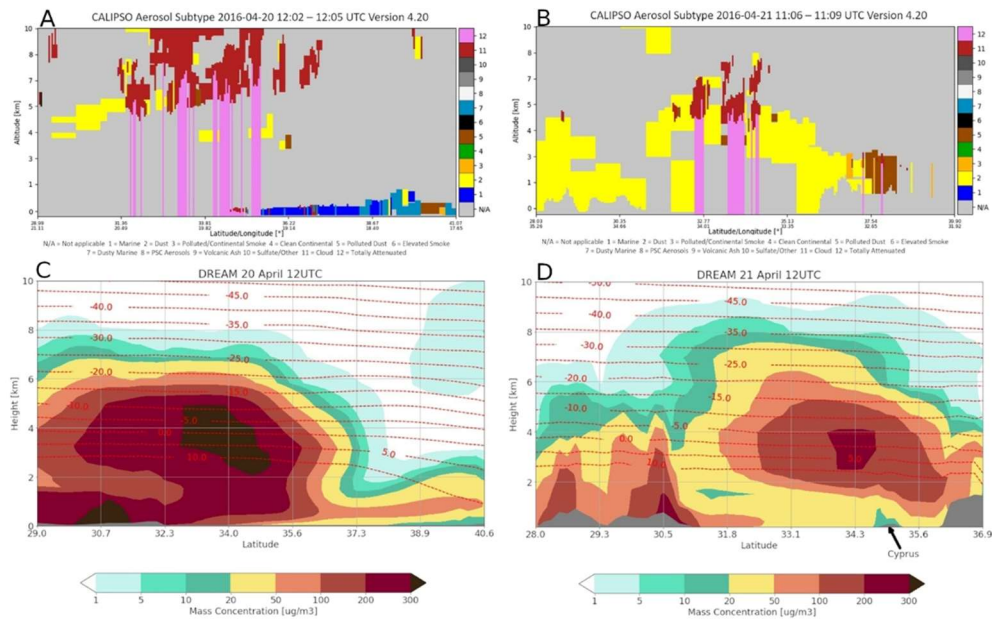


Figure 5.5 CALIPSO aerosol subtype and cloud presence products (A and B) and DREAM vertical cross section of dust concentrations (C and D) with isotherms (dashed red lines), along the satellite path during overpass A on April 20 and during overpass B on April 21. Adapted from Ilic et al. (2022).

Mean simulated dust concentration profiles considered in this part of the discussion show that there is significantly less dust in the atmosphere during the overpass B (Figure 5.6). Peak concentrations decreased from $253 \mu\text{g m}^{-3}$ to $184 \mu\text{g m}^{-3}$ and integrated dust load decreased from 1.1 g m^{-2} to 0.7 g m^{-2} . However, at heights between 6 km and 8 km, where the immersion freezing is likely to occur, there is more dust in the overpass B. Additionally, the model predicts a cooler atmosphere than in overpass A, shifting the immersion range to lower altitudes.

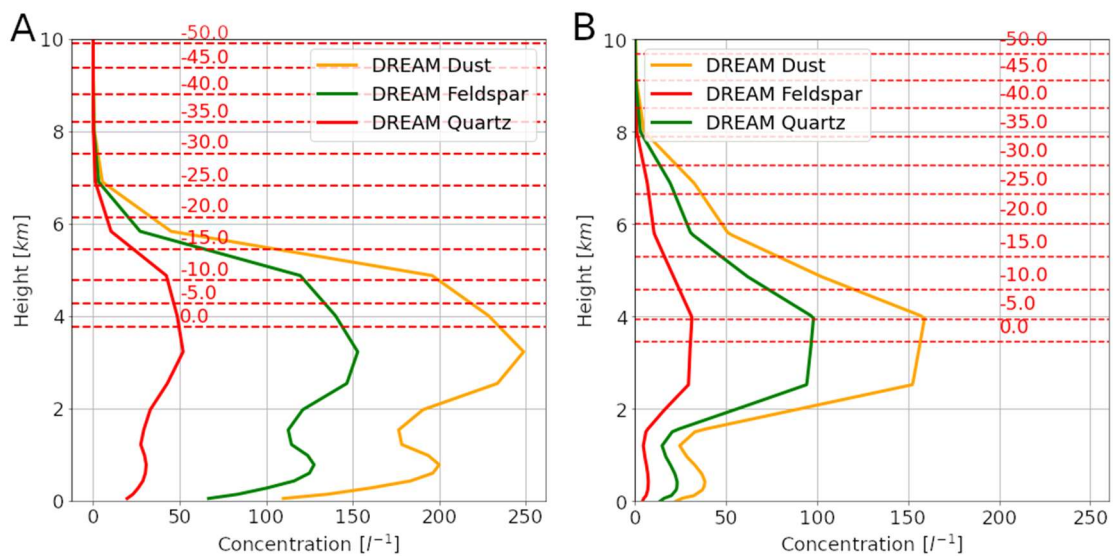


Figure 5.6 Vertical DREAM profiles of total dust (orange), feldspar (red) and quartz (green) concentrations, during overpass A on April 20 12UTC (A) and during overpass B on April 21 12UTC (B). Adapted from Ilić et al. (2022).

The vertical cross sections of DARDAR-Nice products along the satellite ground track during overpass are used to calculate the mean ICNC vertical profiles (Figure 5.7). It should be noted that DARDAR products can have some pixels misclassified as ice instead of mixed-phase clouds (Villanueva et al., 2020). However, in analyzed cases, all the profiles were classified as mixed-phase clouds. Average DARDAR-Nice product is calculated for ice crystal diameters greater than 5 μm , 25 μm and 100 μm . The relative uncertainties in the individual profiles in the overpass A are in the ranges: 15-83%, 14-79%, 10-85% for the mentioned diameters. In the overpass B, the uncertainties are in the ranges: 27-72%, 28-68%, 33-57%. The uncertainties are attributed to the uncertainties in the measurements used in DARDAR validation and possible homogeneous freezing or aggregation influencing the total ICNC. To calculate average INPC profiles from the DREAM model, the satellite track was used to locate the nearest model grid points to the locations of observed clouds

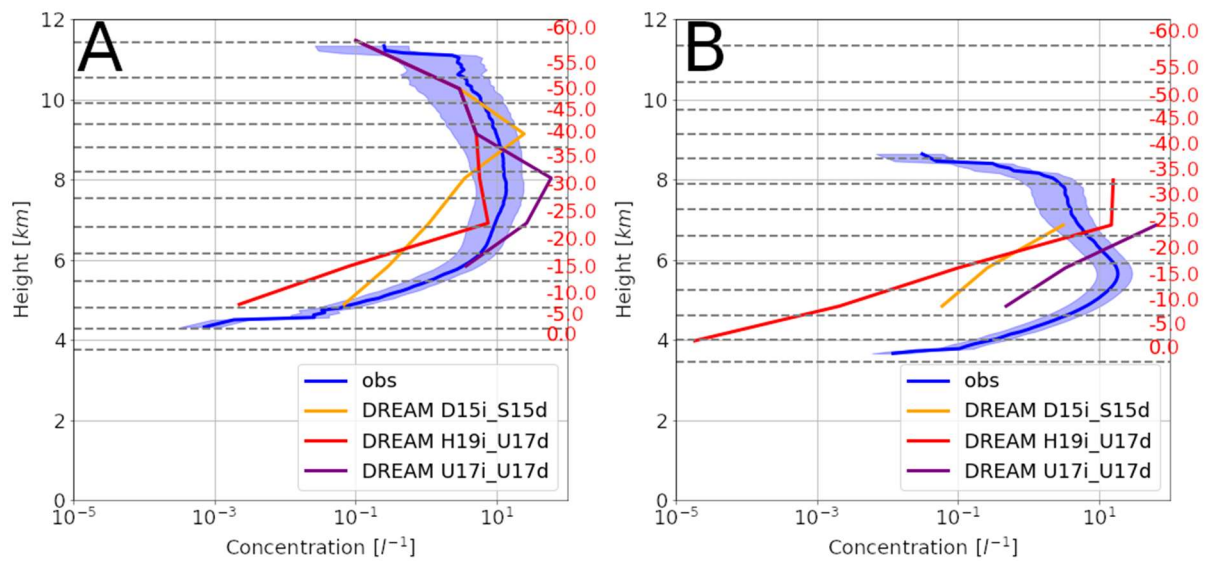


Figure 5.7 Comparison of DREAM-simulated INPC profiles using three model setups and DARDAR-Nice product during overpass A on April 20, 12UTC (A) and during overpass B on April 21, 12UTC (B). Solid blue line represents DARDAR ICNC for $D > 25 \mu\text{m}$, while the shaded blue area indicates $D > 100 \mu\text{m}$ (lower limit) and $D > 5 \mu\text{m}$ (upper limit) values.

Results presented in Figure 5.7 suggest that DREAM INPC parameterizations provide a good proxy of the vertical extent and distribution of the DARDAR ICNC in the mixed phase and cirrus clouds in overpass A. At the top of the cloud the three model setups agree with observations. At temperatures higher than -20°C , more ICNC are retrieved in comparison to the higher altitudes and in comparison, to the estimated INPC. A possible explanation can be in the assumption used by Ansmann et al. (2019) and Marinou et al. (2019) that high INPC values are expected close to the top of the upper aerosol–cloud layers, ice crystals increase in size and fall through the cloud. The model simulates only dust aerosols but the INPs at higher temperatures originating from biogenic sources could contribute to closer agreement with ICNC (Nickovic et al., 2016; O’Sullivan et al., 2018, Marinou et al., 2019). In overpass case B, DARDAR-Nice product shows a much smaller vertical extent, not completely covered by all three model setups, likely because of the coarser model vertical resolution as discussed in Chapter 4.1 and Chapter 5.2. In both A and B cases, DARDAR-Nice product predicts ICNC at heights where homogeneous nucleation is possible (around and below -37°C), so some of the crystals in the deposition temperature range can originate from processes not described by the

parameterizations used in the model setup. In overpass case B, DREAM estimates larger INPC than in overpass case A because of the previously discussed larger dust mass concentrations in the immersion temperature range above 6 km.

During transport, the efficiency of dust as an INP is affected by the physical aging and by the different contribution of quartz and feldspar fractions to total dust concentration. The physical aging of dust within a dust plume can be described as reduction of concentration in larger size bins due to sedimentation of particles (Figure 5.8). The particles in the two silt size bins with the effective radii of 1.3 μm and 2.2 μm are very efficient as INPs at temperatures below -30°C (Niemand et al., 2012). The H19i_U17d- and U17i_U17d-predicted INPC depend on ice nucleation active surface-site density (n_s) and dust particle size bin effective diameter, while the INP fraction in each size bin is strongly dependent on temperature. In overpass case B, U17i_U17d predicts a smaller INP fraction of total dust concentration than in overpass case A due to the warmer temperature at the same altitude. U17i uses some of the same data as the parameterizations by Niemand et al. (2012) and is on average producing n_s values a factor of 1.64 larger. Price et al. (2018) analyzed dust INPC in Atlantic and found that parameterization by Niemand et al. (2012) overestimated INPC in comparison to samples collected in aircraft measurements.

At temperatures higher than -25°C , H19i_U17d INPC maximum is lower than the ICNC maximum values by an order of magnitude. This setup shows the maximum INPC in the immersion mode, at -25°C where K-feldspar is the dominant INP source. The mineral composition of dust in the immersion range is changed during transport as indicated by quartz and feldspar content of dust in overpasses A and B, shown in Figure 5.8. It is estimated that overall, these changes in mineral composition would make the dust produce around 6% higher INPC at -35°C and up to 17% percent higher at -25°C . However, the total mass in silt bins was significantly reduced, mainly through deposition of larger particles, reducing this effect.

D15i_S15d setup estimates peak in INPC in the deposition mode and underestimates concentrations in immersion mode by an order of magnitude in comparison to ICNC. The difference in INPC estimation between overpasses A and B, based on D15i parameterization is caused by higher dust concentration in the immersion temperature range (Figure 5.7) and lower dust concentration in silt bins (Figure 5.8) in the overpass B. It should be considered in this analysis that the D15i parameterization is the only one used in this Thesis which depends only on particle number concentration. Marinou et al. (2019) already established that S15d overestimates the INPC, while D15i values are within an order of magnitude of in situ measurements.

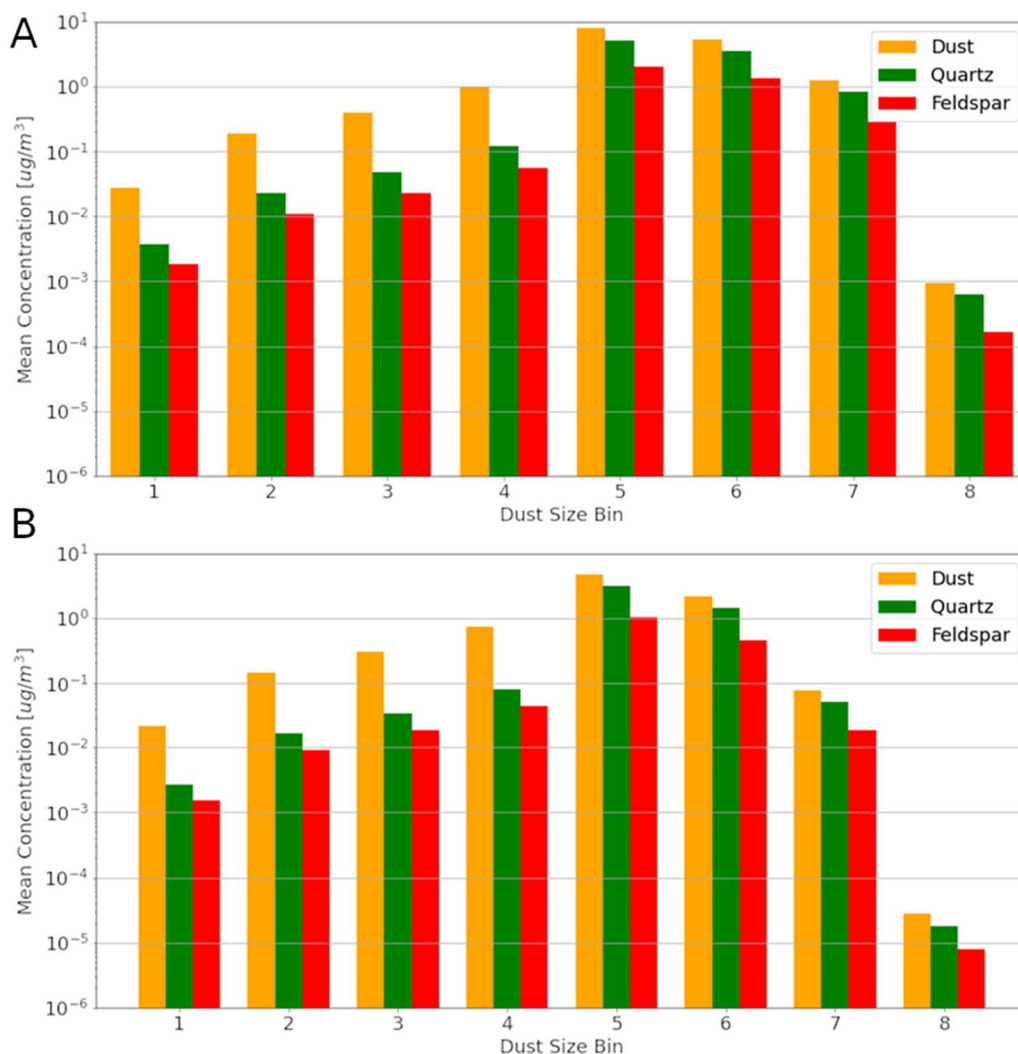


Figure 5.8 Vertically integrated mean dust concentration from DREAM within the DARDAR cross-section and for the immersion range for each size bin on April 20 at 12UTC (A) and April 21 at 12UTC (B). Adapted from Ilić et al. (2022).

Table 3 shows the evaluation of applicability of the three INP parameterization setups in DREAM, with the DARDAR ICNC as a reference in the two studied cases. As discussed previously, H19i_U17d and U17i_U17d INPC capture the general shape of the ICNC profile in case of overpass A. D15i_S15d shows the lowest bias, while positioning the peak concentrations above the observed maximum of INPC. U17i_U17d-predicted INPC is one order of magnitude larger than DARDAR-derived ICNC. These results agree with the results by Marinou et al. (2019) of comparison of lidar-derived INPC with DARDAR-derived ICNC for the two immersion freezing parameterizations (D15i and U17i). In overpass B, DREAM is less successful in predicting the shape of the ICNC profiles and this inevitably largely affect the comparison. D15i INPC prediction is lower than the ICNC, U17i_U17d predicts INPC in a limited altitude range, and H19i_U17d INPC decreases sharply at lower altitudes. In both cases (A and B), H19i_U17d had most success in predicting the vertical extent and the shape of the ICNC profile. Additionally, it shows the least root mean square difference when compared to ICNC.

Table 5.3 Evaluation of DREAM INPC - DARDAR ICNC comparison for three model setups. Adapted from Ilić et al. (2022).

	The Overpass A			The Overpass B		
	H19i_U17d	D15i_S15d	U17i_U17d	H19i_U17d	D15i_S15d	U17i_U17d
Mean difference [$\mu\text{g l}^{-1}$]	-4.1	-2.2	11.1	-1.3	-10.5	7.0
Root Mean Square Difference [$\mu\text{g l}^{-1}$]	4.9	7.6	19.0	10.7	12.1	25.6

5.5 Comparison with the IWP

To discuss the performance of DREAM INPC setups on the prediction of horizontal patterns of ice clouds, the DREAM mineral fractions and INPC values are compared with the MSG-SEVIRI (METEOSAT second generation - Spinning Enhanced Visible and InfraRed Imager) ice water path (IWP) product from the CLAAS-2 dataset (Ničković et al., 2016). Mineral fractions are presented on horizontal maps, using mean concentrations calculated for model levels in the immersion temperature range (Figures 5.9 and 5.11). The corresponding columnar values of IWP and INPC are presented on horizontal maps, as well, in Figures 5.10 and 5.12. Discussion is related to areas of overlap of predicted dust INPs and cloud ice, described by IWP. Following Ničković et al., (2016), to describe the success of dust INPs as cloud ice predictors the areas where columnar INPC and IWP overlap are evaluated as "hits", regions where clouds are observed but INPC are not predicted as "misses", and those where INPC are predicted but clouds are not observed as "false alarms". The usefulness of columnar INP related to dust mineral composition as IWP predictor is also discussed. Two dust events are analyzed: one that was observed as an intermediate dust event from April 14 to 16 at Nicosia corresponding to profiles Ni21 and Ni22 presented in previous sections; and a dust plume related to profiles Po31, Ni31 and Ni32 between April 18 and April 21. The horizontal maps do not correspond exactly in time to the mentioned profiles since MSG-SEVIRI measurements are available only during daytime.

Results of INPC prediction in these two events are similar in terms of model success in predicting presence of clouds. Therefore, the results described here correspond to the specific geographical regions in which consistent model behavior can be seen. In certain cases, it is pointed out if a different prediction pattern occurs. In both dust events, feldspar fraction was between 16% and 26% in most of the model domain, the second event having slightly higher values. Lower values were generally predicted in eastern Europe, which can be attributed to

sedimentation of silt particles. Local maxima of feldspar fraction reached values of up to 30% in Europe and Mediterranean. The vertically integrated INPCs predicted using the three DREAM model setups differ from each other by up to two orders of magnitude in the columnar values of INPC, which is a conclusion also reached when vertical profiles were analyzed. H19i_U17d INPC falls between the U17i_U17d and D15i_S15d values. In columnar INPC values, U17d deposition nucleation parameterization is used in two setups, H19i_U17d and U17i_U17d, which makes differences between mineralogy-indifferent and mineralogy-sensitive parameterizations less pronounced. D15i_S15d setup predicts more localized spots with significant INPC, as opposed to more spread regions of significant INPC predicted by other two setups. This is not a clear indication of whether a certain parameterization setup is a better choice in cloud prediction. INPC represents a reservoir of particles that can participate in formation of clouds, while other processes not represented by this type of parameterizations (e.g., homogenous freezing, secondary ice production) can significantly increase the ice crystal concentration.

In all the presented cases, the largest differences between the setups can be noticed in the southern part of model domain, to the west over the Atlantic and in the northeast near Caspian Sea. In the eastern part of the model domain, consistently, INPC prediction indicates possible presence of clouds which are not observed. H19i_U17d predicts false alarm areas with less probability than U17i_U17d, possibly to the effect of mineralogy-sensitive immersion parameterization. D15i_S15d predicts the lowest concentrations and, therefore, smaller false alarm areas, but also less probability of predicting observed clouds over the Atlantic. In both events, over the Atlantic, south of 40N, model does not predict all the observed clouds. Since these are the areas above the ocean, it is possible that other types of aerosols could have contributed to ice formation. In the first event, the mineralogy-indifferent setup D15 did not predict clouds in west and south-central Mediterranean. However, in the second event, in the southern parts of Europe and in the Mediterranean, the H19i_U17d forecast patterns are close to the observed ones. Results presented here indicate that U17i_U17d and H19i_U17d model setups predict cloud ice with higher probability than D15i_S15d over the Mediterranean Sea and the Atlantic Ocean. Feldspar content does play a role in INPC prediction. The D15i setup can produce overestimations, as seen in the east, although smaller than U17i_U17d, but can maintain a lower area of clouds which are not predicted. Further investigation and possible coupling with a microphysics scheme could provide clearer conclusion about usefulness of increased model complexity when simulating mineral components of dust in predicting the horizontal distribution of clouds.

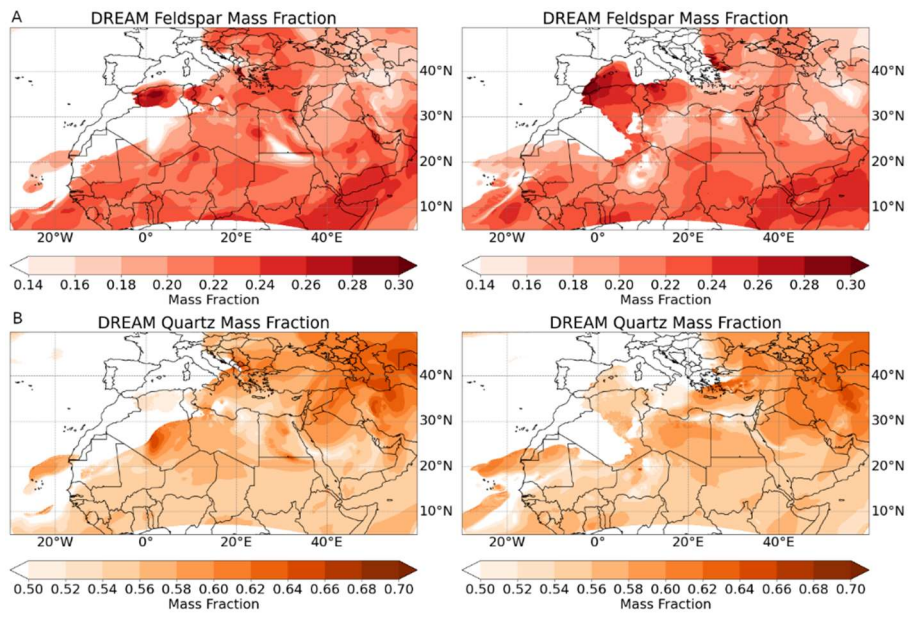


Figure 5.9 DREAM-simulated feldspar (A) and quartz (B) mineral fractions in the immersion temperature range on April 14, 12UTC (1st column) and April 15, 12UTC (2nd column).

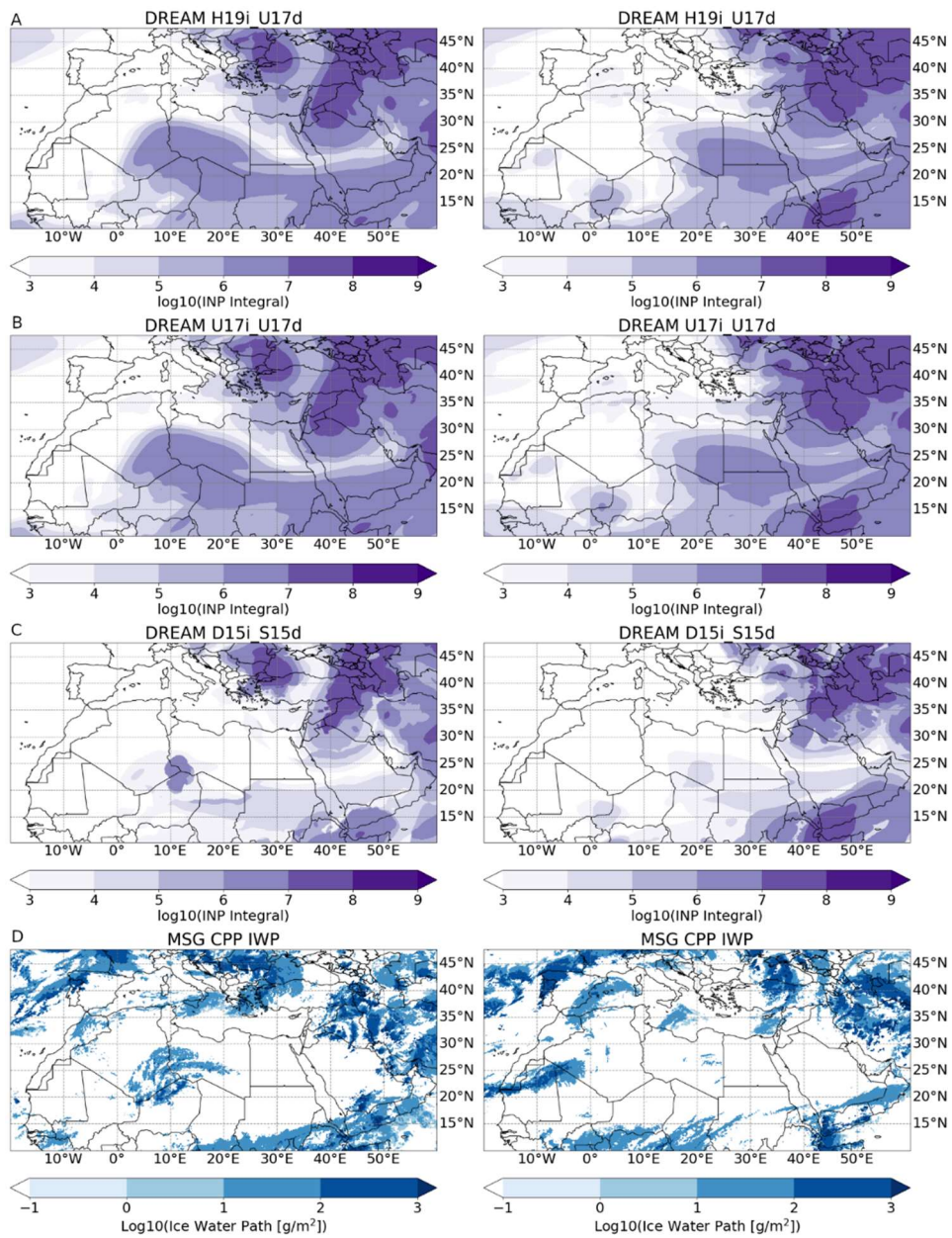


Figure 5.10 DREAM-simulated integrated INPC values for H19i_U17d (A) U17i_U17d (B) and D15i_S15d (C) setups. MSG IWP product (D) on April 14, 12UTC (left) and April 15, 12UTC (right).

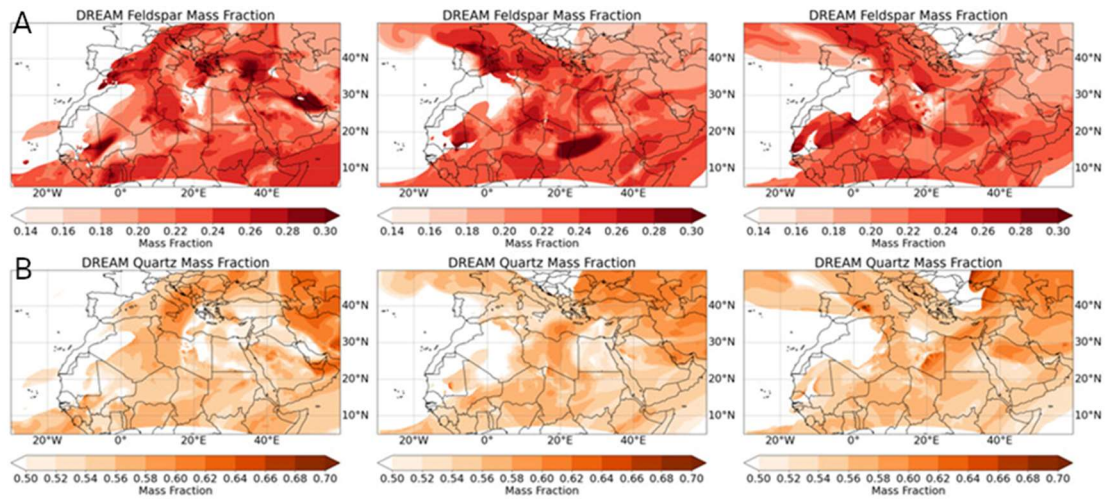


Figure 5.11 DREAM-simulated feldspar (A) and quartz (B) mineral fractions in the immersion temperature range on April 18, 15UTC (1st column); April 20, 12UTC (2nd column); and April 21, 12UTC (3rd column). Adapted from Ilić et al. (2022).

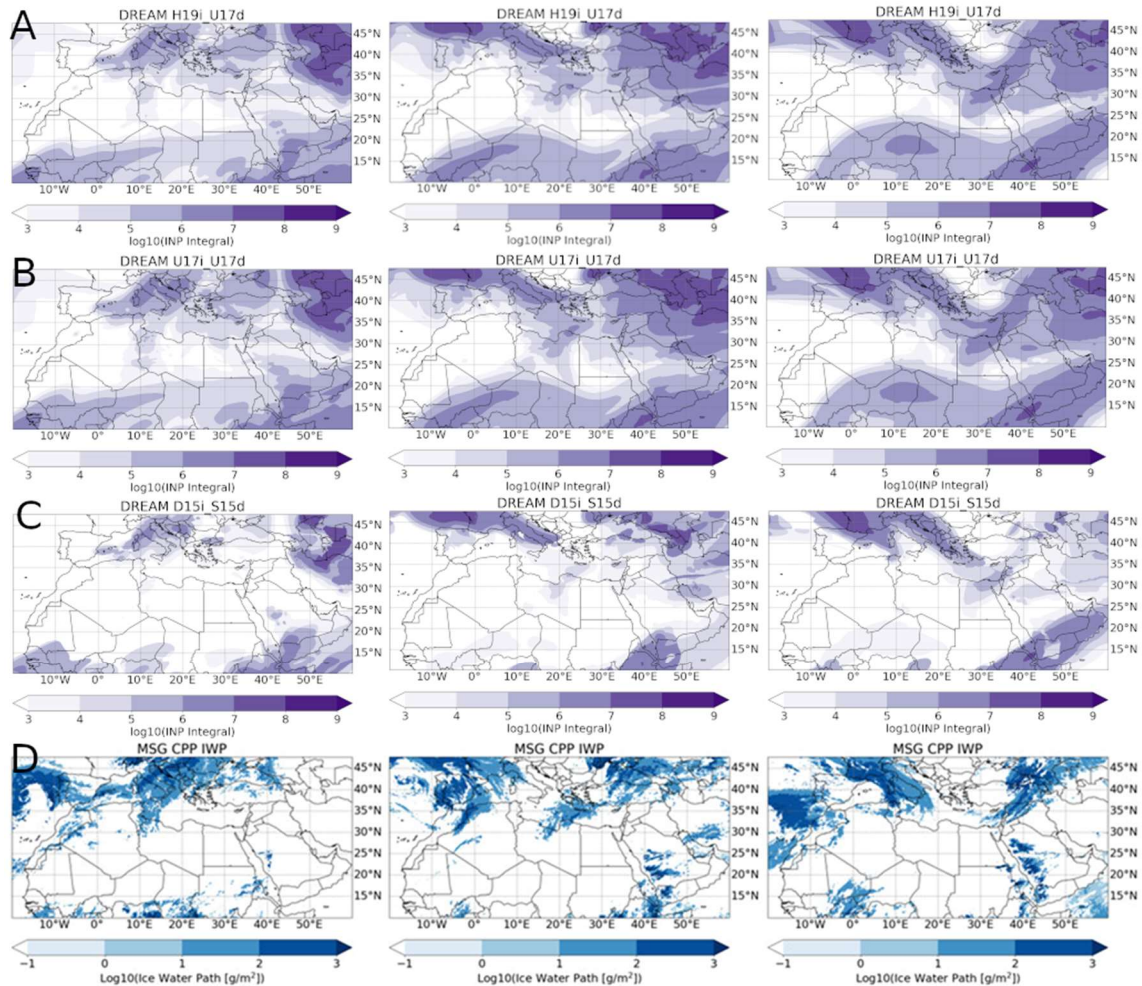


Figure 5.12 DREAM-simulated integrated INPC values for H19i_U17d (A), U17i_U17d (B), and D15i_S15d (C) setups. MSG IWP product (D) on April 18, 15UTC (left); April 20, 12UTC (center) and April 21, 12UTC (right). Adapted from Ilić et al. (2022).

6 Summary and Conclusions

For the first time, a mineralogy-sensitive INPC parameterization has been implemented in an operational, regional dust-atmosphere coupled model. The results of this Thesis present the outcome of implementing such a parameterization in DREAM and comparison of the model results with remote sensing and in situ measurements. The limitations of this approach and the outlooks for a more detailed coupling of dust concentrations with a microphysics scheme, that is on the pathway to future development, are discussed.

Specific numerical experiments were performed to simulate the transport of dust in the case of mineralogy-indifferent parameterizations and of feldspar and quartz minerals for the mineralogy-sensitive parameterizations. For the mineralogy-indifferent parameterizations (D15i, U17i, S15d, U17d), cloud-relevant dust concentrations were used as input. For the mineralogy-sensitive parameterization (H19i), feldspar and quartz concentrations were used. Through analysis of the results of a long-term study of model performance and several analyzed cases of dust episodes in the Mediterranean, the results of mineralogy-sensitive parameterization have been compared to the mineralogy-indifferent parameterizations and observations. Vertical profiles of cloud-relevant dust concentrations, and INPC from the model and ground-based lidar measurements, ICNC satellite retrievals, and in situ INPC were analyzed. Additionally, qualitative comparisons were performed with vertical profiles of IWC from a ground-based cloud radar and horizontal distribution of IWP from satellite retrievals. Differences between the parameterizations and observed values are linked to cloud-relevant dust concentrations and thermodynamic quantities. Based on the results of a long-term systematic study to which the results of DREAM were contributed and based on numerical experiment case studies in the Mediterranean in April 2016, the following conclusions have been drawn:

- Systematic evaluations of dust concentrations forecast, and the selected cases studied in more detail confirmed that the DREAM model successfully simulates the evolution and vertical distribution of the dust plume, slightly overestimating the height of the layer when compared to remote sensing retrievals.
- In the case studies of comparison with POLIPHON, DREAM typically overestimated the dust concentration, especially in the low concentration cases. Furthermore, a lower correlation coefficient than in the systematic study was obtained. The predicted altitude of the dust layer was above the average altitude for the east cluster of EARLINET stations in the systematic study.
- Based on the available data, it is difficult to discriminate which effect could be the dominant cause of differences in dust concentrations between the model and the observations in each case. Parameterizations of the dust source strength, sedimentation, and wet scavenging or a combination of these effects along with the model horizontal and vertical resolutions can all be the cause of the discrepancies. In other studies, it has been shown that the data assimilation scheme included in the model simulation cycle can improve the forecasts.
- In the vertical profiles, the three INPC setups implemented in the model (mineralogy-sensitive H19i_U17d and mineralogy-indifferent D15i_S15d and U17i_U17d) differ by about an order of magnitude. H19i_U17d presents a sharp maximum in INPC at -25°C and a sharper decrease of INPC at temperatures higher than -20°C in comparison with other

setups, as the INPC in H19i parameterization is dominated by the feldspar efficiency as the INP.

- The mineralogy-sensitive immersion freezing parameterization agrees with the in situ INPC measurements at -30°C and -25°C , but underestimates the INPC at -20°C , possibly due to the sedimentation of silt particles and consequent reduction of feldspar fraction of dust.
- The direct comparisons of DREAM INPC and DARDAR ICNC show agreement within an order of magnitude for all model setups. In the two presented cases, the shape of vertical distribution and the vertical extent of the INPC predicted by the H19i_U17d model setup showed the closest agreement with DARDAR ICNC. This implies that the mineralogy-sensitive setup may be the best proxy of ICNC in the atmosphere, but additional experiments and model validation are needed to explore this hypothesis.
- In comparison to mineralogy-indifferent setups, the mineralogy-sensitive setup is more sensitive to particle size, as feldspar is dominantly present in silt particles in the model. Variations in the feldspar content have shown to be able to influence the productivity of dust as an INP by 6% at -35°C and up to 17% at -25°C . This effect is reduced by the reduction in overall feldspar content by physical aging of dust through sedimentation of feldspar silt particles.
- The horizontal distribution of INPs has shown that U17i_U17d and H19i_U17d model setups have a higher probability to predict the presence of cold clouds than D15i_S15d over the Atlantic and Mediterranean. The similarity of the results of U17i_U17d and H19i_U17d implies that the horizontal distribution of the predicted values is strongly influenced by the U17d deposition nucleation parameterization. However, they show differences in predicted INPC over the Atlantic and the Caspian Sea region due to differences in feldspar content.

The modeling results presented in this Thesis agree with previous in situ and laboratory studies on the significance of including the dust mineral composition into INPC prediction by numerical models. Using mineralogy-sensitive parameterizations is a step forward in quantifying the role dust plays as INP. The main limitations of the current version of the model are a consequence of the implementation of the INPC parameterizations. While DREAM is fully coupled in terms of dust transport and INPC predictions, dust concentrations are not coupled with the cloud microphysics scheme. Therefore, the assumption has been made that INPC would correspond to the ICNC which, depending on the secondary ice production, homogeneous nucleation, and ice crystal aggregation, may introduce additional uncertainties. Nevertheless, a more comprehensive evaluation using a database of in situ measurements would give us a clearer view of the importance of representing dust mineral composition when modeling cloud ice initiation processes. Additionally, it would give information about how well the particles collected by the surface measurements or by the low troposphere UAV flights correspond to the particles present at altitudes where, due to the thermodynamic conditions, ice initiation mechanisms are possible. In future development and numerical experiments, a dust model with a fully coupled microphysics scheme would be able to overcome some of the limitations of this study. In such a model, depending on the complexity of the microphysics scheme ICNC concentration may be calculated. Further development of the aerosol model itself can lead to the representation of other aerosol species. Other aerosol types, such as biogenic particles contribute to INPC at higher temperatures or remote ocean locations, especially in the Southern Hemisphere can contribute to INPC. Future experimental campaigns would ideally be able to provide in situ observations of aerosol concentrations, INPC, and ICNC. This would

facilitate further development of current parameterizations and improve the model validation capabilities leading to further refinement and improvements in parametrizing the INPC and constraining the effects of INPs on cloud processes.

7 References

- Abbatt, J. P. , 2003. Interactions of atmospheric trace gases with ice surfaces: Adsorption and reaction. *Chem. Rev.*, 103, 4783– 4800, doi:10.1021/cr0206418.
- Alexandri, G., Georgoulas, A. K., Zanis, P., Katragkou, E., Tsikerdekis, A., Kourtidis, K., and Meleti, C., 2015. On the ability of RegCM4 regional climate model to simulate surface solar radiation patterns over Europe: an assessment using satellite-based observations, *Atmos. Chem. Phys.*, 15, 13195–13216, <https://doi.org/10.5194/acp-15-13195-2015>.
- Althausen, D., Engelmann, R., Baars, H., Heese, B., Ansmann, A., Müller, D., & Komppula, M., 2009. Portable Raman Lidar PollyXT for Automated Profiling of Aerosol Backscatter, Extinction, and Depolarization, *Journal of Atmospheric and Oceanic Technology*, 26(11), 2366-2378. Retrieved Oct 18, 2021, from https://journals.ametsoc.org/view/journals/atot/26/11/2009jtecha1304_1.xml.
- Althausen, D., Engelmann, E., Baars, H., Heese, B., Kanitz, T., Komppula, M., Giannakaki, E., Pfüller, A., Silva, A. M., Preißler, J., Wagner, F., Rascado, J. L., Pereira, S., Lim, J. H., Ahn, J. Y., Tesche, M., and Stachlewska, I. S., 2013. PollyNET – a network of multiwavelength polarization Raman lidars, in: *Proc. SPIE 8894, Lidar Technologies, Techniques, and Measurements for Atmospheric Remote Sensing IX*, 88940I, 22 October 2013, Dresden, Germany, 8894, doi:10.1117/12.2028921.
- Amiridis, V., Marinou, E., Tsekeri, A., Wandinger, U., Schwarz, A., Giannakaki, E., Mamouri, R., Kokkalis, P., Biniotoglou, I., Solomos, S., Herekakis, T., Kazadzis, S., Gerasopoulos, E., Proestakis, E., Kottas, M., Balis, D., Papayannis, A., Kontoes, C., Kourtidis, K., Papagiannopoulos, N., Mona, L., Pappalardo, G., Le Rille, O., and Ansmann, A., 2015 LIVAS: a 3-D multi-wavelength aerosol/cloud database based on CALIPSO and EARLINET, *Atmos. Chem. Phys.*, 15, 7127–7153, <https://doi.org/10.5194/acp-15-7127-2015>.
- Ansmann, A., Tesche, M., Seifert, P., Groß, S., Freudenthaler, V., Apituley, A., Wilson, K. M., Serikov, I., Linné, H., Heinold, B., Hiebsch, A., Schnell, F., Schmidt, J., Mattis, I., Wandinger, U., Wiegner, M., 2011a. Ash and fine-mode particle mass profiles from EARLINET-AERONET observations over central Europe after the eruptions of the Eyjafjallajökull volcano in 2010, *J. Geophys. Res.*, 116, D00U02, doi:10.1029/2010JD015567.
- Ansmann, A., Petzold, A., Kandler, K., Tegen, I., Wendisch, M., Müller, D., Weinzierl, B., Müller, T., and Heintzenberg, J., 2011b. Saharan Mineral Dust Experiments SAMUM–1 and SAMUM–2: what have we learned?, *Tellus B: Chemical and Physical Meteorology*, 63:4, 403-429, DOI: [10.1111/j.1600-0889.2011.00555.x](https://doi.org/10.1111/j.1600-0889.2011.00555.x).
- Ansmann, A., Seifert, P., Tesche, M., & Wandinger, U., 2012. Profiling of fine and coarse particle mass: case studies of Saharan dust and Eyjafjallajökull/Grimsvötn volcanic plumes, *Atmos. Chem. Phys.*, 12, 9399–9415, doi:10.5194/acp-12-9399-2012.
- Ansmann, A., Rittmeister, F., Engelmann, R., Basart, S., Jorba, O., Spyrou, C., Remy, S., Skupin, A., Baars, H., Seifert, P., Senf, F., and Kanitz, T., 2017. Profiling of Saharan dust from the Caribbean to western Africa – Part 2: Shipborne lidar measurements versus

- forecasts, *Atmos. Chem. Phys.*, 17, 14987–15006, <https://doi.org/10.5194/acp-17-14987-2017>.
- Ansmann, A., Mamouri, R.-E., Bühl, J., Seifert, P., Engelmann, R., Hofer, J., Nisantzi, A., Atkinson, J. D., Kanji, Z. A., Sierau, B., Vrekoussis, M., and Sciare, J., 2019a. Ice-nucleating particle versus ice crystal number concentration in altocumulus and cirrus layers embedded in Saharan dust: a closure study, *Atmos. Chem. Phys.*, 19, 15087–15115, <https://doi.org/10.5194/acp-19-15087-2019>.
- Ansmann, A., Mamouri, R.-E., Hofer, J., Baars, H., Althausen, D., & Abdullaev, S. F., 2019b. Dust mass, cloud condensation nuclei, and ice-nucleating particle profiling with polarization lidar: updated POLIPHON conversion factors from global AERONET analysis, *Atmos. Meas. Tech.*, 12, 4849–4865, <https://doi.org/10.5194/amt-12-4849-2019>.
- Antuña-Marrero, J. C., Landulfo, E., Estevan, R., Barja, B., Robock, A., Wolfram, E., Ristori, P., Clemesha, B., Zaratti, F., Forno, R., Armandillo, E., Bastidas, Á. E., de Frutos Baraja, Á. M., Whiteman, D. N., Quel, E., Barbosa, H. M. J., Lopes, F., Montilla-Rosero, E., and Guerrero-Rascado, J. L., 2017. LALINET: The First Latin American–Born Regional Atmospheric Observational Network. *Bulletin of the American Meteorological Society* 98, 6, 1255–1275, available from: < <https://doi.org/10.1175/BAMS-D-15-00228.1>>
- Atkinson, J. D., Murray, B. J., Woodhouse, M. T., Whale, T. F., Baustian, K. J., Carslaw, K. S., Dobbie, S., O’Sullivan, D., Malkin, T. L., 2013. The importance of feldspar for ice nucleation by mineral dust in mixed-phase clouds, *Nature*, 498, 355–358.
- Baars, H., Kanitz, T., Engelmann, R., Althausen, D., Heese, B., Komppula, M., Preißler, J., Tesche, M., Ansmann, A., Wandinger, U., Lim, J.-H., Ahn, J. Y., Stachlewska, I. S., Amiridis, V., Marinou, E., Seifert, P., Hofer, J., Skupin, A., Schneider, F., Bohlmann, S., Foth, A., Bley, S., Pfüller, A., Giannakaki, E., Lihavainen, H., Viisanen, Y., Hooda, R. K., Pereira, S. N., Bortoli, D., Wagner, F., Mattis, I., Janicka, L., Markowicz, K. M., Achtert, P., Artaxo, P., Pauliquevis, T., Souza, R. A. F., Sharma, V. P., van Zyl, P. G., Beukes, J. P., Sun, J., Rohwer, E. G., Deng, R., Mamouri, R.-E., and Zamorano, F., 2016. An overview of the first decade of PollyNET: an emerging network of automated Raman-polarization lidars for continuous aerosol profiling, *Atmos. Chem. Phys.*, 16, 5111–5137, <https://doi.org/10.5194/acp-16-5111-2016>.
- Balkanski, Y., Schulz, M., Claquin, T., and Guibert, S., 2007. Reevaluation of Mineral aerosol radiative forcings suggests a better agreement with satellite and AERONET data, *Atmos. Chem. Phys.*, 7, 81–95, doi:10.5194/acp-7-81-2007.
- Baker, A. R. and Jickells, T. D., 2006. Mineral particle size as a control on aerosol iron solubility, *Geophys. Res. Lett.*, 33, L17608, doi: 10.1029/2006GL026557.
- Basart, S., Pérez, C., Nickovic, S., Cuevas, E., Baldasano, J., 2012. Development and evaluation of the BSCDREAM8b dust regional model over northern Africa, the Mediterranean and the Middle East. *Tellus B* 64, 18539. <https://doi.org/10.3402/tellusb.v64i0.18539>.
- Bellouin, BN., Quaas, J., Gryspeerdt, E., Kinne, S., Stier, P., Watson-Parris, D., Boucher, O., Carslaw, K. S., Christensen, M., Daniau, A.-L., Dufresne, J.-L., Feingold, G., Fiedler, S.,

- Forster, P., Gettelman, A., Haywood, J. M., Lohmann, U., Malavelle, F., Mauritsen, T., McCoy, D. T., Myhre, G., Mülmenstädt, J., Neubauer, D., Possner, A., Rugenstein, M., Sato, Y., Schulz, M., Schwartz, S. E., Sourdeval, O., Storelvmo, T., Toll, S. E., Winker, D., and Stevens, B., 2020. Bounding global aerosol radiative forcing of climate change. *Reviews of Geophysics*, 58, e2019RG000660. Bounding Global Aerosol Radiative Forcing of Climate Change - Bellouin - 2020 - Reviews of Geophysics - Wiley Online Library.
- Benas, N., Finkensieper, S., Stengel, M., van Zadelhoff, G.-J., Hanschmann, T., Hollmann, R., and Meirink, J. F., 2017. The MSG-SEVIRI-based cloud property data record CLAAS-2, *Earth Syst. Sci. Data*, 9, 415-434, <https://doi.org/10.5194/essd-9-415-2017>.
- Benedetti, A., Morcrette, J.-J., Boucher, O., Dethof, A., Engelen, R. J., Fisher, M., Flentjes, H., Huneus, N., Jones, L., Kaiser, J. W., Kinne, S., Mangold, A., Razinger, M., Simmons, A. J., Suttie, M., and the GEMS-AER team, 2009. Aerosol analysis and forecast in the ECMWF Integrated Forecast System: 2. Data assimilation, *J. Geophys. Res.*, 114, D13205, <https://doi.org/10.1029/2008JD011115>.
- Biniotoglou, I., Basart, S., Alados-Arboledas, L., Amiridis, V., Argyrouli, A., Baars, H., Baldasano, J. M., Balis, D., Belegante, L., Bravo-Aranda, J. A., Burlizzi, P., Carrasco, V., Chaikovsky, A., Comerón, A., D'Amico, G., Filioglou, M., Granados-Muñoz, M. J., Guerrero-Rascado, J. L., Ilic, L., Kokkalis, P., Maurizi, A., Mona, L., Monti, F., Muñoz-Porcar, C., Nicolae, D., Papayannis, A., Pappalardo, G., Pejanovic, G., Pereira, S. N., Perrone, M. R., Pietruczuk, A., Posyniak, M., Rocadenbosch, F., Rodríguez-Gómez, A., Sicard, M., Siomos, N., Szkop, A., Terradellas, E., Tsekeri, A., Vukovic, A., Wandinger, U., and Wagner, J., 2015. A methodology for investigating dust model performance using synergistic EARLINET/AERONET dust concentration retrievals, *Atmos. Meas. Tech.*, 8, 3577–3600, <https://doi.org/10.5194/amt-8-3577-2015>.
- Boose, Y., Welti, A., Atkinson, J., Ramelli, F., Danielczok, A., Bingemer, H. G., Plötze, M., Sierau, B., Kanji, Z. A., and Lohmann, U., 2016. Heterogeneous ice nucleation on dust particles sourced from nine deserts worldwide – Part 1: Immersion freezing, *Atmos. Chem. Phys.*, 16, 15075–15095, <https://doi.org/10.5194/acp-16-15075-2016>.
- Bösenberg, J., Ansmann, A., Baldasano, J. M., Balis, D., Böckmann, C., Calpini, B., Chaikovsky, A., Flamant, P., Hagard, A., Mitev, V., Papayannis, A., Pelon, J., Resendes, D., Schneider, J., Spinelli, N., Trickl, T., Vaughan, G., Visconti, G., and Wiegner, M., 2001. EARLINET: a European Aerosol Research Lidar Network, in: *Advances in Laser Remote Sensing*, edited by: Dabas, A., Loth, C., and Pelon, J., Ecole polytechnique, Palaiseau Cedex, France, 155–158.
- Bösenberg, J., Matthias, V., Amodeo, A., Amoiridis, V., Ansmann, A., Baldasano, J. M., Balin, I., Balis, D., Böckmann, C., Boselli, A., Carlsson, G., Chaikovsky, A., Chourdakis, G., Comeron, A., De Tomasi, F., Eixmann, R., Freudenthaler, V., Giehl, H., Grigorov, I., Hågård, A., Iarlori, M., Kirsche, A., Kolarov, G., Komguem, L., Kreipl, S., Kumpf, S., Larchevêque, G., Linné, H., Matthey, R., Mattis, I., Mekler, A., Mironova, I., Mitev, V., Mona, L., Müller, D., Music, S., Nickovic, S., Pandolfi, M., Papayannis, A., Pappalardo, G., Pelon, J., Pérez, C., Perrone, M. R., Persson, R., Resendes, D. P., Rizi, V., Rocadenbosch, F., Rodrigues, J. A., Sauvage, L., Schneidenbach, L., Schumacher, R., Shcherbakov, V., Simeonov, V., Sobolewski, P., Spinelli, N., Stachlewska, I., Stoyanov, D., Trickl, T., Tsaknakis, G., Vaughan, G., Wandinger, U., Wang, X., Wiegner, M.,

- Zavrtanik, M., and Zerefos, C., 2003. EARLINET: a European Aerosol Research Lidar Network to Establish an Aerosol Climatology, MPI-Report 348, Hamburg.
- Boucher, O., Randall, D., Artaxo, P., Bretherton, C., Feingold, G., Forster, P., Kerminen, V.-M., Kondo, Y., Liao, H., Lohmann, U., Rasch, P., Satheesh, S.K., Sherwood, S., Stevens, B., & Zhang, X.Y., 2013. Clouds and aerosols. In *Climate Change 2013: The Physical Science Basis. Contribution of Working Group I to the Fifth Assessment Report of the Intergovernmental Panel on Climate Change*. T.F. Stocker, D. Qin, G.-K. Plattner, M. Tignor, S.K. Allen, J. Doschung, A. Nauels, Y. Xia, V. Bex, and P.M. Midgley, Eds. Cambridge University Press, pp. 571-657, doi:10.1017/CBO9781107415324.016.
- Bowdle, D. A., Hobbs, P. V., and Radke L. F., 1985. Particles in the lower troposphere over the High Plains of the United States. Part III: Ice nuclei. *J. Clim. Appl. Meteor.*, 24, 1370–1376.
- Bundke, U., Nillius, B., Jaenicke, R., Wetter, T., Klein, H., and Bingemer, H., 2008. The Fast Ice Nucleus Chamber FINCH. *Atmos. Res.*, 90, 180–186, doi:10.1016/j.atmosres.2008.02.008.
- Cantrell, W., & Heymsfield, A., 2005. Production of ice in tropospheric clouds: A review. *Bull. Amer. Meteor. Soc.*, 86, 795– 807, doi:10.1175/BAMS-86-6-795.
- Chaikovsky, A., Dubovik, O., Holben, B., Bril, A., Goloub, P., Tanré, D., Pappalardo, G., Wandinger, U., Chaikovskaya, L., Denisov, S., Grudo, J., Lopatin, A., Karol, Y., Lapyonok, T., Amiridis, V., Ansmann, A., Apituley, A., Allados-Arboledas, L., Biniotoglou, I., Boselli, A., D'Amico, G., Freudenthaler, V., Giles, D., Granados-Muñoz, M. J., Kokkalis, P., Nicolae, D., Oshchepkov, S., Papayannis, A., Perrone, M. R., Pietruczuk, A., Rocadenbosch, F., Sicard, M., Slutsker, I., Talianu, C., De Tomasi, F., Tsekeri, A., Wagner, J., and Wang, X., 2016. Lidar-Radiometer Inversion Code (LIRIC) for the retrieval of vertical aerosol properties from combined lidar/radiometer data: development and distribution in EARLINET, *Atmos. Meas. Tech.*, 9, 1181–1205, <https://doi.org/10.5194/amt-9-1181-2016>.
- Sprigg, W.A., Nickovic, S., Galgiani, J.N., Pejanovic, G., Petkovic, S., Vujadinovic, M., Vukovic, A., Dacic, M., DiBiase, S., Prasad, A. and El-Askary, H., 2014. Regional dust storm modeling for health services: the case of valley fever. *Aeolian Research*, 14, pp.53-73.
- Claquin, T., Schulz, M., Balkanski, Y., and Boucher, O., 1998. Uncertainties in modeling the radiative forcing of mineral dust, *Tellus*, 50B, 491–505.
- Claquin, T., Schulz, M., and Balkanski, Y., 1999. Modeling the mineralogy of atmospheric dust sources, *J. Geophys. Res.*, 104, 22243–22256.
- Cziczo, D. J., Froyd, K. D., Hoose, C., Jensen, E. J., Diao, M., Zondlo, M. A., Smith, J. B., Twohy, C. H., and Murphy, D. M., 2013. Clarifying the Dominant Sources and Mechanisms of Cirrus Cloud Formation. *Science* 340, no. 6138 (June 14, 2013): 1320–1324, <http://dx.doi.org/10.1126/science.1234145>.

- D'Amico, G., Amodeo, A., Baars, H., Binietoglou, I., Freudenthaler, V., Mattis, I., Wandinger, U., and Pappalardo, G., 2015. EARLINET Single Calculus Chain – overview on methodology and strategy, *Atmos. Meas. Tech.*, 8, 4891–4916, <https://doi.org/10.5194/amt-8-4891-2015>.
- D'Amico, G., Amodeo, A., Mattis, I., Freudenthaler, V., and Pappalardo, G., 2016. EARLINET Single Calculus Chain – technical – Part 1: Pre-processing of raw lidar data, *Atmos. Meas. Tech.*, 9, 491–507, <https://doi.org/10.5194/amt-9-491-2016>.
- Delanoë, J., Protat, A., Testud, J., Bouniol, D., Heymsfield, A. J., Bansemmer, A., Brown, P. R. A., and Forbes, R. M., 2005. Statistical properties of the normalized ice particle size distribution, *J. Geophys. Res.-Atmos.*, 110, D10201, <https://doi.org/10.1029/2004JD005405>.
- Delanoë, J., and Hogan, R. J.: Combined CloudSat-CALIPSO-MODIS retrievals of the properties of ice clouds, *J. Geophys. Res.*, 115, D00H29, doi:10.1029/2009JD012346, 2010.
- Delanoë, J. M. E., Heymsfield, A. J., Protat, A., Bansemmer, A., and Hogan, R. J.: Normalized particle size distribution for remote sensing application, *J. Geophys. Res. Atmos.*, 119, 4204– 4227, doi:10.1002/2013JD020700, 2014.
- DeMott, P. J., Prenni, A. J., Liu, X., Kreidenweis, S. M., Petters, M. D., Twohy, C. H., and Rogers, D. C., 2010. Predicting global atmospheric ice nuclei distributions and their impacts on climate. *Proceedings of the National Academy of Sciences*, 107(25), 11217–11222. <https://doi.org/10.1073/pnas.0910818107>.
- DeMott, P. J., Möhler, O., Stetzer, O., Vali, G., Levin, Z., Petters, M. D., Murakami, M., Leisner, T., Bundke, U., Klein, H., Kanji, Z. A., Cotton, R., Jones, H., Benz, S., Brinkmann, M., Rzesanke, D., Saathoff, H., Nicolet, M., Saito, A., Nillius, B., Bingemer, H., Abbatt, J., Ardon, K., Ganor, E., Georgakopoulos, D. G., and Saunders, C., 2011. Resurgence in Ice Nuclei Measurement Research, *Bulletin of the American Meteorological Society*, 92(12), 1623-1635. https://journals.ametsoc.org/view/journals/bams/92/12/2011bams3119_1.xml.
- DeMott, P. J., Prenni, A. J., McMeeking, G. R., Sullivan, R. C., Petters, M. D., Tobo, Y., Niemand, M., Möhler, O., Snider, J. R., Wang, Z., and Kreidenweis, S. M., 2015. Integrating laboratory and field data to quantify the immersion freezing ice nucleation activity of mineral dust particles, *Atmos. Chem. Phys.*, 15, 393–409, <https://doi.org/10.5194/acp-15-393-2015>.
- Dubovik, O. and King, M. D., 2000. A flexible inversion algorithm for retrieval of aerosol optical properties from sun and sky radiance measurements, *J. Geophys. Res.*, 105, 20673–20696.
- Dubovik, O., Smirnov, A., Holben, B. N., King, M. D., Kaufman, Y. J., Eck, T. F., and Slutsker, I., 2006. Accuracy assessment of aerosol optical properties retrieved from Aerosol Robotic Network (AERONET) sun and sky radiance measurements, *J. Geophys. Res.*, 105, 9791–9806.

- Dudhia, J., 1989. Numerical study of convection observed during the winter monsoon experiment using a mesoscale two-dimensional model. *J. Atmos. Sci.*, 46, 3077–3107.
- Engelmann, R., Kanitz, T., Baars, H., Heese, B., Althausen, D., Skupin, A., Wandinger, U., Komppula, M., Stachlewska, I. S., Amiridis, V., Marinou, E., Mattis, I., Linné, H., and Ansmann, A., 2016. The automated multiwavelength Raman polarization and water-vapor lidar PollyXT: the neXT generation, *Atmos. Meas. Tech.*, 9, 1767–1784, <https://doi.org/10.5194/amt-9-1767-2016>.
- Escribano, J., Di Tomaso, E., Jorba, O., Klose, M., Gonçalves Ageitos, M., Macchia, F., Amiridis, V., Baars, H., Marinou, E., Proestakis, E., Urbanneck, C., Althausen, D., Bühl, J., Mamouri, R.-E., and Pérez García-Pando, C., 2022. Assimilating spaceborne lidar dust extinction can improve dust forecasts, *Atmos. Chem. Phys.*, 22, 535–560, <https://doi.org/10.5194/acp-22-535-2022>.
- Ferrier, B. S., Jin, Y., Lin, Y., Black, T., Rogers, E. and DiMego, G., 2002. Implementation of a new grid-scale cloud and precipitation scheme in the NCEP Eta model. In 15th Conference on Numerical Weather Prediction, American Meteorological Society, San Antonio, 280–283.
- Fletcher, N. H.: *The Physics of Rain Clouds*. Cambridge University Press, 1962.
- Freudenthaler, V., Esselborn, M., Wiegner, M., Heese, B., Tesche, M., Ansmann, A., et al. (2009). Depolarization ratio profiling at several wavelengths in pure Saharan dust during SAMUM 2006, *Tellus B*, 61, 165–179, <https://doi.org/10.1111/j.1600-0889.2008.00396.x>
- Freudenthaler, V., Linné, H., Chaikovski, A., Rabus, D., and Groß, S.: EARLINET lidar quality assurance tools, *Atmos. Meas. Tech. Discuss.* [preprint], <https://doi.org/10.5194/amt-2017-395>, in review, 2018.
- Georgoulas, A. K., Tsikerdekis, A., Amiridis, V., Marinou, E., Benedetti, A., Zanis, P., Alexandri, G., Mona, L., Kourtidis, K. A., and Lelieveld, J., 2018. A 3-D evaluation of the MACC reanalysis dust product over Europe, northern Africa and Middle East using CALIOP/CALIPSO dust satellite observations, *Atmos. Chem. Phys.*, 18, 8601–8620, <https://doi.org/10.5194/acp-18-8601-2018>.
- Ghan, S. J., Liu, X., Easter, R. C., Zaveri, R., Rasch, P. J., Yoon, J.-H., and Eaton, B., 2012. Toward a minimal representation of aerosols in climate models: Comparative decomposition of aerosol direct, semidirect, and indirect radiative forcing. *J. Climate*, 25, 6461–6476, <https://doi.org/10.1175/JCLI-D-11-00650.1>.
- Giles, D. M., Sinyuk, A., Sorokin, M. G., Schafer, J. S., Smirnov, A., Slutsker, I., Eck, T. F., Holben, B. N., Lewis, J. R., Campbell, J. R., Welton, E. J., Korkin, S. V., and Lyapustin, A. I., 2019. Advancements in the Aerosol Robotic Network (AERONET) Version 3 database – automated near-real-time quality control algorithm with improved cloud screening for Sun photometer aerosol optical depth (AOD) measurements, *Atmos. Meas. Tech.*, 12, 169–209, <https://doi.org/10.5194/amt-12-169-2019>.

- Ginoux, P., Chin, M., Tegen, I., Prospero, J., Holben, B., Dubovik, O., and Lin, S. J., 2001. Sources and distributions of dust aerosols simulated with the GOCART model, *J. Geophys. Res.*, 106(D17), 20255-20273.
- Georgi, F., 1986. A particle dry-deposition parameterization scheme for use in tracer transport models, *J. Geophys. Res.*, 91, 9794-9806.
- Giannadaki, D., Pozzer, A., and Lelieveld, J., 2014. Modeled global effects of airborne desert dust on air quality and premature mortality, *Atmos. Chem. Phys.*, 14, 957–968, <https://doi.org/10.5194/acp-14-957-2014>.
- Groß, S., Tesche, M., Freudenthaler, V., Toledano, C., Wiegner, M., Ansmann, A., et al. (2011). Characterization of Saharan dust, marine aerosols and mixtures of biomass burning aerosols and dust by means of multi-wavelength depolarization and Raman lidar measurements during SAMUM 2, *Tellus B*, 63, 706–724, doi:10.1111/j.1600-0889.2011.00556.x
- Groß, S., Esselborn, M., Abicht, F., Wirth, M., Fix, A., and Minikin, A., 2013. Airborne high spectral resolution lidar observation of pollution aerosol during EUCAARI-LONGREX, *Atmos. Chem. Phys.*, 13, 2435–2444, <https://doi.org/10.5194/acp-13-2435-2013>.
- Gurganus, C. and Lawson, P.: Laboratory and Flight Tests of 2D Imaging Probes: Toward a Better Understanding of Instrument Performance and the Impact on Archived Data, *J. Atmos. Ocean. Tech.*, 35, 1533–1553, <https://doi.org/10.1175/JTECH-D-17-0202.1>, 2018.
- Haarig, M., Ansmann, A., Gasteiger, J., Kandler, K., Althausen, D., Baars, H., Radenz, M., and Farrell, D. A., 2017. Dry versus wet marine particle optical properties: RH dependence of depolarization ratio, backscatter, and extinction from multiwavelength lidar measurements during SALTRACE, *Atmos. Chem. Phys.*, 17, 14199–14217, <https://doi.org/10.5194/acp-17-14199-2017>.
- Haarig, M., Walser, A., Ansmann, A., Dollner, M., Althausen, D., Sauer, D., Farrell, D., and Weinzierl, B., 2019. Profiles of cloud condensation nuclei, dust mass concentration, and ice-nucleating-particle-relevant aerosol properties in the Saharan Air Layer over Barbados from polarization lidar and airborne in situ measurements, *Atmos. Chem. Phys.*, 19, 13773–13788, <https://doi.org/10.5194/acp-19-13773-2019>.
- Harrison, A. D., Whale, T. F., Carpenter, M. A., Holden, M. A., Neve, L., O'Sullivan, D., Vergara Temprado, J., and Murray, B. J., 2016. Not all feldspars are equal: a survey of ice nucleating properties across the feldspar group of minerals, *Atmos. Chem. Phys.*, 16, 10927–10940, <https://doi.org/10.5194/acp-16-10927-2016>.
- Harrison, A. D., Lever, K., Sanchez-Marroquin, A., Holden, M. A., Whale, T. F., Tarn, M. D., McQuaid, J. B., and Murray, B. J., 2019. The ice-nucleating ability of quartz immersed in water and its atmospheric importance compared to K-feldspar, *Atmos. Chem. Phys.*, 19, 11343–11361, <https://doi.org/10.5194/acp-19-11343-2019>.
- Heymsfield, A., and Willis, P., 2014. Cloud Conditions Favoring Secondary Ice Particle Production in Tropical Maritime Convection, *Journal of the Atmospheric Sciences*, 71(12), 4500-4526, <https://journals.ametsoc.org/view/journals/atsc/71/12/jas-d-14-0093.1.xml>.

- Hoff, R. M. and Pappalardo, G., 2010. The GAW Aerosol Lidar Observation Network (GALION) as a source of near-real time aerosol profile data for model evaluation and assimilation, AGU Fall Meeting Abstracts, San Francisco, p. G8.
- Hogan, R. J., Mittermaier, M. P., and Illingworth A. J., 2006. The Retrieval of Ice Water Content from Radar Reflectivity Factor and Temperature and Its Use in Evaluating a Mesoscale Model. *J. Appl. Meteor. Climatol.*, 45, 301–317, <https://doi.org/10.1175/JAM2340.1>.
- Holben, B. N., Eck, T. F., Slutsker, I., Tanré, D., Buis, J. P., Setzer, A., et al. (1998). Aeronet – A Federal Instrument Network and Data Archive for Aerosol Characterization, *Remote Sens. Environ.*, 66, 1–16, doi:10.1016/S0034-4257(98)00031-5.
- Hoose, C. & Möhler, O.: Heterogeneous ice nucleation on atmospheric aerosols: a review of results from laboratory experiments, *Atmos. Chem. Phys.*, 12, 9817–9854, <https://doi.org/10.5194/acp-12-9817-2012>, 2012.
- Huneeus, N., Schulz, M., Balkanski, Y., Griesfeller, J., Prospero, J., Kinne, S., Bauer, S., Boucher, O., Chin, M., Dentener, F., Diehl, T., Easter, R., Fillmore, D., Ghan, S., Ginoux, P., Grini, A., Horowitz, L., Koch, D., Krol, M. C., Landing, W., Liu, X., Mahowald, N., Miller, R., Morcrette, J.-J., Myhre, G., Penner, J., Perlwitz, J., Stier, P., Takemura, T., and Zender, C. S.: Global dust model intercomparison in AeroCom phase I, *Atmos. Chem. Phys.*, 11, 7781–7816, <https://doi.org/10.5194/acp-11-7781-2011>, 2011.
- Illingworth, A. J., R. J. Hogan, E. J. O'Connor, D. Bouniol, M. E. Brooks, J. Delanoë, D. P. et al. (2007). CloudNet - continuous evaluation of cloud profiles in seven operational models using ground-based observations *Bull. Am. Meteorol. Soc.*, 88, 883-898
- Janjic, Z. I.: The step-mountain Eta coordinate model: Further developments of the convection, viscous sublayer, and turbulence closure schemes. *Mon. Wea. Rev.*, 122, 927–945, 1994.
- Janjic, Z. I., Gerrity, J. P., and Nickovic, S.: An alternative approach to nonhydrostatic modeling, *Mon. Weather Rev.*, 129, 1164–1178, 2001.
- Jensen, E. J., Lawson, R. P., Bergman, J. W., Pfister, L., Bui, T. P., and Schmitt, C. G.: Physical processes controlling ice concentrations in synoptically forced, midlatitude cirrus, *J. Geophys. Res.- Atmos.*, 118, 5348–5360, <https://doi.org/10.1002/jgrd.50421>, 2013
- Jickells, T., and C. M. Moore, 2015: The importance of atmospheric deposition for ocean productivity. *Annu. Rev. Ecol. Evol. Syst.*, 46, 481–501, <https://doi.org/10.1146/annurev-ecolsys-112414-054118>.
- Journet, K., Desboeufs, V., Caquineau, S., and Colin, J. L.: Mineralogy as a critical factor of dust iron solubility, *Geophys. Res. Lett.*, 35, L07805, doi: 10.1029/2007GL031589, 2008.
- Kampouri, A., Amiridis, V., Solomos, S., Gialitaki, A., Marinou, E., Spyrou, C., Georgoulas, A.K., Akritidis, D., Papagiannopoulos, N., Mona, L., Scollo, S., Tsihla, M., Tsikoudi, I., Pytharoulis, I., Karacostas, T., Zanis, P.: Investigation of Volcanic Emissions in the Mediterranean: “The Etna–Antikythera Connection”. *Atmosphere* 2021, 12, 40. <https://doi.org/10.3390/atmos12010040>, 2021.

- Kandler, K., Schütz, L., Deutscher, C., Ebert, M., Hofmann, H., Jäckel, S., et al. (2009), Size distribution, mass concentration, chemical and mineralogical composition and derived optical parameters of the boundary layer aerosol at Tinfou, Morocco, during SAMUM 2006. *Tellus B*, 61: 32-50. <https://doi.org/10.1111/j.1600-0889.2008.00385.x>
- Kim, M.-H., Omar, A. H., Tackett, J. L., Vaughan, M. A., Winker, D. M., Trepte, C. R., Hu, Y., Liu, Z., Poole, L. R., Pitts, M. C., Kar, J., and Magill, B. E.: The CALIPSO version 4 automated aerosol classification and lidar ratio selection algorithm, *Atmos. Meas. Tech.*, 11, 6107–6135, <https://doi.org/10.5194/amt-11-6107-2018>, 2018.
- Koehler, K. A., Kreidenweis, S. M., DeMott, P. J., Petters, M.-D., Prenni, A. J., and Carrico, C. M.: Hygroscopicity and cloud droplet activation of mineral dust aerosol, *Geophys. Res. Lett.*, 36, L08805, doi:10.1029/2009GL037348, 2009.
- Kok, J., Ridley, D., Zhou, Q. et al. Smaller desert dust cooling effect estimated from analysis of dust size and abundance. *Nature Geosci* 10, 274–278 (2017). <https://doi.org/10.1038/ngeo2912>
- Kok, J. F., and Coauthors, 2021: Contribution of the world's main dust source regions to the global cycle of desert dust. *Atmos. Chem. Phys.*, 21, 8169–8193, <https://doi.org/10.5194/acp-21-8169-2021>.
- Kokkalis, P., Papayannis, A., Mamouri, E. R., Tsaknakis, G., and Amiridis, V.: The EOLE Radar Conference, Porto Heli, Greece, 25–29 June 2015, 629–632, 2012.
- Konsta, D., Biniotoglou, I., Gkikas, A., Solomos, S., Marinou, E., Proestakis, E., et al. (2018). Evaluation of the BSC-DREAM8b regional dust model using the 3D LIVAS-CALIPSO product. *Atmospheric Environment*, 195, 46–62. <https://doi.org/10.1016/j.atmosenv.2018.09.047>
- Konsta, D., Tsekeri, A., Solomos, S., Siomos, N., Gialitaki, A., Tetoni, E., Lopatin, A., Goloub, P.; Dubovik, O., Amiridis, V., Nastos, P.: The Potential of GRASP/GARRLiC Retrievals for Dust Aerosol Model Evaluation: Case Study during the PreTECT Campaign. *Remote Sens.* 2021, 13, 873. <https://doi.org/10.3390/rs13050873>, 2021.
- Krätschmer, S., van der Does, M., Lamy, F., Lohmann, G., Völker, C., and Werner, M.: Simulating glacial dust changes in the Southern Hemisphere using ECHAM6.3-HAM2.3, *Clim. Past*, 18, 67–87, <https://doi.org/10.5194/cp-18-67-2022>, 2022.
- Kumar, P., Sokolik, I. N., & Nenes, A.: Parameterization of cloud droplet formation for global and regional models: including adsorption activation from insoluble CCN, *Atmos. Chem. Phys.*, 9, 2517–2532, doi:10.5194/acp-9-2517-2009, 2009.
- Kumar, P., Sokolik, I. N., & Nenes, A.: Cloud condensation nuclei activity and droplet activation kinetics of wet processed regional dust samples and minerals, *Atmos. Chem. Phys.*, 11, 8661–8676, doi:10.5194/acp-11-8661-2011, 2011.
- Liu, Z., and Coauthors, 2009: The CALIPSO lidar cloud and aerosol discrimination: Version 2 algorithm and initial assessment of performance. *J. Atmos. Oceanic Technol.*, 26, 1198–1213.

- Madonna, F., Amodeo, A., Boselli, A., Cornacchia, C., Cuomo, V., D'Amico, G., et al. CIAO: the CNR-IMAA advanced observatory for atmospheric research, *Atmos. Meas. Tech.*, 4, 1191–1208, <https://doi.org/10.5194/amt-4-1191-2011>, 2011.
- Mamali, D., Marinou, E., Sciare, J., Pikridas, M., Kokkalis, P., Kottas, M., et al. (2018). Vertical profiles of aerosol mass concentration derived by unmanned airborne in situ and remote sensing instruments during dust events, *Atmos. Meas. Tech.*, 11, 2897–2910, <https://doi.org/10.5194/amt-11-2897-2018>
- Mamouri, R. E. & Ansmann, A.: Estimated desert-dust ice nuclei profiles from polarization lidar: methodology and case studies, *Atmos. Chem. Phys.*, 15, 3463–3477, <https://doi.org/10.5194/acp-15-3463-2015>, 2015.
- Mamouri, R. E. & Ansmann, A.: Potential of polarization lidar to provide profiles of CCN- and INP-relevant aerosol parameters, *Atmos. Chem. Phys.*, 16, 5905–5931, <https://doi.org/10.5194/acp-16-5905-2016>, 2016.
- Matthias, V., et al. (2004), Vertical aerosol distribution over Europe: Statistical analysis of Raman lidar data from 10 European Aerosol Research Lidar Network (EARLINET) stations, *J. Geophys. Res.*, 109, D18201, doi:[10.1029/2004JD004638](https://doi.org/10.1029/2004JD004638).
- Marinou, E., Tesche, M., Nenes, A., Ansmann, A., Schrod, J., Mamali, D., et al. (2019). Retrieval of ice-nucleating particle concentrations from lidar observations and comparison with UAV in situ measurements, *Atmos. Chem. Phys.*, 19, 11315–11342, <https://doi.org/10.5194/acp-19-11315-2019>
- Mattis, I., D'Amico, G., Baars, H., Amodeo, A., Madonna, F., & Iarlori, M. (2016). EARLINET Single Calculus Chain – technical – Part 2: Calculation of optical products, *Atmos. Meas. Tech.*, 9, 3009–3029, <https://doi.org/10.5194/amt-9-3009-2016>
- Meyers, M. P., DeMott, P. J. & Cotton, W. R.: New primary ice nucleation parameterizations in an explicit cloud model. *J. Appl. Meteor.*, 31, 708–721, 1992.
- Mona, L., Papagiannopoulos, N., Basart, S., Baldasano, J., Binietoglou, I., Cornacchia, C., & Pappalardo, G.: EARLINET dust observations vs. BSC-DREAM8b modeled profiles: 12-year-long systematic comparison at Potenza, Italy, *Atmos. Chem. Phys.*, 14, 8781–8793, <https://doi.org/10.5194/acp-14-8781-2014>, 2014.
- Morcrette, J.-J., Boucher, O., Jones, L., Salmond, D., Bechtold, P., Beljaars, A., Benedetti, A., Bonet, A., Kaiser, J. W., Razinger, M., Schulz, M., Serrar, S., Simmons, A. J., Sofiev, M., Suttie, M., Tompkins, A. M., & Untch, A.: Aerosol analysis and forecast in the ECMWF integrated forecast system: Forward modelling, *J. Geophys. Res.*, 114, D06206, <https://doi.org/10.1029/2008JD011235>, 2009.
- Murray, B. J., O'Sullivan, D., Atkinson, J. D., & Webb, M. E.: Ice nucleation by particles immersed in supercooled cloud droplets, *Chem. Soc. Rev.*, 41, 6519–6554, 2012.
- Benjamin J. Murray (January 26, 2017) *Science* 355 (6323), 346–347. [doi: 10.1126/science.aam5320]

- Müller, D., Ansmann, A., Mattis, I., Tesche, M., Wandinger, U., Althausen, D., & Pisani, G. (2007). Aerosol-type-dependent lidar ratios observed with Raman lidar, *J. Geophys. Res.*, 112, D16202, <https://doi.org/10.1029/2006JD008292>
- Nickovic S, Dobricic S.: A model for long-range transport of desert dust. *Mon Weather Rev* 124(11):2537–2544, 1996.
- Nickovic, S., Kallos, G., Papadopoulos, A., & Kakaliagou, O.: A model for prediction of desert dust cycle in the atmosphere *J. Geophys. Res.* 106, 18113-18130, 2001.
- Nickovic, S.: Distribution of dust mass over particle sizes: impacts on atmospheric optics, Forth ADEC Workshop - Aeolian Dust Experiment on Climate Impact, 26-28 January, Nagasaki, Japan, 357-360, 2005.
- Nickovic, S., A. Vukovic, M. Vujadinovic, V. Djurdjevic, & G. Pejanovic (2012). Technical Note: High-resolution mineralogical database of dust-productive soils for atmospheric dust modeling *Atmos. Chem. Phys.*, 12, 845–855, 2012 www.atmos-chem-phys.net/12/845/2012/ doi:10.5194/acp-12-845-2012
- Nickovic, S., Vukovic, A., and Vujadinovic, M.: Atmospheric processing of iron carried by mineral dust, *Atmos. Chem. Phys.*, 13, 9169–9181, <https://doi.org/10.5194/acp-13-9169-2013>, 2013.
- Nickovic, S., Cvetkovic, B., Madonna, F., Rosoldi, M., Pejanovic, G., Petkovic, S., & Nikolic, J.: Cloud ice caused by atmospheric mineral dust – Part 1: Parameterization of ice nuclei concentration in the NMME-DREAM model, *Atmos. Chem. Phys.*, 16, 11367-11378, <https://doi.org/10.5194/acp-16-11367-2016>, 2016.
- Nicolae, D., Vasilescu, J., Talianu, C., Binietoglou, I., Nicolae, V., Andrei, S., & Antonescu, B.: A neural network aerosol-typing algorithm based on lidar data, *Atmos. Chem. Phys.*, 18, 14511–14537, <https://doi.org/10.5194/acp-18-14511-2018>, 2018.
- Tomoaki Nishizawa, Nobuo Sugimoto, Ichiro Matsui, Atsushi Shimizu, Yukari Hara, Uno Itsushi, Kazuaki Yasunaga, Rei Kudo, Sang-Woo Kim, Ground-based network observation using Mie-Raman lidars and multi-wavelength Raman lidars and algorithm to retrieve distributions of aerosol components, *Journal of Quantitative Spectroscopy & Radiative Transfer* 188, 79-93, 2017. doi:10.1016/j.jqsrt.2016.06.031
- Olson, J. S.: Global ecosystem framework-definitions: USGS EROS Data Center Internal Report, Sioux Falls, SD, 37 pp., 1994a.
- Olson, J. S.: Global ecosystem framework-translation strategy: USGS EROS Data Center Internal Report, Sioux Falls, SD, 39 pp., 1994b.
- Omar, A. H., and Coauthors, 2009: The CALIPSO automated aerosol classification and lidar ratio selection algorithm. *J. Atmos. Oceanic Technol.*, 26, 1994–2014.
- Pappalardo, G., Amodeo, A., Apituley, A., Comeron, A., Freudenthaler, V., Linné, H., et al. (2014). EARLINET: towards an advanced sustainable European aerosol lidar network, *Atmos. Meas. Tech.*, 7, 2389–2409, <https://doi.org/10.5194/amt-7-2389-2014>

- Papagiannopoulos, N., D'Amico, G., Gialitaki, A., Ajtai, N., Alados-Arboledas, L., Amodeo, A., Amiridis, V., Baars, H., Balis, D., Biniotoglou, I., Comerón, A., Dionisi, D., Falconieri, A., Fréville, P., Kampouri, A., Mattis, I., Mijić, Z., Molero, F., Papayannis, A., Pappalardo, G., Rodríguez-Gómez, A., Solomos, S., and Mona, L.: An EARLINET early warning system for atmospheric aerosol aviation hazards, *Atmos. Chem. Phys.*, 20, 10775–10789, <https://doi.org/10.5194/acp-20-10775-2020>, 2020.
- Pejanovic G., Nickovic S., Petkovic S., Vukovic A., Djurdjevic V., Vujadinovic M., Dacic M.: Dust operational forecast system with assimilation of dust analysed data, Regional Conference on Dust and Dust Storms, Kuwait, 20-22 November 2012, 2012.
- Pérez García-Pando, Carlos & Nickovic, Slobodan & Baldasano, José & Sicard, Michaël & Rocadenbosch, F. & Cachorro, Victoria. (2006). A long Saharan dust event over the western Mediterranean: Lidar, Sun photometer observations, and regional dust modeling. *Journal of Geophysical Research*. 10.1029/2005JD006579.
- Pérez, C., Nickovic, S., Pejanovic, G., Baldasano, J. M., & Özsoy, E.: Interactive dust-radiation modeling: A step to improve weather forecasts, *J. Geophys. Res.*, 111, D16206, doi:10.1029/2005JD006717, 2006.
- Pérez García-Pando C, Stanton MC, Diggle PJ, Trzaska S, Miller RL, Perlwitz JP, Baldasano JM, Cuevas E, Ceccato P, Yaka P, Thomson MC. Soil dust aerosols and wind as predictors of seasonal meningitis incidence in Niger. *Environ Health Perspect*. 2014 Jul;122(7):679-86. doi: 10.1289/ehp.1306640. Epub 2014 Mar 17. PMID: 24633049; PMCID: PMC4080544.
- Price, H. C., Baustian, K. J., McQuaid, J. B., Blyth, A., Bower, K. N., Choularton, T., ... Murray, B. J. (2018). Atmospheric ice-nucleating particles in the dusty tropical Atlantic. *Journal of Geophysical Research: Atmospheres*, 123, 2175–2193. <https://doi.org/10.1002/2017JD027560>
- Joseph M. Prospero et al, The Discovery of African Dust Transport to the Western Hemisphere and the Saharan Air Layer: A History, *Bulletin of the American Meteorological Society* (2021). DOI: 10.1175/BAMS-D-19-0309.1
- Rauber, R.M.: Microphysical processes in the atmosphere, ch. 18. In *Handbook of Weather, Climate, and Water. Dynamics, Climate, Physical Meteorology, Weather Systems, and Measurements*, ed. T. D. Potter and B. R. Colman. Wiley, pp. 255–299, 2003.
- Ravi, S., and Coauthors, 2011: Aeolian processes and the biosphere. *Rev. Geophys.*, 49, RG3001, <https://doi.org/10.1029/2010RG000328>.
- Reinfried, F., Tegen, I., Heinold, B., Hellmuth, O., Schepanski, K., Cubasch, U., Huebener, H. and Knippertz, P.: Simulations of convectively-driven density currents in the Atlas region using a regional model: Impacts on dust emission and sensitivity to horizontal resolution and convection schemes, *J. Geophys. Res.*, 114, D08127, doi:10.1029/2008JD010844, 2009.

- Reisner, J., Rasmussen, R.M. & Bruintjes, R. T.: Explicit forecasting of supercooled liquid water in winter storms using the MM5 mesoscale model. *Quart. J. Royal Meteor. Soc.*, 124, 1071–1107, 1998.
- Rittmeister, F., Ansmann, A., Engelmann, R., Skupin, A., Baars, H., Kanitz, T., and Kinne, S.: Profiling of Saharan dust from the Caribbean to western Africa – Part 1: Layering structures and optical properties from shipborne polarization/Raman lidar observations, *Atmos. Chem. Phys.*, 17, 12963–12983, <https://doi.org/10.5194/acp-17-12963-2017>, 2017.
- Rogers, R. R., & Yau, M. K.: *A Short Course in Cloud Physics*. 3rd ed. International Series in Natural Philosophy, Vol. 113, Pergamon Press, 290 pp, 1989.
- Sanchez-Marroquin, A. et al. Iceland is an episodic source of atmospheric ice-nucleating particles relevant for mixed-phase clouds. *Sci. Adv.* 6, 8137–8161 (2020).
- Schmetz, J., Pili, P., Tjemkes, S., Just, D., Kerkmann, J., Rota, S., and Ratier, A.: An introduction to Meteosat second generation (MSG), *B. Am. Meteorol. Soc.*, 83, 977–992, 2002.
- Schrod, J., Weber, D., Drücke, J., Keleshis, C., Pikridas, M., Ebert, M., et al. (2017). Ice nucleating particles over the Eastern Mediterranean measured by unmanned aircraft systems, *Atmos. Chem. Phys.*, 17, 4817–4835, <https://doi.org/10.5194/acp-17-4817-2017>
- Schulz, M., Balkanski, Y. J., Guelle, W. & Dulac, F.: Role of aerosol size distribution and source location in a three-dimensional simulation of a Saharan dust episode tested against satellite-derived optical thickness, *J. Geophys. Res.*, 103, 10,579 – 10,592, 1998.
- Shettle, E. P.: Optical and radiative properties of a desert aerosol model, in *Proceedings of the Symposium on Radiation in the Atmosphere*, edited by G. Fiocco, pp. 74 – 77, A. Deepak, Hampton, Va, 1994.
- Sokolik, I., & Toon, O.: Incorporation of mineralogical composition into models of the radiative properties of mineral aerosol from UV to IR wavelengths, *J. Geophys. Res.*, 104, 9423–9444, 1999.
- Solomos, S., Kallos, G., Kushta, J., Astitha, M., Tremback, C., Nenes, A., and Levin, Z.: An integrated modeling study on the effects of mineral dust and sea salt particles on clouds and precipitation, *Atmos. Chem. Phys.*, 11, 873–892, [doi:10.5194/acp-11-873-2011](https://doi.org/10.5194/acp-11-873-2011), 2011.
- Solomos, S., Ansmann, A., Mamouri, R.-E., Biniotoglou, I., Patlakas, P., Marinou, E., and Amiridis, V.: Remote sensing and modelling analysis of the extreme dust storm hitting the Middle East and eastern Mediterranean in September 2015, *Atmos. Chem. Phys.*, 17, 4063–4079, <https://doi.org/10.5194/acp-17-4063-2017>, 2017.
- Solomos, S., Abuelgasim, A., Spyrou, C., Biniotoglou, I., & Nickovic, S.: Development of a dynamic dust source map for NMME-DREAM v1.0 model based on MODIS Normalized Difference Vegetation Index (NDVI) over the Arabian Peninsula, *Geosci. Model Dev.*, 12, 979–988, <https://doi.org/10.5194/gmd-12-979-2019>, 2019.

- Sourdeval, O., Gryspeerd, E., Krämer, M., Goren, T., Delanoë, J., Afchine, A., et al. (2018). Ice crystal number concentration estimates from lidar–radar satellite remote sensing – Part 1: Method and evaluation, *Atmos. Chem. Phys.*, 18, 14327–14350, <https://doi.org/10.5194/acp-18-14327-2018>
- Stengel, M., Kniffka, A., Meirink, J. F., Lockhoff, M., Tan, J., & Hollmann, R.: CLAAS: the CM SAF cloud property data set using SEVIRI, *Atmos. Chem. Phys.*, 14, 4297–4311, <https://doi.org/10.5194/acp-14-4297-2014>, 2014.
- Stephens, G. L., Vane, D. G., Boain, R. J., Mace, G. G., Sassen, K., Wang, Z., et al. (2002). The Cloudsat mission and the A–train, *B. Am. Meteorol. Soc.*, 83, 1771–1790, DOI: <https://doi.org/10.1175/BAMS-83-12-1771>
- Stohl, A.; Forster, C.; Frank, A.; Seibert, P.; Wotawa, G., 2005. Technical note: The Lagrangian particle dispersion model FLEXPART version 6.2. *Atmos. Chem. Phys.* 2005, 5, 2461–2474.
- Tegen, I., & Fung, I. Modeling of mineral dust in the atmosphere: Sources, transport, and optical thickness, *J. Geophys. Res.*, 99(D11), 22897–22914, 1994.
- Tesche, M., Ansmann, A., Müller, D., Althausen, D., Engelmann, R., Freudenthaler, V., & Groß, S.: Vertically resolved separation of dust and smoke over Cape Verde using multiwavelength Raman and polarization lidars during Saharan Mineral Dust Experiment 2008, *J. Geophys. Res.*, 114, D13202, <https://doi.org/10.1029/2009JD011862>, 2009.
- TESCHE, M., MÜLLER, D., GROSS, S., ANSMANN, A., ALTHAUSEN, D., FREUDENTHALER, V., WEINZIERL, B., VEIRA, A. and PETZOLD, A. (2011), Optical and microphysical properties of smoke over Cape Verde inferred from multiwavelength lidar measurements. *Tellus B*, 63: 677–694. <https://doi.org/10.1111/j.1600-0889.2011.00549.x>
- Tsarpalis, K.; Katsafados, P.; Papadopoulos, A.; Mihalopoulos, N.: Assessing Desert Dust Indirect Effects on Cloud Microphysics through a Cloud Nucleation Scheme: A Case Study over the Western Mediterranean. *Remote Sens.* 2020, 12, 3473. <https://doi.org/10.3390/rs12213473>, 2020.
- Tsekeri, A., Amiridis, V., Kokkalis, P., Basart, S., Chaikovsky, A., Dubovik, O., Papayannis, R., and Baldasano, J. M.: Application of a synergetic lidar and sunphotometer algorithm for the characterization of a dust event over Athens, Greece, *British J. Environ. Clim. Change*, 3, 531–546, 2013.
- Tsekeri, A., Lopatin, A., Amiridis, V., Marinou, E., Igloffstein, J., Siomos, N., Solomos, S., Kokkalis, P., Engelmann, R., Baars, H., Gratsea, M., Raptis, P. I., Biniotoglou, I., Mihalopoulos, N., Kalivitis, N., Kouvarakis, G., Bartsotas, N., Kallos, G., Basart, S., Schuettmeyer, D., Wandinger, U., Ansmann, A., Chaikovsky, A. P., & Dubovik, O.: GARLiC and LIRIC: strengths and limitations for the characterization of dust and marine particles along with their mixtures, *Atmos. Meas. Tech.*, 10, 4995–5016, <https://doi.org/10.5194/amt-10-4995-2017>, 2017.

- Tsikerdekis, A., Zanis, P., Steiner, A. L., Solmon, F., Amiridis, V., Marinou, E., Katragkou, E., Karacostas, T., & Foret, G.: Impact of dust size parameterizations on aerosol burden and radiative forcing in RegCM4, *Atmos. Chem. Phys.*, 17, 769–791, <https://doi.org/10.5194/acp-17-769-2017>, 2017.
- U.S. Department of Agriculture: State soil geographic (STATSGO) data base-data use information, miscellaneous publication number 1492 (rev. ed.): Fort Worth, Texas, Natural Resources Conservation Service (variously paged), 1994.
- Veefkind, J.P., Aben, I., McMullan, K., Förster, H., de Vries, J., Otter, G., Claas, J., Eskes, H.J., de Haan, J.F., Kleipool, Q., et al. TROPOMI on the ESA Sentinel-5 Precursor: A GMES mission for global observations of the atmospheric composition for climate, air quality and ozone layer applications. *Remote Sens. Environ.* 2012, 120, 70–83.
- Veselovskii, I., Goloub, P., Podvin, T., Bovchaliuk, V., Derimian, Y., Augustin, P., et al. (2016). Retrieval of optical and physical properties of African dust from multiwavelength Raman lidar measurements during the SHADOW campaign in Senegal, *Atmos. Chem. Phys.*, 16, 7013–7028, <https://doi.org/10.5194/acp-16-7013-2016>
- Vukovic, A., Vujadinovic, M., Pejanovic, G., Andric, J., Kumjian, M. R., Djurdjevic, V., et al. (2014). Numerical simulation of "an American haboob", *Atmos. Chem. Phys.*, 14, 3211–3230, doi:10.5194/acp-14-3211-2014
- Wagner, J., Ansmann, A., Wandinger, U., Seifert, P., Schwarz, A., Tesche, M., Chaikovsky, A., & Dubovik, O.: Evaluation of the Lidar/Radiometer Inversion Code (LIRIC) to determine microphysical properties of volcanic and desert dust, *Atmos. Meas. Tech.*, 6, 1707–1724, <https://doi.org/10.5194/amt-6-1707-2013>, 2013.
- Walker, A. L., Liu, M., Miller, S. D., Richardson, K. A., & Westphal, D. L.: Development of a dust source database for mesoscale forecasting in southwest Asia, *J. Geophys. Res.*, 114, D18207, doi: 10.1029/2008JD011541, 2009.
- Wandinger, U., Freudenthaler, V., Baars, H., Amodeo, A., Engelmann, R., Mattis, I., Groß, S., Pappalardo, G., Giunta, A., D'Amico, G., Chaikovsky, A., Osipenko, F., Slesar, A., Nicolae, D., Belegante, L., Talianu, C., Serikov, I., Linné, H., Jansen, F., Apituley, A., Wilson, K. M., de Graaf, M., Trickl, T., Giehl, H., Adam, M., Comerón, A., Muñoz-Porcar, C., Rocadenbosch, F., Sicard, M., Tomás, S., Lange, D., Kumar, D., Pujadas, M., Molero, F., Fernández, A. J., Alados-Arboledas, L., Bravo-Aranda, J. A., Navas-Guzmán, F., Guerrero-Rascado, J. L., Granados-Muñoz, M. J., Preißler, J., Wagner, F., Gausa, M., Grigorov, I., Stoyanov, D., Iarlori, M., Rizi, V., Spinelli, N., Boselli, A., Wang, X., Lo Feudo, T., Perrone, M. R., De Tomasi, F., & Burlizzi, P.: EARLINET instrument intercomparison campaigns: overview on strategy and results, *Atmos. Meas. Tech.*, 9, 1001–1023, <https://doi.org/10.5194/amt-9-1001-2016>, 2016.
- Wang, Y., Sartelet, K. N., Bocquet, M., Chazette, P., Sicard, M., D'Amico, G., León, J. F., Alados-Arboledas, L., Amodeo, A., Augustin, P., Bach, J., Belegante, L., Biniotoglou, I., Bush, X., Comerón, A., Delbarre, H., García-Vizcaino, D., Guerrero-Rascado, J. L., Hervo, M., Iarlori, M., Kokkalis, P., Lange, D., Molero, F., Montoux, N., Muñoz, A., Muñoz, C., Nicolae, D., Papayannis, A., Pappalardo, G., Preissler, J., Rizi, V., Rocadenbosch, F., Sellegri, K., Wagner, F., & Dulac, F.: Assimilation of lidar signals: application to aerosol

- forecasting in the western Mediterranean basin, *Atmos. Chem. Phys.*, 14, 12031–12053, <https://doi.org/10.5194/acp-14-12031-2014>, 2014.
- Welton, E.J., J. R. Campbell, J. D. Spinhirne, & V. S. Scott, 2001. Global monitoring of clouds and aerosols using a network of micro-pulse lidar systems, *Proc. SPIE*, 4153, 151-158.
- Weinzierl, B., Ansmann, A., Prospero, J. M., Althausen, D., Benker, N., Chouza, F., Dollner, M., Farrell, D., Fomba, W. K., Freudenthaler, V., Gasteiger, J., Groß, S., Haarig, M., Heinold, B., Kandler, K., Kristensen, T. B., Mayol-Bracero, O. L., Müller, T., Reitebuch, O., Sauer, D., Schäfler, A., Schepanski, K., Spanu, A., Tegen, I., Toledano, C., & Walser, A.: The Saharan Aerosol Long-Range Transport and Aerosol–Cloud-Interaction Experiment: Overview and Selected Highlights, *Bulletin of the American Meteorological Society*, 98(7), 1427-1451. Retrieved Oct 18, 2021, from <https://journals.ametsoc.org/view/journals/bams/98/7/bams-d-15-00142.1.xml>, 2017.
- Winker, D. M., Vaughan, M. A., Omar, A., Hu, Y., Powell, K. A., Liu, Z., Hunt, W. H., & Young, S. A.: Overview of the CALIPSO Mission and CALIOP Data Processing Algorithms, *Journal of Atmospheric and Oceanic Technology*, 26(11), 2310-2323. Retrieved Oct 18, 2021, from https://journals.ametsoc.org/view/journals/atot/26/11/2009jtecha1281_1.xml, 2009.
- Winker, D. M., Tackett, J. L., Getzewich, B. J., Liu, Z., Vaughan, M. A., & Rogers, R. R.: The global 3-D distribution of tropospheric aerosols as characterized by CALIOP, *Atmos. Chem. Phys.*, 13, 3345–3361, doi:10.5194/acp-13-3345-2013, 2013.
- Wu, C., Lin, Z. & Liu, X.: The global dust cycle and uncertainty in CMIP5 (Coupled Model Intercomparison Project phase 5) models. *Atmos. Chem. Phys.*, 20, 10 401–10 425, <https://doi.org/10.5194/acp-20-10401-2020>, 2020.
- Zender, C. S., Bian, H. & Newman, D.: Mineral Dust Entrainment and Deposition (DEAD) model: Description and 1990s dust climatology, *J. Geophys. Res.*, 108(D14), 4416, doi:10.1029/2002JD002775, 2003.

Appendix

Publications

Journals

- Ilić, L., Jovanović, A., Kuzmanoski, M., Lazić, L., Madonna, F., Rosoldi, M., et al. (2022). Mineralogy sensitive immersion freezing parameterization in DREAM. *Journal of Geophysical Research: Atmospheres*, 127, e2021JD035093. <https://doi.org/10.1029/2021JD035093>
- Barreto, Á., Cuevas, E., García, R. D., Carrillo, J., Prospero, J. M., Ilić, L., Basart, S., Berjón, A. J., Marrero, C. L., Hernández, Y., Bustos, J. J., Ničković, S., and Yela, M. (2022) Long-term characterisation of the vertical structure of the Saharan Air Layer over the Canary Islands using lidar and radiosonde profiles: implications for radiative and cloud processes over the subtropical Atlantic Ocean, *Atmos. Chem. Phys.*, 22, 739–763, <https://doi.org/10.5194/acp-22-739-2022>
- Vudragovic, D., Ilic, L., Jovanovic, P., Nickovic, S., Bogojevic, A., and Balaz, A., (2018) VI-SEEM DREAMCLIMATE Service, Scalable Computing: Practice and Experience, 19(2), <https://doi.org/10.12694/scpe.v19i2.1396>
- Ilić, L., Kuzmanoski, M., Kolarž, P., Nina, A., Srećković, V., Mijić, Z., Bajčetić, J., Andrić, M., (2018) Changes of atmospheric properties over Belgrade, observed using remote sensing and in situ methods during the partial solar eclipse of 20 March 2015, *Journal of Atmospheric and Solar-Terrestrial Physics*, Volume 171, 2018, Pages 250-259, ISSN 1364-6826, <https://doi.org/10.1016/j.jastp.2017.10.001>
- Granados-Muñoz, M. J., Navas-Guzmán, F., Guerrero-Rascado, J. L., Bravo-Aranda, J. A., Biniotoglou, I., Pereira, S. N., Basart, S., Baldasano, J. M., Belegante, L., Chaikovsky, A., Comerón, A., D'Amico, G., Dubovik, O., Ilic, L., Kokkalis, P., Muñoz-Porcar, C., Nickovic, S., Nicolae, D., Olmo, F. J., Papayannis, A., Pappalardo, G., Rodríguez, A., Schepanski, K., Sicard, M., Vukovic, A., Wandinger, U., Dulac, F., and Alados-Arboledas, L. (2016) Profiling of aerosol microphysical properties at several EARLINET/AERONET sites during the July 2012 ChArMEx/EMEP campaign, *Atmos. Chem. Phys.*, 16, 7043–7066, <https://doi.org/10.5194/acp-16-7043-2016>
- Lazić, L., Aničić Urošević, M., Mijić, Z., Vuković, G., Ilić, L. (2016) Traffic contribution to air pollution in urban street canyons: Integrated application of the OSPM, moss biomonitoring and spectral analysis, *Atmospheric Environment*, Volume 141, 2016, Pages 347-360, ISSN 1352-2310, <https://doi.org/10.1016/j.atmosenv.2016.07.008>
- Stojic, A., Stanišić Stojic, S., Šoštaric, A., Ilic, L., Mijic, Z., Rajšic, S., (2015) Characterization of VOC sources in an urban area based on PTR-MS measurements and receptor modelling. *Environ Sci Pollut Res* 22, 13137–13152, <https://doi.org/10.1007/s11356-015-4540-5>
- Biniotoglou, I., Basart, S., Alados-Arboledas, L., Amiridis, V., Argyrouli, A., Baars, H., Baldasano, J. M., Balis, D., Belegante, L., Bravo-Aranda, J. A., Burlizzi, P., Carrasco, V., Chaikovsky, A., Comerón, A., D'Amico, G., Filioglou, M., Granados-Muñoz, M. J., Guerrero-Rascado, J. L., Ilic, L., Kokkalis, P., Maurizi, A., Mona, L., Monti, F., Muñoz-

Porcar, C., Nicolae, D., Papayannis, A., Pappalardo, G., Pejanovic, G., Pereira, S. N., Perrone, M. R., Pietruczuk, A., Posyniak, M., Rocadenbosch, F., Rodríguez-Gómez, A., Sicard, M., Siomos, N., Szkop, A., Terradellas, E., Tsekeri, A., Vukovic, A., Wandinger, U., and Wagner, J. (2015) A methodology for investigating dust model performance using synergistic EARLINET/AERONET dust concentration retrievals, *Atmos. Meas. Tech.*, 8, 3577-3600, <https://doi.org/10.5194/amt-8-3577-2015>

Papayannis, D. Nicolae, P. Kokkalis, I. Biniotoglou, C. Talianu, L. Belegante, G. Tsaknakis, M.M. Cazacu, I. Vetres, L. Ilic (2014) Optical, size and mass properties of mixed type aerosols in Greece and Romania as observed by synergy of lidar and sunphotometers in combination with model simulations: A case study, *Science of the Total Environment* 500–501 (2014) 277–294 <https://doi.org/10.1016/j.scitotenv.2014.08.101>

Kotroni, V., Floros, E., Lagouvardos, K., Pejanovic, G., Ilic, L., and Zivkovic, M., (2010) Multi-model multi-analysis ensemble weather forecasting on the Grid for the South Eastern Mediterranean Region, *Earth Science Informatics*, 3, 209-218, <http://dx.doi.org/10.1007/s12145-010-0071-2>

Conferences

Ilić, L., Marinou, E., Jovanović, A., Kuzmanoski, M., and Ničković, S. (2021) Ice nucleating particle concentrations in Dust Regional Atmospheric Model (DREAM) – going one step further, *Geophysical Research Abstracts*, EGU2021-7754, 2020, EGU General Assembly 2021, <https://doi.org/10.5194/egusphere-egu21-7754>

Ilić, L., Cvetković, B., Pejanović, G., Petković, S., Kuzmanoski, M., Ničković, S. (2020) Mineralogy sensitive ice nucleation parameterizations in Dust Regional Atmospheric Model (DREAM), *Geophysical Research Abstracts*, EGU2020-15857, 2020, EGU General Assembly 2020, <https://doi.org/10.5194/egusphere-egu2020-15857>

Ilić, L., Jovanović, A., Kuzmanoski, M., Ničković, S., (2019) Modeling of immersion freezing initiation of mineral dust in dust regional atmospheric model DREAM, *The 7th international WeBIOPATR Workshop and Conference*, Belgrade

Ilić, L., Cvetković, B., Pejanović, G., Petković, S., Kuzmanoski, M., Ničković, S. (2018) Modeling of mineral composition effects on ice nucleation due to dust in Dust Regional Atmospheric Model (DREAM), *Geophysical Research Abstracts*, Vol. 20, EGU2018-16921, 2018, EGU General Assembly 2018, <https://meetingorganizer.copernicus.org/EGU2018/EGU2018-16921.pdf>

Cvetković, B., Ilić, L., Madonna, F., Weber, D., Ničković, S., Vuković, A., Pejanović, G., Nikolić, J., Bingemer, H., Vujadinović, M., Đurđević, V. (2018) Modeling heterogeneous ice nucleation due to mineral dust using Dust Regional Atmospheric Model (DREAM-NMME), *Geophysical Research Abstracts*, Vol. 20, EGU2018-10050, 2018, EGU General Assembly 2018, <https://meetingorganizer.copernicus.org/EGU2018/EGU2018-10050.pdf>

Ničković, S., Cvetković, B., Pejanović, G., Ilić, L., Madonna, F., Weber, D., Vuković, A., Pejanović, G., Nikolić, J., Petković, S. (2018) Predicting atmospheric dust process from Icelandic soil sources, *Geophysical Research Abstracts*, Vol. 20, EGU2018-10338, 2018,

- Vassilis, A., Marinou, E., Tsekeri, A., Solomos, S., Kottas, M., Proestakis, E., Konsta, D., Gkikas, A., Daskalopoulou, V., Tetoni, E., Gialitaki, A., Nicolae, D., Belegante, L., Ene, D., Andrei, S., Carstea, E., Stefanie, H., Dandocsi, A., Komppula, M., Kanakidou, M., Michalopoulos, N., Kalivitis, N., Kouvarakis, G., Rosoldi, M., Pappalardo, G., Campanelli, M., Biniotoglou, I., Kazadzis, S., Raptis, P., Ulanowski, J., Tesche, M., Mueller, D., Kezoudi, M., Smith, H., Marengo, F., Balis, D., Voudouri, K., Siomos, N., Nickovic, S., Cvetkovic, B., Ilic, L., Goloub, P., Diemoz, H., Aslanoglu, Y., Estelles, V., Basart, S., Eleftheriadis, K., Hloupis, G., Weinzierl, B. (2018) The Pre-TECT campaign - Revealing the secrets of desert dust, ELC, European Lidar Conference
- Kuzmanoski, M., Ilić, L., Mijić, Z., (2017) Aerosol remote sensing study of a Saharan dust intrusion episode in Belgrade, Serbia, XIX International Eco-Conference, September 25-27, Belgrade, Serbia, 73-81
- Ilić, L., Cvetković, B., Ničković, S. (2017) Assessment of health effects of exposure to atmospheric mineral dust using the NMME-DREAM model, Earth's climate changes and impacts, Book of Abstracts, p. 67, October 11-13, 2017, Belgrade, Serbia
- Kuzmanoski, M., Ilić, L., Todorović, M., Mijić, Z., (2017) A study of a dust intrusion event over Belgrade, Serbia, The 6th international WeBIOPATR Workshop and Conference, Book of Abstracts, 6-8 September 2017, Belgrade, Serbia, p. 36
- Mijić, Z., Ilić, L., Kuzmanoski, M., (2017) Raman lidar for atmospheric aerosol profiling in Serbia, 49th International October Conference on Mining and Metallurgy, Proceedings, pp. 65-68, October 18-21, 2017. Bor Lake, Serbia
- Mijić, Z., Ilić, L., Kuzmanoski, M. (2017) Vertical Raman LIDAR profiling of atmospheric aerosol optical properties over Belgrade, PHOTONICA 2017, Book of Abstracts, p. 210, August 28 - September 1, 2017, Belgrade, Serbia
- Mijić Z., Perišić, M., Stojić, A., Kuzmanoski, M., Ilić, L., (2017) Estimation of atmospheric aerosol transport by ground-based remote sensing and modeling, XIX International Eco-Conference, September 25-27, 2017, Belgrade, Serbia, 375-382
- Kuzmanoski, M., Ničković, S., Ilić, L., (2016) Spatial distribution of mineral dust single scattering albedo based on DREAM model, Geophysical Research Abstracts, Vol. 20, EGU2016-4425, 2016, EGU General Assembly 2016, <https://meetingorganizer.copernicus.org/EGU2016/EGU2016-4425.pdf>
- Ilić, L., Kuzmanoski, M., Mijić, Z., (2015) Planetary Boundary Layer and Elevated Aerosol Layer Height Retrieval from Lidar Signal in Belgrade, 5th International WeBIOPATR Workshop & Conference Particulate Matter: Research and Management, October 14-16, 2015, Belgrade, Serbia, 77-84
- Mijić, Z., Ilić, L., Kuzmanoski, M. (2017) Vertical Raman LIDAR profiling of atmospheric aerosol optical properties over Belgrade, PHOTONICA 2017, Book of Abstracts, p. 210, August 28 - September 1, 2017, Belgrade, Serbia

Mijić Z., Perišić, M., Stojić, A., Kuzmanoski, M., Ilić, L., (2017) Estimation of atmospheric aerosol transport by ground-based remote sensing and modeling, XIX International Eco-Conference, September 25-27, 2017, Belgrade, Serbia, 375-382

Kuzmanoski, M., Ničković, S., Ilić, L., (2016) Spatial distribution of mineral dust single scattering albedo based on DREAM model, Geophysical Research Abstracts, Vol. 20, EGU2016-4425, 2016, EGU General Assembly 2016, <https://meetingorganizer.copernicus.org/EGU2016/EGU2016-4425.pdf>

Ilić, L., Kuzmanoski, M., Mijić, Z., (2015) Planetary Boundary Layer and Elevated Aerosol Layer Height Retrieval from Lidar Signal in Belgrade, 5th International WeBIOPATR Workshop & Conference Particulate Matter: Research and Management, October 14-16, 2015, Belgrade, Serbia, 77-84

Presentations

Klimatske promjene - koliko je čovjek pokvario svijet? (Climate Change – How Much Have Humans Affected the Planet?) Presentation at The Seventh Symposium Theology in the Public Sphere, Trebinje, Bosnia and Herzegovina, February 2020.

Presentation of the PhD research, Computational Research of Young Talents in Serbia, The Milanković Day event, Mathematical Institute of the Serbian Academy of Sciences and Arts, May 28th, 2019.

Presentation on parameterization of dust-induced ice nuclei concentration in DREAM model. The talk was organized at Prof. Jennifer Kay's Polar and atmospheric science group meeting, at the Department of Atmospheric and Oceanic Sciences, University of Colorado at Boulder, July 5th, 2017.

Presentation on dust modeling using DREAM model at Prof. Ulrike Lohmann's Atmospheric Physics Group Seminar at Institute for Atmospheric and Climate Science, ETH Zurich on November 26, 2016.

Biography

Luka Ilić was born in Belgrade, Serbia in 1985. He graduated from the Institute of Meteorology, Faculty of Physics, the University of Belgrade in 2012. During his undergraduate studies, he started his professional career in the private sector. He worked SEWA on operational numerical weather prediction (NWP) workflow based on GFS, Eta, and NMM models running on an in-house developed and maintained Linux cluster. At SEWA, NWP models were used to produce tailored forecast products for different business sectors (e.g., road weather, energy sector, media).

Through collaborations with the Institute of Physics Belgrade, he ported the Eta and NMM models to an HPC infrastructure. In a project between Maxeler, Meteos, and the School of Electrical Engineering, University of Belgrade, he participated in porting the geostrophic adjustment code, originally written by Dr. Vladimir Đurđević to a Maxeler FPGA chip.

In 2012, Luka started his Ph. D. studies in the field of meteorology at the Faculty of Physics, University of Belgrade. After a brief post at SEEVCCC of RHMSS, in 2013, he joined the Institute of Physics Belgrade (IPB). At that time, his research focus shifted toward the field of atmospheric aerosols. Relying on previous education and experience in numerical modeling, he started working with the Dust Regional Atmospheric Model (DREAM) with the support and supervision of DREAM's original author Dr. Slobodan Ničković.

The work at IPB had a strong experimental side bringing him closer to aerosol Raman lidar measurements within the EARLINET.

While finalizing his Ph.D. Thesis, Luka got an opportunity to join the BSC Atmospheric Composition group. At BSC, he is modeling atmospheric mineral dust radiative effects in the Earth System.

Изјава о ауторству

Име и презиме аутора Лука Илић

Број индекса 2012 8004

Изјављујем

да је докторска дисертација под насловом

NUMERICAL MODELING OF ICE NUCLEATING PROPERTIES OF ATMOSPHERIC
MINERAL AEROSOL

НУМЕРИЧКО МОДЕЛИРАЊЕ НУКЛЕАЦИОНИХ ОСОБИНА АТМОСФЕРСКОГ
МИНЕРАЛНОГ АЕРОСОЛА

- резултат сопственог истраживачког рада;
- да дисертација у целини ни у деловима није била предложена за стицање друге дипломе према студијским програмима високошколских установа;
- да су резултати коректно наведени и
- да нисам кршио ауторска права и користио интелектуалну својину других лица.

Потпис аутора

У Београду, 11.04.2022.

Изјава о истоветности штампане и електронске верзије докторског рада

Име и презиме аутора Лука Илић

Број индекса 2012 8004

Докторски студијски програм Метеорологија

Наслов рада

NUMERICAL MODELING OF ICE NUCLEATING PROPERTIES OF ATMOSPHERIC MINERAL AEROSOL

НУМЕРИЧКО МОДЕЛИРАЊЕ НУКЛЕАЦИОНИХ ОСОБИНА АТМОСФЕРСКОГ МИНЕРАЛНОГ АЕРОСОЛА

Ментори: Др Лазар Лазић, редовни професор

Др Маја Кузманоски, научни сарадник

Изјављујем да је штампана верзија мог докторског рада истоветна електронској верзији коју сам предао ради похрањивања у **Дигиталном репозиторијуму Универзитета у Београду**.

Дозвољавам да се објаве моји лични подаци везани за добијање академског назива доктора наука, као што су име и презиме, година и место рођења и датум одбране рада.

Ови лични подаци могу се објавити на мрежним страницама дигиталне библиотеке, у електронском каталогу и у публикацијама Универзитета у Београду.

Потпис аутора

У Београду, 11.04.2022.

Изјава о коришћењу

Овлашћујем Универзитетску библиотеку „Светозар Марковић“ да у Дигитални репозиторијум Универзитета у Београду унесе моју докторску дисертацију под насловом:

NUMERICAL MODELING OF ICE NUCLEATING PROPERTIES OF ATMOSPHERIC MINERAL AEROSOL

НУМЕРИЧКО МОДЕЛИРАЊЕ НУКЛЕАЦИОНИХ ОСОБИНА
АТМОСФЕРСКОГ МИНЕРАЛНОГ АЕРОСОЛА

која је моје ауторско дело.

Дисертацију са свим прилозима предао сам у електронском формату погодном за трајно архивирање.

Моју докторску дисертацију похрањену у Дигиталном репозиторијуму Универзитета у Београду и доступну у отвореном приступу могу да користе сви који поштују одредбе садржане у одабраном типу лиценце Креативне заједнице (Creative commons) за коју сам се одлучио.

1. Ауторство (CC BY)
2. Ауторство - некомерцијално (CC BY - NC)
3. Ауторство - некомерцијално - без прерада (CC BY - NC - ND)
4. Ауторство - некомерцијално - делити под истим условима (CC BY - NC - SA)
5. Ауторство - без прерада (CC BY - ND)
6. Ауторство - делити под истим условима (CC BY - SA)

(Молимо да заокружите само једну од шест понуђених лиценци.
Кратак опис лиценци је саставни део ове изјаве).

У Београду, 11.04.2022.

Потпис аутора
